A Remeshing Technique for Large Strain Analysis of Fine-blanking

By

LEUNG Yau Chuen

A thesis submitted in the requirements

for the Degree of Master of Philosophy

At

Department of Industrial and Systems Engineering

The Hong Kong Polytechnic University

October 2003

CERTIFICATE OF ORIGINALITY

I hereby declare that this thesis is my own work and that, to the best of my knowledge and belief, it reproduces no material previously published or written nor material which has been accepted for the award of any other degree or diploma, except where due acknowledgement has been made in the text.

_____(Signed)

Leung Yau Chuen_____(Name of student)

Abstract of thesis entitled:

"A Remeshing Technique for Large Strain Analysis of Fine-blanking"

submitted by Leung Yau Chuen

for the degree of Master of Philosophy

at the Hong Kong Polytechnic University in October 2003

Abstract

Fine-blanking is a well-known metal forming process, growing in popularity due to high quality, reproducible formation of near net shape parts. Strain analysis is an important quantitative measure for investigating metal deformation. A deeper understanding of the strain analysis of fine-blanking could bring forth further applications and breakthroughs in this technology. However, only limited literatures are available on strain analysis of fine-blanking, despite the fact that this technology had been used for years. This is mostly due to the severe and localized deformation of fine-blanking obstructing the measurement of strain. To solve this problem, a new experimental remeshing technique was developed for the large strain analysis of fine-blanking in this research project.

In this project, large strain analysis of fine-blanking was investigated through the use of a new remeshing technique on major deformation area. Grid patterns

were etched on the meridian planes of specimens of low carbon steel sheets by photochemical method. These prepared specimens were then fine-blanked, with a step increment of 20% till the total punch penetration reached 80% of the material thickness. Results of the experimental remeshing showed the highest effective strain values at the punch tip and die corner, where the deformation was highly localized. The effective strain values at the punch tip were found to be 1.19, 2.90, 6.77and 11.78 for a total punch penetration of 20%, 40%, 60% and 80% of the material thickness respectively, indicating that an increase in total punch penetration was associated with an increase of effective strain value. The severity of deformation augmented with the percentage of the increase of total punch penetration.

This study clearly shows that, by employing this newly developed remeshing technique, the measurement of large strain is no longer hindered by the severe deformation usually occurring in fine-blanking. This study also demonstrates that a more intensive strain analysis of fine-blanking is able to be achieved with the aid of this novel technique.

Acknowledgements

First of all, I would like to thank the Industry Department (Industry Support Fund: AF/150/98) and the Research Committee of the Hong Kong Polytechnic University for financial support. Special thanks go to Mr. Michael Leung, Managing Director of Falcon Industries Ltd., who supported my MPhil study, both mentally and financially.

Thanks also due to my respected chief research supervisor, Dr. L.C. Chan, for his extraordinary guidance, enthusiasm, encouragement and boundless support throughout my research years. Deep gratitude is also expressed to Dr. C.Y. Tang for his invaluable guidance and suggestions. My gratitude is also accorded to Prof. T.C. Lee for a great deal of encouragement and constructive comments.

To my wife, Isis Ng, I owe a great debt of gratitude for keeping me going when the road seemed long. Moreover, a big "thank you" to my parents, without whose love and support, I would surely not have enjoyed such a full and successful life.

Finally, thanks to Mr. J.P. Fan, Mr. David Lai, Mr. S.Y. Lau, Mr. Rico Cheung and many others for their valuable advice, assistance and encouragement.

Nomenclature

$\bar{\varepsilon}$	Effective Strain
$\bar{\sigma}$	Effective Stress
F_b	Blanking Force
F_v	Vee-ring Force
F_c	Counter Force
T	Tensile Load
ε^L	Lagrangian Strain
l_i	Initial Length
ε^E	Eulerian strain
l_f	Final Length
ε^N	Natural (true or Logarithmic) strain
Δl	Change of Length
l	Length of a Bar
$x, y, z,$	Axes of Cartesian Coordinates
$u, v, w,$	Displaces in $x, y, z,$ Directions
$\varepsilon_{xx}, \varepsilon_{yy}, \varepsilon_{zz}$	Normal Strains
$\gamma_{xy}, \gamma_{yz}, \gamma_{zx}$	Shear Strains
θ_1, θ_2	Angular Distortions
ε_1	Maximum Principal Strain
ε_2	Minimum Principal Strain
ε_3	Circumferential Strain
R	Resistance

r	Specific Resistance
ε_a	Axial Strain
ε_t	Transverse Strain
μ	Poisson's ratio
S_a	Strain Sensitivity
p_m	Pitch of Master Grating
p_s	Pitch of Specimen Grating
d_m	Density of Master Grating
d_s	Density of Specimen Grating
G_l	Gauge Length of Moiré Fringes
δ	Centre-to-centre Distance
$[K^{(e)}]$	Stiffness Matrix
$\overline{F}^{(e)}$	Load Vector
"e"	Element
{U}	Vector of Nodal Displacements
{F}	Vector of Nodal Forces
d	Die-roll Height
h	Burr Height
K	Shear of Blanked Edge Quality
S_g	Thickness of purely shear of blanking edge
S	Thickness of the material

Table of Contents

List of Tables

List of Figures

CHAPTER 1

INTRODUCTION

1.1 Research Background and Motivation

Nowadays, global competition is forcing the manufacturing industry to increase quality productivity and efficiency. A larger number of higher quality parts must be produced at a lower cost. Every aspect of the production process must be examined and inefficiency eliminated. In addition to improvements in manufacturing plants, there are many opportunities for the improvement of product design as well.

Fine-blanking is a metal stamping process, famous for its ability to produce near net shape parts with excellent quality. Through the application of fine-blanking, time and cost savings can be realized by eliminating secondary operations on the parts. High quality parts must combine good strength and low costing. In general, initial set-up expenses are required for mass production. For example, a stamping plant spends 22.6% of total expenditure on the adjustment of tools and the modification of product design (Dong and Lin, 2000). Therefore, improvement of products in the design phase can greatly reduce the set-up costs and increase productivity.

Fine-blanking is regarded as a more effective metal forming process than conventional (ordinary) blanking, because of the reduction of secondary operations on parts after initial formation. With the existence of vee-ring and small clearance, the sheared surface of the fine-blanked part could be free of cracks and tearing over the whole material thickness. Neither stamping,

counter-blanking nor laser-cutting can produce this result. Effective use of the counter force in the fine-blanking process ensures that the fine-blanked parts are inherently flatter than those produced by stamping. The burr, an unavoidable feature of the blanking process, is very small and easily rectified by deburring process. Another remarkable feature of fine-blanked parts is strain hardening. The sheared edge is hardened due to the severe shearing deformation which takes place in the fine-blanking operation. This hardened edge can extend the service life of the fine-blanked parts. Final products can be made with a precise and good surface finishing after a simple deburring process.

Today, with the increase in application of fine-blanking technology, fine-blanked parts are widely used in many areas. However, there is limited theoretical information relating to the mechanics and the mechanism of fine-blanking technology, forcing workers in this area to rely mainly on their own knowledge and experience. To further understanding on fine-blanking, the deformation process has to be intensively studied, in order to improve the design of fine-blanking parts and tooling. So far, the theoretical analysis of the fine-blanking process is still scarcely reported. Despite some empirical studies, there have been relatively few reports on the deformation mechanism of fine-blanking. Investigations into fine-blanking are far from adequate, especially theoretical ones.

However, there has been a growing trend towards analysing the fine-blanking process by using Finite Element Method (FEM). FEM is a computer simulation method that gives approximate solutions to differential equations modelling problems arising in physics and engineering. However, the accuracy of the

solutions produced by FEM is not guaranteed. For example, in the metal forming process, the rigid-plastic FEM employs computer simulation to simulate the deformation process, when the initial finite-element mesh progressively distorts. As a result, the accuracy of the solution decreases with increasing distortion, until eventually a converged solution is no longer possible.

Experimental strain analysis, is therefore, needed to further explore the deformation mechanism of fine-blanking. Deformation in the metal forming process is very large, especially in the fine-blanking region. The severe and localized deformation of the fine-blanking induces a rigorously distorted grid pattern, immeasurable by conventional methods. Consequently, there is a need to develop an experimental approach to measure these distorted grid patterns, so that a prove intensive strain analysis of fine-blanking can be made practically. In order to reach this goal, a newly developed remeshing technique for large strain analysis of fine-blanking, has been explored and implemented in this research project.

1.2 Scope of this Research

Strain measurement for fine-blanking operation is limited, at low punch penetration of about 20% of the material thickness, due to the severe and unidentifiable deformation of the grids. Without identifying the deformed grids, their strain cannot be measured. In order to make use of the deformed grid for strain analysis, the concept of remeshing in FEM was adopted in the experimental research. In addition, an experimental remeshing technique was developed and performed in a simple tensile test before being applied directly to the

fine-blanking operation. The experimental remeshing technique was verified by comparing the experimental results and FE simulation results. An initial pilot study confirmed the suitability and applicability of this method to fine-blanking. Large strain analysis of fine-blanking was therefore studied by using this experimental remeshing technique, and the experiments were designed and performed. In the experiments, specimens with the fine-element mesh 0.4mm x 0.4mm square grid pattern on the meridians were fine-blanked for punch penetration of 20% step-increment of the material thickness. For each fine-blanking operation, the distorted mesh was taken to measure the strain, and then replaced by etching a new square grid pattern mesh on the meridian plan before the next operation. The procedure of remeshing for the fine-blanking operation were performed and repeated, until a distorted mesh with deformed square grid pattern was obtained up to a maximum of total punch penetration of 80% of the material thickness. By measuring the nodal coordinates for all distorted meshes, large strain analysis of the fine-blanking process was can be carried out adopting the experimental remeshing technique.

1.3 Research Objectives

The goal of the research was to investigate the deformation mechanism of the fine-blanking operation. Large strain analysis was adopted as the analysis method, due to the large deformation during the fine-blanking operation. The strain was measured by one of the traditional strain measurements, the grid method. However, the severe and localized deformation of fine-blanking induces rigorously distorted grid patterns, which are impossible to measure,

explaining the lack of experimental strain analysis on fine-blanking. Therefore, an experimental remeshing technique was developed in this study to overcome this difficulty, making large strain analysis of fine-blanking achievable. The objectives of this research work can be briefly summarized as follows:

- To develop and verify a remeshing technique for large strain analysis, through an experimental approach.
- To design an experiment for application of the remeshing technique, incrementally for the strain measurement of fine-blanking.
- To analyse results for the investigation of the deformation mechanism of the fine-blanking operation.
- To compare the results obtained by the experimental remeshing technique with those obtained by FEM.

1.4 Layout of the Thesis

This thesis intends to report the investigation on the deformation of fine-blanking through experimental strain analysis. Better accuracy could be obtained by using the technique of remeshing, a process of rezoning mesh distortions at each stage of the fine-blanking.

This thesis comprises seven chapters. Each of these chapters has been written to be either read and considered as an individual topic or in combinations to provide information and references on fine-blanking technology.

Chapter 1 provides an introduction to this research project: displaying background research information and the motivation behind this project. It also outlines the main objectives and the steps taken for this research work.

Chapter 2 surveys the literature to provide a thorough coverage of the process of fine-blanking and related analysis methods. In addition to fine-blanking, literatures relating to experimental strain analysis, FEM and the application of the remeshing technique in FEM are also included in this chapter.

Following on from the necessary theoretical and technical background reviewed in Chapter 2, Chapter 3 illustrates the development of the experimental remeshing technique. By adopting the mathematical formulation of the large strain analysis technique, a program is proposed for handling the tedious calculation of strain values. It also describes the simple tension test employed as the validation experiment to verify the proposed technique for fine-blanking.

Chapter 4 then describes the details of the methodological analysis and practical implementation. It includes the criteria for material and equipment selection, preparation of testing specimens, experimental procedures and the necessary measurement techniques.

Chapter 5 describes the strain analysis performed on the material deformation phenomena in the fine-blanking process. The results are then presented, and a discussion session follows, with comments on the experimental analysis approach.

Conclusions for the whole study are presented in Chapter 6, and several major recommendations for further investigation in Chapter 7. Finally, the possible contribution to knowledge made by this research is iterated in Chapter 8.

CHAPTER 2

LITERATURE REVIEW

Detailed literature reviews of the fine-blanking technology, experimental strain analysis and finite element method are provided in this chapter. Information used for the development of experiment and analysis in this project is summarized.

2.1 Fine-blanking Technology

The inception of the fine-blanking industry dates back to 1923 when F. Schiess studied and invented the "fine-blanking method" (Feorrer, 1970), and obtained his patents in the same year. There were additional patents that followed in Switzerland, France, Great Britain, and the United States. The fine-blanking process, which is essentially a hybrid between stamping and cold extrusion, was developed in Switzerland in the 1920s for the watch industry. However, it was not until 1959 that this advanced technique was widely used in industrial applications, especially the watch industry because of its ability to produce accurate smooth-sheared edges over the full work piece thickness in one single operation (Zhou et al., 1993).

2.1.1 Concept of Fine-blanking

Fine-blanking is widely accepted as "the most operation-minimized while value-maximized" manufacturing methods for the production of fine and accurate units in the sheet metal forming process. Fine-blanking technology covers all blanking processes that achieves high blanking surfaces. Fine-blanking is also

known as precision blanking or fine stamping (Schuler, 1998). This precision-stamping process produces complex "net shape" finished parts in just one or two operations. It can replace castings, forgings, fabrication and all subsequent machining operations. Originally, fine-blanked parts were primarily utilized by the watch/clock as well as office machine industry. Nowadays, the range of applications has expanded considerably and fine-blanking is firmly established and prevalently employed in electronic industry and automotive industry for fine-blanked parts. Typical components fabricated this way included camshaft sprocket and pivot plates for a twin mass flywheel where savings of as much as 50% could be made, as compared to more conventional means.

The production process of fine-blanking involves shear blanking for the manufacture of parts with a smooth cut surface. Fine-blanking involves special type of press and tooling. The system includes fine-blanking press, fine-blanking tool, input material, finished part geometry and lubrication at tool and work piece. The single-stroke shearing method of fine blanking uses an annular serrated blank holder and a counterforce pad. Thus the generated blanked surface is free of any incipient burr or flaws, which is frequently used as a functional surface, see Fig.2.1.

2.1.2 Advantages of Fine-blanking

Fine-blanking is regarded as a separated group of conventional stamping. Fig.2.2 illustrates the main differences between the principles of the tools used for the conventional blanking process (left) and of those for fine-blanking. Conventional blanking forces the stock material through a cavity in a die plate with a punch that is smaller than the cavity in the die plate. In order to produce an

acceptable finished edge on the component and to prolong tool life by reducing loading on the punch and die plate, a clearance gap between the punch and the die plate is employed. This gap is usually about 5 - 10% (Jana and Ong, 1989) of the stock material thickness depending on the mechanical properties of the material being cut. This concept works fine, but has some major drawbacks - the two most notable being that the cut edge is not square throughout the thickness of the component, and that the component will be slightly concave in shape. The resulting edge will be cleanly cut for approximately one third of the material thickness, and then have a tear-away equal in width to the punch to die gap for the remaining two thirds of the material thickness. The concavity arises when unsupported parts are forced through the die cavity.

While these conditions may be acceptable for certain products, there are cases where flatness, edge squareness and edge condition are critical, for example gear teeth and cam faces. In these cases, the fine-blanking process has more advantages. The key to fine-blanking is the triple acting hydraulic press, on the material in the fine-blanking cycle. These presses are built to extreme precision standards and have variable stroke lengths, counterforce, vee-ring force and the blanking force, approach and cutting speeds within the specifications of the press model. This allows for the stock material to be securely clamped between the die plate and a pressure plate (the vee-ring plate), while the area that the component is to be cut from is clamped independently between the punch and counterforce pad. As the press closes, the pressure on the ring groove plate is overcome by the force of the press ram and thus the component is effectively lifted out of the stock material. This degree of control also permits a zero gap between the punch and the die plate

(theoretically the punch never enters the die plate). As these pressures are completely varied, it is possible to produce a component that is completely flat and have smooth unbroken square edges through the entire thickness of the component.

Moreover, the essential advantages of fine-blanking are high quality and low cost. These advantages spans a number of area of consideration including repeatability, cleanly sheared edges, close tolerance on holes and profiles, narrow sections and small diameter holes, flatness and surface finish and various shapes such as counter sinks, half shears, coined sections and self rivets. The close tolerance design of the tool, and the fact that all operations are contained within the tool so that special features are created as the basic component is produced, lead to inherent quality and reliability. There is little or no edge break, eliminating the need for shaving, broaching or profile grinding and the process is better than conventional pressing in the close tolerances permissible on holes and profiles. With fine-blanking, extrusions and collars can be formed to make complex three-dimensional net shapes that do not require any further machining. Extremely strong and thin section components can be produced with consequential weight savings by using rolled steel stock and the steel used for fine-blanking is easily machined.

2.1.3 Analysis of Fine-blanking Process

Although fine-blanking is not a new metal forming technology, limited researches on fine-blanking are published in the past several decades. These researches investigated areas including the placement of vee-ring, hardening behaviour, punch and die clearance, deformations, material selection and

lubrication.

Maeda and Nakagawa (1968) systematically studied the effects of positions of vee-ring and blank holder on the properties of blank edge, when subjected to cracking (Maeda and Nakagawa, 1968). They examined how the impingement ring affected the percent of fracture on the blanked surface, and formed that placement and size of the vee-ring had a significant effect on blanking quality. A flat toped projection was also found to be effective in producing quality shearing, but this feature was seldom used in industry. This research and other experience have generated guidelines for vee-ring size and distance from the shear line (Grimm, 1984): For most application, the vee-ring can be most effectively placed on the die, (Maeda and Nakagawa, 1968); but for thicker stock and critical applications vee-rings on both the die and blank holder are required (Haack, 1984); for non-critical areas of the part, the vee-ring may not be needed at all.

Lee, et al. (1993; 1995; 1997) studied the hardening behaviour in fine-blanking and estimated the strain distribution on the cross-section of fine blanked specimens. They reported that the vee-ring, imposing a wedging force perpendicular to the shearing force, would reinforce and harden the surrounding material inside shear zone, resulting in early crack growth.

To explain why the cracks occur on the shearing surface and how to avoid it, a number of studies were conducted (Rotter, 1990) and (Zhou et al., 1993) and a model was proposed. Using the proposed model, the maximum degree of deformation was estimated and the effect of the small radius of the blanking edge on crack formation was explained. At the same period, another model for stress analysis during fine-blanking deformation was suggested by Tu et al. (1990, 1993),

and further illustrated by Mohr's stress circle (Zhou et al., 1993). From these analysis, conclusion was drawn that the hydrostatic stress exerted on the material can be strengthened by means of increasing vee-ring pressure or counter pressure, and decreasing punch-die clearance, achieving an increase in the material's plasticity, thus reducing cracks and tearing on the shearing surface.

Johnston, et al. proposed a slip line field model to analyze fine-blanking deformation in 1968 (Johnston et al., 1968). A decade later, a modified slip line field model was proposed by Gunasekera and Hobbs (1979). They pointed out that the blank holder's indenting ridge on the stress state at the shear zone could provide an increased hydrostatic stress, lowering the tensile stress in the region, thereby inhibiting the propagation of macro-cracks at the edge of the blank. Similar analysis investigating fine-blanking process can also be found in literatures (Thomson and Gunasekera, 1980), (Rotter, 1990) and (Zhou et al., 1993), where analysis on the deformation by punch penetration and effect of vee-ring indenter were reported.

The study of Rotter on thick metal plate fine-blanking techniques suggested that the accuracy of size and shape of the blanked parts could be improved if the punch-die clearance was kept small, to increase blank holding force and counter force (Rotter, 1990). His study also agrees with the research by Maeda and Nakagawa that performance increased as punch and die clearance decreased, with 0.5% of material thickness being the clearance beyond which only small gains were possible. Optimal clearance is determined by the material, material thickness and part geometry (Haack, 1984).

Proper material selection is important for fine-blanking. Hot rolled steel with a ferrite and pearlite structure is poor for fine-blanking. The hard lamellar planes of

pearlite are difficult to shear, leading to tears on the sheared edge. Spheroidize annealing causes reprecititation of cementite into a spherical shape (Garc, 1982). The cementite is pushed through the softer ferrite, producing smooth surfaces. Alloy steels can reach 95-100% spheroidizatoin through cold rolling which enhances cementite nucleation (Haack, 1984) and (Birzer, 1984). This softer material also reduces the pressure required for forming, with a reduction from 51 kPa for ferridic / pearlitic steel to as little as 41 kPa for fully spheroidized material suitable for fine-blanking. It is possible to get good results from harder materials such as 80 ksi yield high strength low alloy (HSLA) steel. Difficulty in forming is experienced when HSLA hardness exceeds 99 Rockwell B. An annealing step may be required for good results. The blanking of harder materials coupled with the edge hardening effect of the process, can make secondary heat treatment unnecessary.

Lubrication is a significant part of fine-blanking, without which fine-blanking is impossible. The high pressure and slow speed force the lubricant from the critical surfaces of the punch to the die, especially in thicker materials. The heat from yielding material, together with insufficient lubrication, could lead to galling of tooling surfaces (Birzer, 1984). This microwelding of the blank material onto the fine-blanking tool lead to poor surface quality and chipping of the parts. To help the lubricant reach the friction zones, non-critical edges of the blank holder and counter punch are chamfered to provide a pocket, from which lubricant is delivered into material clamped in the tool. As material thickness increases, higher viscosity oils must be used (Birzer, 1984). The pressurized vapour deposition (PVD) coating guard against tool wear. The coatings used are mainly titanium nitride (TiN) and

titanium carbon nitride (TiCN) which help resist galling and also reduce friction.

2.2 Experimental Strain Analysis

When a body is subjected to force, individual points of the body will move and the movement of an arbitrary point is a vector quantity known as a displacement. As the various points in the body undergo different movements, each can be represented by its own unique displacement vector. Each vector can be resolved into components parallel to the Cartesian coordinate axes which are displacement components u, v and w in the x, y, z directions respectively. The movement of the points of a body relative to each other is known as a deformation. The term of strain is used to describe deformation of solid material. It is a geometric quantity depending on the relative movements of two or three points in the body. Therefore strain is related only to the deformation displacements. In other words, when the relative position of points in a continuous body is altered, the body is strained, and strain analysis is the study of this altered states. Strain analysis is important because strain is closely related to stress and ductility. Hooke determined strain in tensile specimens by noting the change in length between two scribed lines, a simple and direct approach hardly warrants designation as a method. However, as the number and direction of lines are increased, and as the geometry becomes more complex, there are certain techniques that aid in the process of measuring the distance between two lines. A normal strain is defined as the change in length of a line segment between two points divided by the original length of the line segment. A shearing strain is defined as the angular change between two line segments initially perpendicular to each other.

In the strain analysis, three definitions of strain were found commonly use (Durelli and Parks, 1967). Considering the axial strain for uniaxial case, a bar with an initial length of l_i would be elongated to l_f under the tensile load T as shown in Fig.2.3.

1) Lagrangian (engineering or nominal) strain, ε^{L} is defined as the change in length divided by its initial length, l_i (commonly associated with a coordinate system on the undeformed body). In symbols this is

$$\varepsilon^{L} = \lim_{l_i \to 0} \frac{l_f - l_i}{l_i} \tag{2.1}$$

2) Eulerian strain, ε^{E}, is defined as the change in length divided by its final length, l_f (commonly associated with a coordinate system on the deformed body). In symbols this is

$$\varepsilon^{E} = \lim_{l_f \to 0} \frac{l_f - l_i}{l_f} \tag{2.2}$$

3) Natural (true or Logarithmic) strain, ε^{N}, is most generally defined by a mathematical expression

$$\varepsilon^{N} = \lim_{l \to 0} \lim_{\Delta l \to 0} \sum_{l_i}^{l_f} \frac{\Delta l}{l} = \ln \frac{l_f}{l_i} \tag{2.3}$$

where l is the length of the bar at any load level and Δl is the change in length due to a change of load at that load level. If the total loading, carrying l from l_i to l_f, is sub-divided in such a manner that all the increments Δl approach zero then the sum of the ratios $\Delta l/l$ will approach ε^{N} and will be equal to ε^{N} in the limit.

Each of the three definitions of strain specifies exactly the geometry of the deformation and as such each strain so defined has a fixed relationship with strain defined in the other two ways

$$\varepsilon^N = \ln(1+\varepsilon^L) \tag{2.4}$$

$$\varepsilon^L = \varepsilon^E/(1-\varepsilon^E) \tag{2.5}$$

$$\varepsilon^N = \ln[1/(1+\varepsilon^E)] \tag{2.6}$$

2.2.1 Definition of Strain

Deformations can be small or large. Therefore, in strain analysis, there are small (infinitesimal) strains and large strains. The concept developed from the fact that the large change in geometry due to large strains limited the usefulness of the conventional definition of strain. Ragab and Abdel-Rahman (1999) proposed calculation method for large deformation problems in engineering. The deformed length dl of a line segment dl_0 shown in Fig.2.4 can be calculated,

$$dl^2 - dl_0^2 = [(dx+du)^2 + (dy+dv)^2 + (dz+dw)^2] - [dx^2 + dy^2 + dz^2]$$

$$dl^2 - dl_0^2 = 2(dudx + dvdy + dwdz) + (du^2 + dv^2 + dw^2) \tag{2.7}$$

The above formulae are known as Lagrangian description, in which the independent variables (x, y, z) are the coordinates of a material particle in its initial, undeformed state. Substituting the result of the chain rule of differentiation into Eq.2.7, it becomes:

$$
\begin{aligned}
dl^2 - dl_0^2 = & 2\left[\left(\frac{\partial u}{\partial x}\right) + \frac{1}{2}\left[\left(\frac{\partial u}{\partial x}\right)^2 + \left(\frac{\partial v}{\partial x}\right)^2 + \left(\frac{\partial w}{\partial x}\right)^2\right]\right]dx^2 \\
& + 2\left[\left(\frac{\partial v}{\partial y}\right) + \frac{1}{2}\left[\left(\frac{\partial u}{\partial y}\right)^2 + \left(\frac{\partial v}{\partial y}\right)^2 + \left(\frac{\partial w}{\partial y}\right)^2\right]\right]dy^2 \\
& + 2\left[\left(\frac{\partial w}{\partial z}\right) + \frac{1}{2}\left[\left(\frac{\partial u}{\partial z}\right)^2 + \left(\frac{\partial v}{\partial z}\right)^2 + \left(\frac{\partial w}{\partial z}\right)^2\right]\right]dz^2 \\
& + 2\left[\left(\frac{\partial v}{\partial x} + \frac{\partial u}{\partial y}\right) + \frac{\partial u}{\partial x}\frac{\partial u}{\partial y} + \frac{\partial v}{\partial x}\frac{\partial v}{\partial y} + \frac{\partial w}{\partial x}\frac{\partial w}{\partial y}\right]dxdy \\
& + 2\left[\left(\frac{\partial w}{\partial x} + \frac{\partial u}{\partial z}\right) + \frac{\partial u}{\partial x}\frac{\partial u}{\partial z} + \frac{\partial v}{\partial x}\frac{\partial v}{\partial z} + \frac{\partial w}{\partial x}\frac{\partial w}{\partial z}\right]dxdz \\
& + 2\left[\left(\frac{\partial w}{\partial y} + \frac{\partial v}{\partial z}\right) + \frac{\partial u}{\partial y}\frac{\partial u}{\partial z} + \frac{\partial v}{\partial y}\frac{\partial v}{\partial z} + \frac{\partial w}{\partial y}\frac{\partial w}{\partial z}\right]dydz
\end{aligned}
\tag{2.8}
$$

The quantity (dl^2-dl_0^2) could provide a convenient means for describing deformation if Eq.2.8 is rewritten as

$$
dl^2 - dl_0^2 = 2\varepsilon_{xx}dx^2 + 2\varepsilon_{yy}dy^2 + 2\varepsilon_{zz}dz^2 + 2\gamma_{xy}dxdy + 2\gamma_{xz}dxdz + 2\gamma_{yz}dydz \tag{2.9}
$$

where

$$
\begin{aligned}
\varepsilon_{xx} &= \left(\frac{\partial u}{\partial x}\right) + \frac{1}{2}\left[\left(\frac{\partial u}{\partial x}\right)^2 + \left(\frac{\partial v}{\partial x}\right)^2 + \left(\frac{\partial w}{\partial x}\right)^2\right] \\
\varepsilon_{yy} &= \left(\frac{\partial v}{\partial y}\right) + \frac{1}{2}\left[\left(\frac{\partial u}{\partial y}\right)^2 + \left(\frac{\partial v}{\partial y}\right)^2 + \left(\frac{\partial w}{\partial y}\right)^2\right] \\
\varepsilon_{zz} &= \left(\frac{\partial w}{\partial z}\right) + \frac{1}{2}\left[\left(\frac{\partial u}{\partial z}\right)^2 + \left(\frac{\partial v}{\partial z}\right)^2 + \left(\frac{\partial w}{\partial z}\right)^2\right] \\
\gamma_{xy} &= \left(\frac{\partial v}{\partial x} + \frac{\partial u}{\partial y}\right) + \left(\frac{\partial u}{\partial x}\frac{\partial u}{\partial y} + \frac{\partial v}{\partial x}\frac{\partial v}{\partial y} + \frac{\partial w}{\partial x}\frac{\partial w}{\partial y}\right) \\
\gamma_{xz} &= \left(\frac{\partial w}{\partial x} + \frac{\partial u}{\partial z}\right) + \left(\frac{\partial u}{\partial x}\frac{\partial u}{\partial z} + \frac{\partial v}{\partial x}\frac{\partial v}{\partial z} + \frac{\partial w}{\partial x}\frac{\partial w}{\partial z}\right) \\
\gamma_{yz} &= \left(\frac{\partial w}{\partial y} + \frac{\partial v}{\partial z}\right) + \left(\frac{\partial u}{\partial y}\frac{\partial u}{\partial z} + \frac{\partial v}{\partial y}\frac{\partial v}{\partial z} + \frac{\partial w}{\partial y}\frac{\partial w}{\partial z}\right)
\end{aligned}
\tag{2.10}
$$

The Eq.2.10 constitutes the strain-displacement relations for large deformations.

Concerning the shear strain, the undeformed states of two lines are oriented along the x and y direction. After deformation, these two lines undergo large strains ε_{xx} and ε_{yy} respectively, together with a change of γ_{xy} in the right angle originally included between them. This change is given by

$$\sin\gamma_{xy} = \frac{\gamma_{xy}}{\sqrt{1+2\varepsilon_{xx}}\sqrt{1+2\varepsilon_{yy}}} \tag{2.11}$$

In a wide variety of engineering problems, the displacements and strains produced by the applied loads are very small. Infinitesimal strain at a given point is defined by considering the undeformed and deformed geometrical configurations of the solid. The relationships between strains and displacements can be determined by considering the deformation of an arbitrary cube in a loaded body system. This deformation is illustrated in Fig.2.4, in which a general point P is moved through a distance u in the x direction, v in the y direction and w in the z direction. For small deformations, the derivatives of displacements are infinitesimal and their products or powers of higher orders could be neglected in practice. Hence the state of strain at a given point, in a deformable solid in Cartesian coordinates, is determined by the following six infinitesimal strain-displacement relations (Dally, 1991):

$$\varepsilon_{xx} = \frac{\partial u}{\partial x} \tag{2.12}$$

$$\varepsilon_{yy} = \frac{\partial v}{\partial y} \tag{2.13}$$

$$\varepsilon_{zz} = \frac{\partial w}{\partial z} \tag{2.14}$$

$$\gamma_{xy} = \frac{\partial v}{\partial x} + \frac{\partial u}{\partial y} \tag{2.15}$$

$$\gamma_{yz} = \frac{\partial w}{\partial y} + \frac{\partial v}{\partial z} \tag{2.16}$$

$$\gamma_{zx} = \frac{\partial u}{\partial z} + \frac{\partial w}{\partial x} \tag{2.17}$$

Although infinitesimal displacements and strains describe the deformation of most engineering structures, there are certain applications where large or finite deformations encountered, such as sheet metal forming, ductile fracture and buckling. Therefore, strains should not be restricted to small ones, which could be viewed as special case of large strains.

In the application of large strain, T. C. Hsü (1966) developed a homogenous large strain analysis technique. This technique involves a marking of small square grids on the surface of the specimen before deformation. The assumption of the technique is that deformation in every square would be homogeneous and the square would become a parallelogram after deformation. Large deformations with rigid body rotation are also taken into consideration in this technique. Based on these assumptions, a matrix algebra method was developed to calculate the strain distribution over surfaces of specimens. Since this is an axisymmetric problem, the square grids must be marked on the meridian plane of the specimen before deformation.

In Fig.2.5, the original square grid *abcd* is supposed to be deformed into a parallelogram $a_1b_1c_1d_1$ and the radial location of point *a* remains unchanged after deformation. After the deformation, the size of the original square $l \times l$ and the

coordinates of the nodal points are defined as $a_1(x_{a_1}, y_{a_1})$, $b_1(x_{b_1}, y_{b_1})$, $c_1(x_{c_1}, y_{c_1})$ and $d_1(x_{d_1}, y_{d_1})$. It can be obtained that

$$\begin{cases} \Delta x_1 = x_{b_1} - x_{a_1} \\ \Delta y_1 = y_{b_1} - y_{a_1} \\ t_1 = \dfrac{\Delta y_1}{\Delta x_1} \end{cases} \tag{2.18}$$

$$\begin{cases} \Delta x_2 = x_{d_1} - x_{a_1} \\ \Delta y_2 = y_{d_1} - y_{a_1} \\ t_2 = \dfrac{\Delta y_2}{\Delta x_2} \end{cases} \tag{2.19}$$

$$l_1 = \sqrt{\Delta x_1^2 + \Delta y_1^2} \tag{2.20}$$

$$\beta = \tan^{-1} \frac{t_2 - t_1}{1 + t_1 t_2} \tag{2.21}$$

$$\begin{aligned} \gamma &= \tan\left(\frac{\pi}{2} - \beta\right) \\ &= \cot \beta \\ &= \frac{1 + t_1 t_2}{t_2 - t_1} \\ &= \frac{\Delta x_1 \Delta x_2 + \Delta y_1 \Delta y_2}{\Delta x_1 \Delta y_2 - \Delta x_2 \Delta y_1} \end{aligned} \tag{2.22}$$

According to the matrix algebra method developed in literature (Hsü, 1966), the strain in the parallelogram $a_1 b_1 c_1 d_1$ can be obtained as

$$\cosh \varepsilon = \frac{1}{2}\left(\frac{l_1}{l} + \frac{l}{l_1}\right)\cos\delta - \frac{l}{l_1}\frac{\gamma}{2}\sin\delta \tag{2.23}$$

where

$$\delta = \tan^{-1}\left(-\frac{l^2\gamma}{l_1^2 + l^2}\right), \tag{2.24}$$

$$\cosh\varepsilon = \frac{1}{2}\left(\frac{l_1}{l} + \frac{l}{l_1}\right)\cos\delta - \frac{\gamma}{2}\frac{l}{l_1}\sin\delta$$

$$= \frac{1}{2}\cos\delta\left(\frac{l_1}{l} + \frac{l}{l_1} - \frac{l}{l_1}\gamma\tan\delta\right)$$

$$= \frac{1}{2}\frac{l^2 + l_1^2}{\sqrt{(l^2 + l_1^2)^2 + \gamma^2 l^4}}\left(\frac{l_1}{l} + \frac{l}{l_1} + \frac{l}{l_1}\frac{\gamma^2 l^2}{l^2 + l_1^2}\right)$$

$$= \frac{1}{2ll_1}\frac{1}{\sqrt{(l^2 + l_1^2)^2 + \gamma^2 l^4}}\left[(l^2 + l_1^2)^2 + \gamma^2 l^4\right]$$

$$= \frac{1}{2ll_1}\sqrt{(l^2 + l_1^2)^2 + \gamma^2 l^4}$$

$$= \frac{1}{2}\sqrt{\left(\frac{l}{l_1} + \frac{l_1}{l}\right)^2 + \gamma^2\left(\frac{l}{l_1}\right)^2} \tag{2.25}$$

the ε is one of the principal strains in parallelogram $a_1b_1c_1d_1$ and the $-\varepsilon$ is another one accordingly. Therefore, the effective strain in parallelogram $a_1b_1c_1d_1$ can be expressed as

$$\bar{\varepsilon} = \frac{\sqrt{2}}{3}\sqrt{(\varepsilon - 0)^2 + (-\varepsilon - 0)^2 + (-\varepsilon - \varepsilon)^2} = \frac{2}{\sqrt{3}}\varepsilon \tag{2.26}$$

For an axi-symmetric case, the circumferential strain generated from the radial displacement is considered. In Fig.2.5, the original square before deformation can be represented by $a_0b_0c_0d_0$ and the deformed parallelogram by $a_1b_1c_1d_1$. By comparing the parallelogram $a_1b_1c_1d_1$ with the square $a_0b_0c_0d_0$, it was found that not only the shape, but also the size of the square $a_0b_0c_0d_0$ changed. Therefore, it would be convenient to consider the deformation in two steps: First the square $a_0b_0c_0d_0$ deforms to *abcd* which is smaller due to the circumferential strain; Then the square *abcd* further deforms to parallelogram $a_1b_1c_1d_1$.

For incompressible condition, $x_0 = x_{a_0}$ and $x_1 = x_{a_1}$, the first deformation could be obtained from,

$$l = l_0\sqrt{\frac{x_0}{x_1}} \tag{2.27}$$

Substituting l into (2.23) and (2.24):

$$\cosh\varepsilon = \frac{1}{2}\left(\frac{l_1}{l_0}\sqrt{\frac{x_1}{x_0}} + \frac{l_0}{l_1}\sqrt{\frac{x_0}{x_1}}\right)\cos\delta - \frac{l_0}{l_1}\sqrt{\frac{x_0}{x_1}}\frac{\gamma}{2}\sin\delta$$

$$\delta = \tan^{-1}\left(-\frac{x_0 l_0^2\gamma}{x_1 l_1^2 + x_0 l_0^2}\right) \tag{2.28}$$

$$\cosh\varepsilon = \frac{1}{2}\sqrt{(\frac{l}{l_1}+\frac{l_1}{l})^2 + \gamma^2(\frac{l}{l_1})^2}$$

Obviously the circumferential strain is

$$\varepsilon_c = \ln\frac{x_1}{x_0} \tag{2.29}$$

Thus the two principal strains in the meridian plane can be further expressed as $\varepsilon_1 = \left(\varepsilon - \frac{\varepsilon_c}{2}\right)$ and $\varepsilon_2 = -\left(\varepsilon + \frac{\varepsilon_c}{2}\right)$. Finally, the effective strain in the parallelogram $a_1b_1c_1d_1$ could be calculated as

$$\bar{\varepsilon} = \tfrac{\sqrt{2}}{3}\sqrt{(\varepsilon_1-\varepsilon_2)^2 + (\varepsilon_2-\varepsilon_c)^2 + (\varepsilon_c-\varepsilon_1)^2} = \tfrac{2}{\sqrt{3}}\sqrt{\varepsilon^2 + \tfrac{3}{4}\varepsilon_c^2}$$

$$= \sqrt{\frac{4}{3}\varepsilon^2 + \varepsilon_c^2} \tag{2.30}$$

Zheng (2000) used this calculation of effective strain in the development of finite element analysis of a combined fine-blanking and extrusion process. However, this technique is used for solving homogenous problems and the deformed quadrilaterals are assumed to be parallelograms. The application of this technique

to fine-blanking is inappropriate because the deformation process in fine-blanking is not homogenous and some of the deformed quadrilaterals are not exact parallelograms.

2.2.2 Strain Measurement

In experimental stress analysis, stress cannot be obtained directly. Therefore, the usual practice is to measure the strain and calculate the state of stress by using the stress-strain equations. In most experimental work involving strain measurement, the strains are measured on a free surface of a membrane where a state of plane stress exists. Obviously, stresses and strains are mathematical concepts that cannot be measured directly. Displacements can be measured and from the physical measurement of displacements, strain is determined. Fine-blanking process is one of the material deformation operations. Strain analysis is the study of quantitative deformation process. Measuring the strain occurs in the fine-blanking process can achieve a better understanding of deformation, which is helpful for applying this technology efficiently and effectively. Therefore, measuring strain of fine-blanking is important to promote the application of fine-blanking as well as provide foundation in the design of fine-blanking products and tooling.

Strains could be measured by many methods but only the measurements of large strain will be reviewed in this section. It was found that electrical-resistance strain gauges, moiré method and grid method are commonly used in strain measurements.

Electrical-resistance strain gauge is probably the most widely used strain

analysis technique, as it offers a simple and quick method of strain measurement. The operative principle of the electrical-resistance strain gauge is known for more than a century. To describe the electrical resistance change of a conductor cause by the change of its length, the term strain sensitivity is introduced. In 1856, Lord Kelvin reported that certain metal wires exhibited a "change of electrical resistance with the change in strain" (Khan and Wang, 2001). The electrical-resistance strain gauge is the most versatile device for strain measurement, on surfaces of machine components and structural members. The total electrical-resistance of a rectangular uniform-cross-section conductor is described by the equation

$$R = \frac{rL}{ab} \tag{2.31}$$

where R, r, L, a and b are the resistance, specific resistance, length, and the lateral dimensions of the rectangular cross section of the conductor respectively. Taking logarithms and differentiating Eq.2.31, it becomes

$$\frac{dR}{R} = \frac{dr}{r} + \frac{dL}{L} - \frac{da}{a} - \frac{db}{b} \tag{2.32}$$

For an axial strain, $\varepsilon_a = dL/L$, there is a transverse strain ε_t, which is given by

$$\varepsilon_t = -\mu\varepsilon_a = -\mu\frac{dL}{L} = \frac{-da}{a} = \frac{-db}{b} \tag{2.33}$$

where μ is the Poisson's ratio. Substituting the Eq.2.33 into Eq.2.32 and gives

$$\frac{dR}{R} = \frac{dr}{r} + (1+2\mu)\frac{dL}{L} \tag{2.34}$$

To describe the change of electrical resistance in a conductor, caused by the change of its length, the term strain sensitivity is introduced. It can be defined as the resistance change (ΔR) per unit of initial resistance (R) per unit of applied axial

strain. Strain sensitivity is denoted by S_a, which is defined as:

$$S_a = \frac{\Delta R / R}{\Delta L / L} = \frac{\Delta R / R}{\varepsilon_a} \tag{2.35}$$

where ε_a is the nominal strain in the axial direction. Since Poisson's ratio is approximately 0.3 for most metal alloys used as the resistance element, the strain sensitivity would be about 1.6 if only the dimensional changes are considered. For large strain, the resistance element undergoes plastic deformation and high strain sensitivity is useful to measure both elastic as well as plastic strain in many engineering problems. Therefore, it is important to employ the proper adhesive and bonding procedures to achieve precise strain measurements, when measuring large strain, by using bonded resistance strain gauge. For high-elongation strain measurements of more than 3% but not exceeding 15%, epoxy adhesive is employed. Different epoxy systems are commercially available in kits today. Some elongation capabilities will be increased to 20% for an uniaxial compression test.

The use of electrical–resistance gauges for dynamic deformation measurement was investigated by Sharpe (1974) and Khan and Hsiao (1988). Sharpe noted that, except for a slightly distorted wave front, foil gauges are "reasonably accurate for measurements of dynamic plastic strain". The maximum strain measured by Sharpe was eight percent. Khan and Hsiao, after comparing their own foil strain gauges results with Bell's ones by diffraction grating technique (Bell 1956), concluded that "the maximum strains and wave speeds, two parameters which are used to infer dynamic response of a solid during plastic wave propagation, are accurately obtained by using foil resistance gauges". Like Karnes and Ripperger (1966), the

maximum strain they obtained was about two percent. However, Huang and Khan (1991) modified the split-Hopkinson pressure-bar technique and measured the strain in the specimen directly by electrical-resistance foil gauges with gauge lengths of 2mm. Since the gauge factor provided by the manufacturer was valid only for small strains, a linear relation between gauge factor and strain was found and used for correction of the strain data. So the gauge factor varies linearly with strain and the measurement of large strain with electrical-resistance foil strain gauge is made possible. The maximum nominal strain obtained was 35 percent in compression, 27 percent in tension.

Other than electrical-resistance strain gauges, the moiré method is another strain measurement procedure. The word moiré comes from the name of a silk fabric which, when folded, exhibits patterns of light and dark bands. The moiré effect is, similar to light and dark bands or fringes, produced by the superposition of two sets of gratings under certain circumstances. Moiré is generally used in engineering to describe interference fringes produced by superimposing two sets of gratings. The historical background information of applications of moiré methods may be found in Durelli and Parks (1970). All moiré methods use silk as the gauge element. Moiré fringe patterns can be used to measure various quantities for example in-plane and out-of-plane displacements, rotations, strains and curvatures. As a geometric interference method, the moiré method could be applied to large deformation measurements, dynamic displacement, elastic-plastic strain measurements, etc.

In the experimental measurement, two gratings are necessary to produce moiré fringes, one is called the specimen grating and the other is known as the master

grating. The centre-to-centre distance between the master grating lines is called pitch, designated by the symbol p_m; the number of lines per unit length for the master grating is known as the density of the master and presented by d_m. The corresponding pitch and density of the specimen are changing during deformation and denoted by p_s and d_s respectively. The direction perpendicular to the lines of the master grating is know as the primary direction and the direction parallel to the lines of the master grating is called the secondary direction.

In Fig.2.6 (Durelli and Parks, 1970), the interference of two gratings with lines parallel to each other but of different pitches p_m and p_1, can bring about visualization of the master grating and the specimen grating, are under uniform deformation. A light fringe would be observed at the place where two opaque strips coincide (point A' in Fig.2.6) and the neighbouring transparent area having maximal average transmitted light intensity. Conversely, a dark fringe will be observed at the points where a transparent strip is covered by an opaque strip, in this case the average transmitted light is minimum. The fringe direction coincides with the secondary direction. Let δ be the centre-to-centre distance between the light (or dark) fringes (known as the fringe spacing). We will have

$$\delta = mp_m = (m \pm 1)p_s \tag{2.36}$$

If the pitches of the master grating and the specimen grating were originally the same, the difference of the pitches would be produced purely by the uniform deformation (either contraction or elongation) of the specimen. If the master grating and the specimen grating were initially coincident and the specimen grating is fixed at the left end, as shown if Fig.2.6, point A in the undeformed state displaced p amount would now be A' at the centreline of a light fringe (called first light fringe).

The engineering or nominal strain, ε, can be computed by

$$\varepsilon = \frac{\Delta L}{Lh} = \frac{p_m}{\delta - p_m} \cong \frac{p_m}{\delta} \tag{2.37}$$

where p_m is known and δ can be directly measured from the moiré fringe patterns. Similarly, at the centreline of the second light fringe, the displacement is $2p_m$, while at the centreline of the mth light fringe, the displacement is mp_m. In other words, moiré fringes are the loci of points with equal relative displacement u in the primary direction. Let m be the number of moiré fringes within the gauge length G_l.

$$\varepsilon = \begin{cases} \dfrac{\Delta L}{\Delta L_0} = \dfrac{mp_m}{G_l - mp_m} \\ -\dfrac{\Delta L}{\Delta L_0} = -\dfrac{mp_m}{G_l + mp_m} \end{cases} \tag{2.38}$$

Fig.2.7 (Khan, 2001) shows a simplified moiré fringes formed by a combination of different pitches and rotations. Firstly determine the angle β, which is closely related to the shear strain and the segment AB gives

$$\frac{p_m}{\sin\beta} = \frac{\delta}{\sin(\alpha - \beta)} \tag{2.39}$$

Angle β will be:

$$\beta = \tan^{-1} \frac{\sin\alpha}{\delta / p_m + \cos\alpha} \tag{2.40}$$

When the rotation β is very small, α approaches $\pi/2$ as p_s approaches p_m, then

$$\beta \approx \frac{p_m}{\delta} \tag{2.41}$$

Similarly for the segment BC,

$$\frac{p_s}{\sin(\alpha - \beta)} = \frac{p}{\sin(\pi - \alpha)} = \frac{p}{\sin\alpha} \tag{2.42}$$

By solving Eq.(2.39) and Eq.(2.42),

$$p_s = \frac{p_m \sin(\alpha - \beta)}{\sin \alpha} = \frac{\delta \sin \beta}{\sin \alpha} \tag{2.43}$$

Using Eq.(2.40) to eliminate θ gives

$$p_s = \frac{\delta}{\sqrt{1 + (\delta / p_m)^2 + 2(\delta / p_m)\cos\alpha}} \tag{2.44}$$

Hence p_s can be computed by using Eq. (2.44), since p_m is known and δ and α can be measured from the moiré fringe patterns. In practice, the centreline of light fringes is easier to locate than those of dark fringes. From Eq. (2.43) it can be seen that α is 0 or π when β is zero. For many applications, rotation β is very small so that α approaches 0 or π. As a result, Eq.(2.44) can be simplified as

$$p_s = \frac{p_m \delta}{|p_m \pm \delta|} \tag{2.45}$$

It should be noted that Eqs.(2.40) and (2.45) cannot be used simultaneously, even in the case when β is very small because the different approximations made in deriving these two equations. When the deformed specimen pitch p_s is known, the nominal strain ε can be found as

$$\varepsilon = \frac{p_s - p_m}{p_m} \tag{2.46}$$

Sciammarella (1982) and Colin (1994) provided thorough reviews of the Moiré method. In experimental mechanics, the moiré technique is defined as the utilization of the moiré patterns to measure displacements of surfaces. The relationship between the specimen and master grating depends on the particular method utilized. There are three basic methods:

1) *Intrinsic-moiré method* – it provides displacements of the points of a surface with respect to their initial position. In this method, the grating is fixed directly to the surface to be studied. The deformations of the model grating directly provide information concerning the displacements and strains of the studied surface. The intrinsic-moiré method is an extremely powerful technique to investigate a wide variety of problems in solid mechanics, both under static and dynamic conditions. The intrinsic-moiré method is particularly convenient to analyse plasticity problems. The geometrical nature of the moiré patterns, the need of recording strain histories, and the presence of large deformations make moiré the best choice for this kind of problem.

2) *Projection moiré* – it provides the slopes of the surface with respect to the reference state. The moiré-pattern is formed by the projection of the shadow of a grating on a surface with collimated light. The limitation of this method is the shadow cast by the features of the surface. To overcome this, two-point light sources or two gratings projection are used. However, the contrast of the fringes is poor (additive moiré) and this is an inconvenience. It is used not only in the area of experimental mechanics, such as the aeronautical industry, but also in the area of medicine.

3) *Reflection moiré* – it provides the slopes of the surface with respect to the reference state. In theories of plates and shells, the second derivatives of the deflections are the quantities of interest; the slope of the surface and the derivative of the slope provide the required information. High sensitivity could be brought about when deflection is of the order of a few

microns. The reflective-moiré method has been very much utilized in the area of civil-engineering structures.

The techniques of moiré-pattern recording can be divided into two basic groups: incoherent-light and coherent-light techniques. For incoherent light technique, a reference grating is put in front of the surface of study. The moiré pattern is formed in the back focal plane of the camera. This technique can be applied with very modest expenses, as it does not need high-quality optics. However, there are three major limitations:

1) Low sensitivity
2) The master line grating must be rotated in order to separate the patterns corresponding to the two directions of reference
3) The gap effect between the model surface and the master grating has to be minimized

Coherent techniques use optical filtering to obtain a diffraction pattern, which provides information (diffraction order) of the displacement of deformed grid.

The grid method of strain analysis is one of the oldest techniques known in experimental strain analysis (Parks, 1982), (Dally, 1991) and (Sevenhuijsen, 1993). There are various types of grids in used on the surface of a specimen, some of them are shown in Fig.2.8.

The grid method requires placement of a grid on the surface of the specimen and or sometimes on an interior plane of a specimen, measuring the distance between discrete points on the grid both before and after loading, and analysis of these measurements. By studying the spacing between the lines, or by studying their movement, the displacements and hence strains developed could be quantified.

The array usually has a repetitive pattern, with lines or dots occurring at some regular frequency. Often the array is rectangular, with dots or lines repeated in two perpendicular directions. Polar grids of radial and circumferential lines are also common and have special usefulness in axisymmetric problems (Danckert and Wanheim, 1979). Occasionally, irregular scratches are used. However, the more commonly used grid has a regular frequency which is specified to some extent by the problem. There are two common methods for the measurement of the distortions of the grid lines.

1) As the strains remain after load removal, a micrometer microscope could be used to measure the spacing of the grid lines directly on the specimen both before and after the loading.

2) Two sets of pictures of the specimens taken, at zero load and at maximum load, will furnish a permanent record of the distortion of the grid for later analysis. Measurements on the spacing of the grid lines are made on these two sets of pictures instead of the specimens.

The grid method has been a standard engineering tool of measuring large strains for many years. There are several characteristics of the grid method which complement the experimental techniques and make it particularly attractive for use in deformation measurements. Grid method in the simplest form can be used to give a gross or fine determination of strain, depending on the size and the number of patterns used. Fig.2.9 illustrated a two dimensional measurement of strain, which requires at least three markers (A, B, C) on the plane of the body. The lengths between these markers are initially normal to each other, which are denoted by l_x and l_y. The corresponding final lengths, l_x' and l_y', for markers A', B' and C' are

separated by angle θ_{xy}.

Practical use of the grid method requires determination of the relative positions of the designed marker, before and after deformation. Once the relative position determined, the normal strain are found by,

$$\varepsilon_{xx} = \frac{l_{x'} - l_x}{l_x} \tag{2.47}$$

$$\varepsilon_{xx} = \frac{l_{y'} - l_y}{l_y} \tag{2.48}$$

and the shear strain is defined by,

$$\gamma_{xy} = \frac{\pi}{2} - \theta_{xy} \tag{2.49}$$

The strain values can be easily determined using these equations, after calculation of the relative position of the markers.

When using the grid method, different methods of marking grids could be used on specimens and printing, etching, scribing, embossing are common for metal. Photographic printing is probably the most common method. The grid method has been described by Brewster as a mean of measuring plastic strains in formed metals (Parks, 1982). He referred to the method as "photogrid" because of the photographic method he had earlier developed to print a 100 line per inch (lpi) grid on metal specimens. Other investigators have suggested a number of variations such as itemized several solutions used to print photogrids (including a nonsoluble solution for use under water), inking technique and using a diazole compound.

Metal etching techniques were described by Holister and Luxmoore (1968) in a paper on moiré. As indicated by Holister, etching is a photographic process. Many of the products used to etch metal can also be used to print grid, without etching.

Today many commercial products are available for etching. Some etching systems even include a dye to enhance the printed image.

Scribing is a common approach to apply grids to metal and plastic models. Box presented a technique to machine scribe grid lines (Parks, 1982). Any competent machine shop can suggest numerous hand and machine scribing methods. Random scratches with emery can be considered as a type of scribing. Usually an area is rubbed with emery in two directions to provide intersection points. Random scratches are often used in conjunction with the replica technique, although unnecessarily. Even the irregularities of the surface itself may be used as a grid. Analysis of random scratches, or the surface itself, usually requires some sort of superposition for measurements.

Early applications of grid method were limited by three major difficulties: it was difficult to apply a well-defined grid onto specimen; the analysis was performed manually by eye and the accuracy and precision of the results were poor; and the manual analysis of the deformed grid could be time consuming. However, with the recent advancements in photographic and computer technology, various approaches have been used to perform this analysis by computer, including spot centroid (Sirkis, 1990) and crossed-grid tracking (Andersen and Helsch, 1988). Others have used the Fourier transform of the grid pattern obtained either optically or by computer (Smith and Burger, 1986 and Bremand and Lagarde, 1988) to obtain local measurements of grid spacing.

Rae et al. (1999) applied the grid method to measure the dynamic large-strain deformation maps. With a high-speed camera, images of impacts at velocities over 500 m/s were captured. An automatic analysis of the dynamic deformation of grid

lined, onto a specimen's surface, permits whole-field measurement of both in-plane displacement components. The Fourier transform method and phase unwrapping, were used to calculate planes of phase coordinates deformed. The strains were found to be about 25%, 28% and 14% in the samples of aluminium, composite and Pyrex respectively.

A new automated approach to the grid method has been developed using digital image processing techniques (Gonzalez and Woods, 1992 and Sevenhuijsen, 1993). In this method, a photoelectronic camera, digitising board and a computer-based image-processing system are used to capture a digital image of the grid. This digital image is then analysed using grey-level threshold techniques and centroid algorithms (Fail and Taylor, 1990) to determine the positions of the centroids of the grid and subsequently the grid deformation and strain. Goldrein et al. (1995) described a new method of analysing images of deforming samples prepared with a grid. They developed an automated approach to digitise images of a sample prepared with a grid, and analysed it by Fourier transform method. After processing data, displacement and strain maps over whole surface of the sample were made. The displacement accuracy is of the order of one-hundredth of the grating pitch, though varies according to the degree of over sampling of the grid pattern and the size of window used in frequency domain. Strains up to 30% could be measured.

Goldrein et al. (1995) and Rae et al. used the automated grid method in their research, but there are some disadvantages: the method requires expensive state-of-the-art equipment; photo electronic camera technology currently limits the grid size analysable to approximately 200mm^2; and accuracy can be poor (typically

around 500 micro strain).

Circular grid is one of the grid pattern commonly used in strain analysis especially in the sheet metal forming such as producing car body panel. The circular grid is turned into ellipse during the forming process. The actual engineering strain can be calculated by measuring the length of the long and short axes of the ellipse. Researcher Buchar (1996) applied circular grid to investigate the problem in car body panel production. In his research, the strain distribution and strain history in the severe deformed area of car body were obtained through the circular grid analysis. The finding helps to reduce not only the scrap in the press shop but also the risk of faulty designs. Other than Buchar (1996), Dong and Lin (2000) also made use of circular grid as the experimental validation for numerical simulation of forming car body panel. From the experimental results, Dong and Lin found that the maximum principal strains ε_1 and ε_2 were 32% and –24.65% respectively.

2.3 Finite Element Method (FEM)

Finite Element Method is a numerical technique, which gives approximate solutions to differential equations that model problems arising in physics and engineering. This method came into existence since the mid 1950s. Early work on numerical solution of boundary value problems can be traced to the use of finite difference schemes. Southwell discussed the use of such methods in his book published in 1946. The beginnings of the finite element method actually stem from these early numerical methods and the frustration associated with attempting to use finite difference methods on more difficult, geometrically irregular problems

(Rouche, 1972). The actual coining of the term "finite element" appeared in a paper by Clough (1960).

2.3.1 Concept of FEM

In the finite element method, the actual continuum or body of matter like solid, liquid or gas is represented as an assemblage of subdivisions called finite elements. These elements are interconnected at specified joints called nodes or nodal points. The nodes usually lie on the element boundaries where adjacent elements are connected. Since the actual variation of the field variable, such as displacement, stress, temperature, pressure or velocity, inside the body is not known, the variation of the field variable inside a finite element is assumed to be approximated by a simple function. These approximating functions are known as interpolation models, which are defined in terms of the values of the filed variables at the nodes. When field equations such as equilibrium equations for the whole body are defined, the new unknowns will be the nodal values of the field variable. By solving the field equations, the nodal values of the field variable are obtained. Once these are known, the approximating functions define the field variable throughout the assemblage of elements.

The solution of a general continuum problem by the finite element method always follows an orderly step-by-step procedure, as follows:

Step (1): Discretization of the structure

The first step in the finite element method is to divide the structure or solution region into subdivisions or elements. Hence the structure is to be modelled with suitable finite elements. The number, type, size and arrangement of the elements are

to be decided.

Step (2): Selection of a proper interpolation or displacement model

Since the displacement solution of a complex structure under any specified load conditions cannot be predicted exactly, it is appropriate to assume that a suitable solution within an element can approximate the unknown solution. The assumed solution must be simple from a computational point of view, but it should also satisfy desired convergence requirements. In general, the solution or the interpolation model is taken in the form of a polynomial.

Step (3): Derivation of element stiffness matrices and load vectors

From the assumed displacement model, the stiffness matrix $[K^{(e)}]$ and the load vector $\overline{F}^{(e)}$, of element "*e*" are to be derived by using either equilibrium conditions or a suitable variational principle.

Step (4): Assemblage of element equations to obtain the overall equilibrium equations

Since the structure is composed of several finite elements, the individual element stiffness matrices and load vectors are to be assembled in a suitable manner and the overall equilibrium equations have to be formulated as

$$[K]\{U\}=\{F\} \tag{2.50}$$

where {} denotes a vector, and [] denoted a matrix. [K] is called assembled stiffness matrix, {U} is the vector of nodal displacements and {F} is the vector of nodal forces for the complete structure.

Step (5): Solution for the unknown nodal displacements

The overall equilibrium equations have to be modified to account for the boundary conditions of the problem. After the incorporation of the boundary

conditions, the equilibrium equations at the element level can be expressed as

$$[k]_e \{u\}_e = \{f\}_e \tag{2.51}$$

For linear problems, the $\{u\}_e$ can be solved very easily. But for nonlinear problems, the solution has to be obtained in a sequence of steps, each step involving the modification of the stiffness $[k]_e$ and /or the load $\{f\}_e$.

Step (6): Computation of element strains and stresses

From the known nodal displacements $\{u\}_e$, the element strains and stresses can be computed by using the necessary equations of solid or structural mechanics.

Researchers in the field started to apply the finite element method (FEM) to model the blanking process in 1980's. Many simulating blanking processes using FEM have been published in the past two decades. Popat, et al. used the elastic-plastic finite element method to analyse the blanking operation (Brokken et al., 1998). With this model, the optimum punch-die clearance and the optimum punch penetration for given values of the parameters could be determined by postulating a crack initiation criterion. They also found that deformation is most severe at the punch and die corners and concluded that the strains are facilitated the initiation of cracks. A recent investigation carried out by Brokken et al. (1998) and co-workers studied the blanking process using a combined technique (Arbitrary Lagrangian Eulerian method and remeshing technique) in which, simulations of two-dimensional transient shearing was performed to simulate the deformation pattern. The blanking forces vs. punch penetration curves for the different clearances were obtained and the site of fracture initiation was predicted. In addition, the geometrical properties like burr size, length of sheared and fractured zone as well as the roll over shape were simulated successfully. Similar work has

been reported in other literatures (Taupin, et al. 1996 and Frauchiger, 1997). The plastic deformation, the shear zone and the material fracture could be predicted. Therefore, the shape of the part such as the roll over, shear zone, rupture zone and burr could be determined. The influences of process variables such as punch-die clearance, material properties and punch and die wear were studied. Furthermore, the optimum punch-die clearance and the effects of cutting tool wear on the part quality were discussed.

The studies of Rotter et al. evaluated stress distributions using the FEM (Frauchiger, 1997), (Johnson et al., 1968) and (Gunaskera and Hobbs, 1979), obtained the stress distributions for no more than 1/30 of the whole material thickness being blanked. They tried to increase the punch-die clearance deliberately; but the results can only be used for reference due to lack of normality and precision even in conventional blanking. In addition, the stress distribution caused by vee-ring indention was also evaluated and the resultant hydrostatic stress acting on the shearing zone was found. Subsequently, the effect of vee-ring indenter on improving the material's plasticity could be verified. However, the relationship between effect of vee-ring indention and punch-die clearance was not investigated simultaneously and demonstrated in their stress distribution diagrams.

Sun, et al. (1990) did further analysis on the fine-blanking process with the rigid-plastic finite element method in 1990, applying the penalty function method to handle incompressible condition. They reported that the reason for the crack initiation in the fine-blanking process could be explained to some extent. However, there was an obvious weakness in their analysis. The whole fine-blanking process was divided into only 10 deformation steps, which is against the working principle

and repeated addition principle based on the small deformation steps of the rigid-plastic finite element method.

Hambli has performed a comparative study between the experimental data and the results obtained by the simulations using two different models: the Lemaitre damage model (LMD) taking into account the influence of triaxiality; and a damage model accumulation allowing the exponential dependence on triaxiality, which is mainly based on the Rice and Tracey ductile fracture criterion. He showed that the LMD model is unable to predict the fracture propagation path in a realistic way. Only the exponential evolution gives good results.

The study of Koni et al. (1984) and his co-workers evaluated the distribution of stresses for no more than 1/30 of the material thickness being penetrated, using the elasto-plastic FEM. In their computation, a large clearance was employed deliberately to avoid the tendency of divergence during the balance iteration. In order to solve the problem, reduced integration and constant volume strain within the elements were employed. However, a relatively large clearance was adopted in the simulation and the effect of heat generation was not taken into account. Moreover, the edge radius of the tools was not modelled in the finite element mesh. Lee and co-workers have identified the effective stress and strain distribution within the clearance zone by using the rigid–plastic finite-element model (Thomson and Gunasekera, 1980). Even though the element remeshing technique was applied, the maximum punch penetration could only reach less than 20% of the material thickness and the edge radius of the tools was still neglected. Moreover, since the R-P model could not be used to handle the unloading problem, a numerical error may be inevitable in the unloading or elastic loading region. Based on the updated

Lagrange formulation, Chen, et al adopted the large deformation elastic-plastic FEM in the simulation of fine-blanking (Lee et al., 1997). In order to avoid the accumulation of errors due to rigid body rotations, an incrementally objective mid-interval integration algorithm has been used. Because the deformation in fine-blanking is very severe and localized, it is still difficult to carry the numerical calculation through to the end.

Furthermore, in order to achieve a more intensive understanding of the forming mechanism of fine-blanking process, Chen et al. (2002) developed a numerical simulation by using a mixed FEM. The simulation was carried out by mixing the displacement and pressure in the finite element analysis. This model can simulate punch penetration up to nearly 100% of the material thickness. Despite the fact that large punch penetration was simulated, questions remained about whether the simulation results agree with the actual deformation mechanism of fine-blanking process.

2.3.2 Remeshing Technique

In most of the numerical or FEM analysis of metal forming process, one of the intrinsic difficulties in large deformation analysis is the initial finite element mesh becomes progressively distorted. The constantly changing configuration of the deforming body leads to computational errors and convergence problems. The accuracy of the solution decreases with increasing distortion, until eventually a converged solution is no longer possible. This causes discrepancies in the process modelling, for instance, where part of the finite element grid moves outside of the boundary conditions. Another potential problem is computational errors caused by

the severe distortion of the finite element mesh where intensive shear takes place.

To overcome these problems in FEM, Gelten et al. (1981; 1982) introduced the remeshing technique into finite element program to solve the metal forming problems, by periodically redefining the mesh system on the distorted mesh. Their proposed remeshing technique consists of four steps:

1) Definition of the new mesh;
2) Definition of a continuous field for all nodal and element variables using a triangulated mesh;
3) Determination of the value of all variables in the nodes of the new mesh;
4) Interpolation of the element variables to the integration points of the new elements.

Later on, similar studies were carried out by other researchers Badawy et al. (1983), Oh et al. (1984), Al-sened et al. (1984) and Im and Kobayashi (1985, 1986). In those studies, remeshing procedure can be mainly described in two steps: generating a new mesh and transferring all field variables from the distorted mesh to the new one. Since remeshing is one of the major procedures the FEM of metal forming, Zhu et al. (1997) have developed a fully automatic remeshing procedure for modelling a whole forming process in FEM. Their proposed remeshing procedure can be spitted into the following steps:

1) Geometric definition of the workpiece and tools;
2) Generation of initial mesh;
3) Finite element simulation;
4) Remeshing decision;
5) Geometric definition of the deformed workpiece deduced from the previous

simulation results;

6) Generation of new adaptive mesh;
7) Transformation of history deformation from the previous mesh to the new one; and
8) Automatic restart of the interrupted simulation.

In metal forming simulation, steps 3-8 are repeating until the prescribed process has been reached.

In the remeshing process, re-generation of new mesh is a step included in remeshing. The shape and size of the re-generated mesh have a direct effect on the accuracy of the solution. In general, the finer the mesh, the more accurate the solution will be. However, finer mesh has a higher computational cost. In order to balance between computational cost and accuracy, different mesh structures are proposed (Lackner and Mang 2002). A mesh can be classified into structured or unstructured ones. A structured mesh is one which is designed according to the topology of the structure. The structure is divided into subdomains. For each subdomain, the user may specify a different mode of mesh design. The different modes result in the following different discretizations:

1) Unstructured discretization: These parts of mesh will be changed in the course of adaptive mesh refinement:
2) Structured discretizations: These parts of the mesh will not be affected by remeshing;
3) Variable-structured discretizations: This mode of mesh design is required for preserving compatibility between the structured and the unstructured parts of the FE mesh during meshing refinement.

The new mesh after remeshing can be adaptive in the way that both structured and unstructured meshes are combined. Depending on the spatial distribution of the estimated error of the FE results, remeshing may result in an increase or decrease of the elemental size.

The more fundamental requirement of remeshing comes form the elemental geometric distortions because of large deformation. Remeshing decision is one of the important steps in remeshing procedure. Remeshing is needed when the original meshing is badly deformed such that computation cannot be performed. The assessment of "how bad" the mesh is distorted forms the Remeshing Decision Criteria. Some common decision indicators are summarized below (PavanaChand and KrishnaKumar, 1998):

1) Error estimates based on the error norms on stresses or strains computed in the finite-element mesh
2) The use of distortion criteria characterizing the geometric distortion of the elements. For example, % of distorted elements of the whole mesh
3) The analysis of the conditioning of the tangent stiffness matrix of the elements

In the commercial FE simulation package, the remeshing criteria are often based on mesh distortion criterion and interface criterion (Zhu et al., 1997). Combining the mesh distortion criterion, interface criterion and numerical convergence options, the remeshing starts when following cases are encountered:

1) Percentage of the too-distorted element reaches a defined critical value, which may be defined by the user;
2) Penetration distance is larger than a given allowable value;

3) Loading step size is reduced to a given minimum value due to bad convergence; and

4) Total number of loading step within one simulation stage reached a specified maximum number.

The frequency of remeshing always depends on the above four specified values. However, if the remeshing is done too frequently, it does not only increase in cost, but also becomes inaccurate because of the accumulation of errors in the remapping state.

Once the state parameters are available at the old mesh nodes, these have to be transferred to the nodal points of the new mesh. There are two basic approaches to carry out this operation. The first approach, suggested by Yang et al. (1989), Jayadeva and Narasimhan (1995) and Lee and Bathe (1994), involves the direct transfer of the old mesh nodal values to the new mesh Gauss point, using the shape functions of the bounding old mesh element. The second approach used by Cheng and Kikuchi (1986), first transferred the nodal values of the old mesh to the new using the shape functions of the bounding old mesh element with new nodes, then use the new mesh element shape functions to calculate the Gauss point values of the state parameters. In both approaches, one needs to determine whether a given point lies within an element in the old mesh or new and the natural coordinates of this point within an element, given its global coordinates. The common mapping procedure includes three steps (Zhu et al., 1997):

1) Transfer all variables of the old mesh from the Gauss points to the element nodes using a shape function

2) Interpolate the state variables from the nodal points of the old mesh to

nodal points of the new mesh

3) Determine the Gauss integration point data by the same shape function

For the mapping of information at the solid boundary, these steps were proposed (Habraken and Cescotto, 1990):

1) Smooth the normal and tangent pressures in the old mesh
2) Define new contact elements that are located on the corrected boundaries of the new solid elements
3) Compute the contact pressures at the new integration points on the boundary by linear interpolation of correspondent variables of the two closest integration points of the old mesh

Various mapping models and functions were proposed in literature for transferring data from the old mesh to the new mesh in FEM. The most common one uses the Lagrangian method. However, depending on the application, other methods are also used.

2.4 Problems Identification

According to most of the literature, it was found that fine-blanking was being studied by FEM recently. Most of these studies were performed for the predictive purpose. To verify the FEM results, some of the researchers used large strain analysis as a validation method. However, their experimental verifications were limited because these researches could not study the fine-blanking operation with punch penetration more than 28% of material thickness. The FE simulations of the whole fine-blanking operation, evaluated by the tentative experiments of punch penetration less than 28% of material thickness, were not sufficient. Therefore,

there is a need for the study of deformation in fine-blanking with more than 28% of its whole thickness through experiments.

Besides, severe deformation of fine-blanking is a major difficulty for strain analysis because strains cannot be measured through changes of grid patterns as punch penetration exceeding 28% of material thickness. So experimental study of the whole fine-blanking operation by strain analysis is restricted. On the other hand, the same problem is also found in FE simulation. But this problem is solved by remeshing in the FE simulation. Due to this characteristic, remeshing technique is able to resolve the experimental problem of measuring strains in the fine-blanking operation.

When using the remeshing technique practically, two problems should have to be overcome. They are the alignment of specimens and crack formation during the subsequent blanking operation. When the specimens are placed into the fine-blanking die, it should be aligned to the previous position or else the vee-ring could not be indented at the same location and fine-blanking operation could not performed at the same region of the specimens. Even though the specimens could be aligned at the same position of the previous operation, crack would be formed in the subsequent operation due to the low formability after the first fine-blanking. Therefore, post-process treatment will be essential to increase the formability of the fine-blanked specimens for further operations.

In order to study the real deformation mechanism of fine-blanking process, an experimental remeshing technique for large strain analysis of fine-blanking is necessary.

CHAPTER 3

DEVELOPMENT OF THE EXPERIMENTAL REMESHING TECHNIQUE

In order to achieve the research objectives, a research methodology was developed. Before applying the developed method to the strain analysis of fine-blanking, a tension test was performed as an evaluation measure to ensure feasibility of the proposed method. In this chapter, details regarding the strategy and the evaluation measure are explained and described.

3.1 Large Strain Analysis Technique

Strain is the quantity used to measure the intensity of a deformation, and the study of deformations is within the scope of strain analysis. Certain techniques for the experimental determination of large strains were discussed in the previous chapter. The grid method is a surface phenomenon and the strain determination is reduced into a two-dimensional problem. Therefore, strain in metal forming process is typically evaluated by measurements of grid deformations on the surface of specimens. In this study, the grid method has been employed for strain measurement. The methodology of strain measurement and calculation of strains are presented in this section.

3.1.1 Strain Measurement and Calculation

A non-homogeneous deformation in two dimensions is illustrated in Fig.3.1, which shows the initial and deformed state of a square grid. The initial square grid ABCD is deformed into a quadrilateral OPQR. The original dimensions of the square ABCD are $l \times l$, and the coordinates of the nodal point in OPQR are

defined as $O(x_o, y_o)$, $P(x_p, y_p)$, $Q(x_q, y_q)$ and $R(x_r, y_r)$, respectively. By definition, the large strain is defined as Eq.3.1, mentioned in Ragab. (1999)

$$\varepsilon = \frac{1}{2}\left[\left(\frac{dl}{dl_0}\right)^2 - 1\right] \tag{3.1}$$

where dl is the deformed length of a line segment dl_0.

Using the Eq.3.1, the engineering strains ε_{xx} and ε_{yy} and the shear strain γ_{xy} can be obtained as follows:

$$\varepsilon_{xx} = \frac{1}{2}\left[\left(\frac{OP}{AB}\right)^2 - 1\right] \tag{3.2}$$

$$\varepsilon_{yy} = \frac{1}{2}\left[\left(\frac{OR}{AC}\right)^2 - 1\right] \tag{3.3}$$

$$\gamma_{xy} = \sin(\theta_1 + \theta_2)(\sqrt{1+2\varepsilon_{xx}})(\sqrt{1+2\varepsilon_{yy}}) \tag{3.4}$$

As $(\theta_1 + \theta_2) = (\frac{\pi}{2} - \phi)$, Eq.3.4 becomes,

$$\gamma_{xy} = \cos\phi(\sqrt{1+2\varepsilon_{xx}})(\sqrt{1+2\varepsilon_{yy}})$$

$$\gamma_{xy} = (\frac{OP^2 + OR^2 - PR^2}{2(OP)(OR)})\{\sqrt{1+2[\frac{1}{2}(\frac{OP^2}{AB^2}-1)]}\}\{\sqrt{1+2[\frac{1}{2}(\frac{OR^2}{AC^2}-1)]}\}$$

$$\gamma_{xy} = (\frac{OP^2 + OR^2 - PR^2}{2(AB)(AC)}) \tag{3.5}$$

The grid method is a two-dimensional measurement and the 'z' axis is not considered in this case. Since these strains are on different axes, Mohr's Circle for plane strain is applied to translate them into principal strains. The translation of principal strains can be obtained by the equations presented in Ragab (1999):

$$\varepsilon_1 = \frac{\varepsilon_{xx} + \varepsilon_{yy}}{2} + \sqrt{(\frac{\varepsilon_{xx} - \varepsilon_{yy}}{2})^2 + (\frac{\gamma_{xy}}{2})^2} \tag{3.6}$$

$$\varepsilon_2 = \frac{\varepsilon_{xx} + \varepsilon_{yy}}{2} - \sqrt{(\frac{\varepsilon_{xx} - \varepsilon_{yy}}{2})^2 + (\frac{\gamma_{xy}}{2})^2} \tag{3.7}$$

where ε_1 and ε_2 are the maximum and minimum principal strains. In the axisymmetrical deformation, the meridian plane remains plane, by symmetry, hence it is used to measure the deformation in such a plane. A square is deformed into a quadrilateral owing to the circumferential strain from radial displacement. The circumferential strain was defined as ε_3 by Hsü in 1966.

$$\varepsilon_3 = \ln(\frac{x_o}{x_a}) \tag{3.8}$$

It is meaningful to calculate the accumulated strain during the deformation process when the strains are large, as in the case of the metal forming process. Since effective strain is used for measuring the overall plastic deformation, it should be should be determined by taking into account the incremental changes in the configuration of the body during the deformation. The equation developed by Backofen (1972) to calculate the effective strain of the deformed quadrilateral is as follows:

$$\begin{aligned} \bar{\varepsilon} &= \frac{\sqrt{2}}{3}\sqrt{(\varepsilon_1 - \varepsilon_2)^2 + (\varepsilon_2 - \varepsilon_3)^2 + (\varepsilon_3 - \varepsilon_1)^2} \\ &= \frac{1}{3}\sqrt{2[(\varepsilon_{xx} - \varepsilon_3)^2 + (\varepsilon_{yy} - \varepsilon_3)^2 + (\varepsilon_{xx} - \varepsilon_{yy})^2] + 3(\gamma_{xy})^2} \end{aligned} \tag{3.9}$$

The coordinates of nodal points O, P, Q and R could be found by measuring the deformed grids directly through experiments. Hence, the values of the effective strain could be computed by substituting the measured values into the equations.

3.1.2 Linear Interpolation Technique

In an FEM simulation, mapping the field variables from the old mesh to the

new is an important procedure. Generally, it is subdivided into two steps: (a) searching for elements within the old mesh, where nodes of the new one are located; and (b) transferring field variables from the old mesh to the new one. To perform the same procedure in this experimental study, the linear interpolation technique was applied.

In order to transfer the field variables from the old mesh to the new one, identification must be carried out for every nodal point in the new mesh. Fig.3.2 shows a square before deformation, and P_0 is a point located inside the square. The coordinates of P_0 can be defined in terms of M_0 and N_0. When the square grid has undergone deformation into a quadrilateral as shown in Fig.3.3, point P_0 is moved to P. The locations identification of points M and N can be achieved by:

$$\vec{OM} = r\ \vec{OP}_2 + (1-r)\ \vec{OP}_1$$

$$\vec{ON} = r\ \vec{OP}_3 + (1-r)\ \vec{OP}_4$$

After locating the positions of points M and N, the location of point P can also be defined in terms of points M and N. As a result, the location of point P can be found by knowing the locations of P_1, P_2, P_3 and P_4.

$$\begin{aligned}\vec{OP} &= s\ \vec{ON} + (1-s)\ \vec{OM} \\ &= s\,[r\ \vec{OP}_3 + (1-r)\ \vec{OP}_4] + (1-s)\,[r\ \vec{OP}_2 + (1-r)\ \vec{OP}_1] \\ &= (1-r)(1-s)\ \vec{OP}_1 + r(1-s)\ \vec{OP}_2 + rs\ \vec{OP}_3 + (1-r)s\ \vec{OP}_4\end{aligned}$$

Therefore, the co-ordinates of point P (x, y) can be formulated as follows:

$$\begin{aligned}x &= s(rx_3 + (1-r)x_4) + (1-s)(rx_2 + (1-r)x_1) \\ &= (1-s)(1-r)x_1 + r(1-s)x_2 + srx_3 + s(1-r)x_4\end{aligned} \tag{3.16}$$

$$y = s(ry_3 + (1-r)y_4) + (1-s)(ry_2 + (1-r)y_1)$$
$$= (1-s)(1-r)y_1 + r(1-s)y_2 + sry_3 + s(1-r)y_4 \quad (3.17)$$

In this experimental study, besides performing experiments, bulk volume of experimental data also has to be handled for strain analysis. According to the obtained data, the straining behaviour is calculated and analysed routinely with a computing programme. The programme is therefore developed to handle tedious calculations of effective strains at all nodal points and to transfer distorted nodal coordinates after deformation. Fig.3.4 shows the flow chart of the programme.

3.2 Validation of the Remeshing Technique

In this section, the main investigation is directed towards the development and evaluation of an experimental remeshing technique capable of performing large strain analysis on fine-blanking process. A simple tension test was carried out for the validation of the experimental remeshing technique. In this tension test, measurements of nodal points of a grid marked on the deformed specimens were analysed to determine effective strain distributions. Specimens without remeshing were undergone tension tests until they were nearly ruptured. Furthermore, tension tests on specimens with remeshing were also carried out. Effective strain distributions both with and without remeshing were measured and compared to evaluate the effectiveness of the proposed remeshing method. In addition to the experimental tension test, an FE simulation was used to predict the behaviour of strain during the tension test. The effectiveness of remeshing technique could be confirmed by the findings acquired from experiments and the

FE simulation.

3.2.1 Tension Test without Remeshing

In the tension test, a rectangular specimen of SPCC steel sheet with thickness 1.0mm was designed, as shown in Fig.3.5. Additional information about the mechanical properties and the chemical composition of SPCC are shown in Table 3.1. The tension test was performed by an MTS tension test machine (Model No.: 812.21), which is shown in Fig.3.6. The crosshead of the maximum loading of 5kN was installed on the tension test machine. A mask of square grids (0.4mm x 0.4mm) was installed on the specimen, as shown in Fig.3.7. The upper edge of the mask was located 10mm from the reference point. Since the necking region would be elongated during the tension test, the reference point was sited outside the necking region and was easily identifiable. The reference point is very important for the strain measurement, because all of the coordinates of the nodal points are obtained with reference to this point.

Before clamping the specimen onto the testing machine, the parameters, such as width, thickness and crosshead speed of 0.5mm/min, were input into the computer to control the testing process. Then, the specimens were gripped on the crosshead, and the extensometer was attached to the specimen and properly aligned. After that, the specimen underwent a tension test as loads were applied to the crosshead till the breaking point was reached. Five of the specimens without a mesh of grid pattern had undergone a trial test to ensure that the equipment was set-up properly. The results of the experiments are shown in Table 3.2. It was found that the total elongation of the specimens at the breaking

point was 3.7mm and the strain at breaking point was 26.12%. The stress-strain curve obtained from the trial test is illustrated in Fig.3.8. The strain obtained in the trial test was nearly identical to the strain of the overall deformation process, which was different from the strain within the necking region.

A specimen with a mesh of grid pattern was held by the crosshead to undergo the tension test for the evaluation of the proposed remeshing technique. The deformation of the grid pattern was captured by a digital camera in every elongation of 0.5mm, until the specimen reached the point of rupture. Fig.3.9 shows the ruptured specimen. In order to find out the strain of the ruptured specimen, it is necessary to measure the deformation of grids. However, it is difficult to identify the grids at the point of rupture as shown in Fig.3.9. As a result, it is hard to measure the large strain at the point of rupture.

The sequence of grid deformation before reaching the point of rupture during the tension test is shown in Fig.3.10. Fig.3.10(d) shows a clear picture of a deformed grid with an elongation of 3.5mm which is close to the point of rupture. The coordinates of the deformed grid were also measured for the strain analysis. Effective strain values were calculated by inputting the measured coordinates into the strain calculation programme. The contour of the effective strain distributions was plotted according to the coordinate system defined in Fig.3.11. In Fig.3.11, point 'A' is the centre of the necking region, the coordinates of which are (0,11). The x-axis is the cross-section of the width of the necking region, which displays the effective strain distributions along the x-axis. The y-axis is the centre line of the specimen. A contour map of the tension test with 3.5mm elongation is shown in Fig.3.12. Clearly, the highest effective strain value was

1.8, located at point 'A'. The effective strain values were localized at the centre of the necking region, and the maximum effective strain value was 1.8 when the elongation was 3.5mm. The width of the necking region was 6.2mm prior to the tension test, and became 4.4mm afterwards. It was found that the width of the necking region had narrowed by 1.8mm during the test.

3.2.2 Tension test with Remeshing

Before applying the experimental remeshing technique to the strain analysis of fine-blanking, a validation of this technique was carried out through tension testing. In the previous section, a tension test without remeshing showed that the specimen was ruptured at an elongation of 3.7mm, and that it was hard to identify the deformed grids. To keep the balance between getting measurable deformed grid patterns and the greatest possible stretch, the maximum elongation was limited to 3.5mm. Fig.3.10 shows that noticeable deformations of the grid patterns were found when the elongation was greater than 2.0mm. Remeshing was carried out when the specimen was stretched to 2.0mm. A specimen with etched grid pattern was mounted on the tension test machine with attachment of an extensometer. Then, load was applied to the crosshead and the specimen was stretched by 2.0mm. The stretched specimen was ungripped and the image of the deformed grid pattern was captured by digital camera, as shown in Fig.3.13. Then the deformed nodal coordinates were measured and recorded for the calculation of effective strain.

After that, a new grid pattern was printed on another surface of the specimen and the specimen was then gripped into the crosshead of the tension test machine.

Fig.3.14 shows the specimen with a new remeshed grid before being gripped onto the tension machine. A tension test was performed with the remeshed specimen, stretched by 1.5mm until the total elongation became 3.5mm. The deformation of the remeshed grid pattern after a second tension test is shown in Fig.3.15. The deformed coordinates of the remeshed specimen were obtained and the effective strain values were calculated by inputting data into the strain program. Subsequent to the strain calculation, the effective strain distributions an elongation of 2.0mm and those of the remeshed tension test are plotted and illustrated in Fig.3.16. As shown in Fig.3.16, the value of the largest effective strain is 0.9 located at the highest point of the profile, which is the centre of the necking region. Fig.3.17 shows the effective strain distributions of the second tension test after remeshing.

In order to validate the remeshing technique, it is necessary to find out the total deformation for the two tension tests, and interpolation of the two sets of deformed coordinates should be made by linear interpolation technique. Using the transformed nodal coordinates of the total deformation, effective strain values obtained by remeshing technique could be calculated. The contour of the effective strain distributions is plotted and shown in Fig.3.18, in which the maximum effective strain value is 1.9 at the centre of the necking region. The maximum effective strain value obtained through the experimental remeshing is 0.1 more than that obtained by the tension test without remeshing. By comparison, the effective strain values (without experimental remeshing) obtained by direct tension test are slightly lower than those with experimental remeshing.

3.2.3 FE Simulation of Tension Test

The use of FE simulation becomes more and more popular for the investigation and the prediction of certain engineering and manufacturing process. One of the greatest benefits of using finite element analysis is to enable the evaluation of different concepts at the very early stage in the design process. Therefore, in this research, an FE simulation of the tension test was performed by using the commercially available finite element software, ABAQUS. ABAQUS/Standard PC version 5.8 was therefore employed.

In this research FE simulation was used as a numerical method to predict the effective strain of tension tests. The effective strain values predicted from the FE simulation were used to compare with the experimental ones. The material properties of SPCC were employed in the FE analysis. Table 3.1 and Fig.3.8 show the material properties of SPCC. The simulation of the tension test was performed using the element mesh of a quarter of the symmetrical specimen, which is shown in Fig.3.19. Since this experiment is a displacement case, the tension test has been simulated by changing the displacement along the 'Y' direction, as shown in Fig.3.20, which illustrates the boundary condition of the FE simulation model. With reference to Fig 3.20, the boundaries of x and y were assumed to be fixed and the tension force was applied to the y-axis in terms of nodal force. Therefore, the displacement is the nodal displacement. The predicted effective strain distributions with elongations of 2.0mm and 3.5mm are illustrated in Fig.3.21. The maximum effective strain values with an elongation of 2.0mm and 3.5mm are 0.749 and 1.56 respectively, locating at the bottom left hand corner. As in Fig.3.11, it was found that the effective strain values

decreased as increased in distance from the centre 'A'. The predicted maximum effective strain value was localised at centre 'A'.

A summary of the experimental (with and without remeshing) and predicted effective strain values are shown in Fig.3.22. It was found that the experimental effective strain values are slightly greater than those from the FE simulation. The results of the FE simulation are ideal for prediction. Although, in some real conditions, such as gripping forces and shape change, are not included in the FE simulation, the disparity between the FE simulation and the experimental results is reasonable and acceptable. Even though there is a disparity, the FE simulation can be used to predict the trend of effective strain distributions in tension tests. Fig.3.22 shows that there are three effective strain curves obtained by FE simulation and experiments (both with remshing and without remeshing). In fact, the result obtained without remeshing should show a more realistic strain distribution in the tension test. The average deviations between the results of FE and experiment with remeshing with respect to the results of experiment without remeshing indicated nearly the same discrepancies, 15% and 12% respectively. It seems that both results of FE and experiment with remeshing show almost the same agreement with that of experiment without remeshing. Furthermore, the measurement of strain in fine-blanking without remeshing is only limited to about 30% of punch penetration as shown in Fig.5.33 (Chan 1998) because the deformed grids cannot be measured when the punch penetration is greater than 30% of material thickness. In order to perform a complete strain analysis of fine-blanking, the proposed remeshing technique is believed to be useful and contributive.

CHAPTER 4

STRAIN ANALYSIS OF FINE-BLANKING

In this chapter, in order to implement the developed technique for the strain analysis of fine-blanking, details regarding material selection, equipment set-up and experimental procedures are explained and described in this chapter.

4.1 Materials Selection

Material selection is a very important step in the experimental study, because using inappropriate material could lead to failure. It is known that the hardness and strength of a material depends upon its carbon content and the alloying elements. In the blanking process, the harder the material, the more difficult the process. A hard material is not suitable for fine-blanking, and the best result can be achieved by using material with good flow and cold forming characteristics. High quality of fine-blanked parts with good finish on sheared edges can best be made from alloy steels with a tensile strength ranging from 30 to 60 kgf/mm^2 and carbon content up to 0.35%. Non-alloy steels with maximum carbon content up to 0.7% and non-ferrous alloys such as brass and aluminium also provide a good quality finishing on sheared edges. Overall, in the fine-blanking industry, over 90% of all fine-blanked parts are made out of mild or alloy steels, about 8% aluminium alloy, 2% copper alloy and other materials (Birzer, 1997). However, other than the carbon content and tensile strength of a material, the internal structure also has a great influence on the quality of fine-blanked parts. A laminated pearlitic structure of steel, consisting of alternated layers of hard cementite and soft ferrite, could increase the difficulty in fine-blanking. For this

reason, a low carbon steel sheet JIS G3101 of Japanese Standard has been selected and used in this research. Table 5.1 shows the properties and the chemical composition (%) of the selected materials.

4.2 Equipment Design and Set Up

To carry out the experimental study, a large amount of equipment had to be employed in the laboratory for specimen preparation and processing, measurement and testing. In this study, equipment such as the fine-blanking system, a micro-hardness tester, hand grinders, a universal polisher, a sawing machine and a tool-maker's microscope have been employed. Most of this testing and measuring equipment are readily available in the laboratory, except the fine-blanking system, which will be described further. Other than the fine-blanking system, details of specimen design and preparation, experimental set-up and procedures are described in the following paragraphs.

4.2.1 Conventional Fine-blanking Press

The fine-blanking process is only workable through the effect of three forces: the blanking force, the vee-ring force and the counterforce. Thus, a special triple-action press is used for the fine-blanking operation. Fine-blanking presses are required to comply with high precision standards such as slide gibes; high frame rigidity and the parallelism of die clamping surfaces. Fig.4.1 shows the layout of a mechanical fine-blanking press. The central supports in the upper and lower die clamping plates ensure optimum die support and the introduction of forces to the die. Controlled and infinitely variable DC motor drives the press

via the flywheel, a disk clutch and a worm gear pair on two synchronously running crankshafts with different eccentricity. The crankshafts drive a double knuckle-joint system generating sequential movements of the slide required for fine blanking. The vee-ring force and counterforce are applied by hydraulic systems.

4.2.2 Tailor-made Fine-blanking Simulation System

In the metal forming production industry, fine-blanking technology can produce complex finishing on parts, achieving high quality by using highly priced fine-blanking press. It effectively reduces production costs by minimizing machining operations to one or two. But the installation of a fine-blanking press involves very huge capital investment. Installation of one fine-blanking press costs several million Hong Kong dollars, and only large enterprises can afford that. Up to date, only one fine-banking press has been installed in Hong Kong, and it was imported from Switzerland in 1989 (Chan 1998). Most metal manufacturers, medium and small firms (SME) especially in Hong Kong, cannot afford to install a fine-blanking press, even though they realise the outstanding and remarkable advantages of using the fine-blanking technology over the conventional one.

This expensive equipment is usually installed for carrying out mass production. In order to promote fine-blanking technology in Hong Kong industry with a lower initial cost, the Hong Kong Polytechnic University has developed a tailor-made fine-blanking simulation system. This fine-blanking simulation system can carry out the operation by mounting a specially designed hydraulic activation system onto a conventional mechanical press, as shown in

Fig.4.2. When the hydraulic activation system is connected to the additional hydraulic supply system, it can provide a vee-ring force and a counter force for the conventional mechanical press. The hydraulic supply system and the hydraulic activation system were made in accordance with the recommendation of Tu (1990). When a specially constructed die set was built and installed into the hydraulic activation system, the conventional mechanical press was able to carry out fine-blanking operation in the same way as a fine-blanking Press. By applying this tailor-made simulation system, a fine-blanking force could be provided by the conventional mechanical press indirectly, whilst the vee-ring force and the counter force by the hydraulic activation system through the additional hydraulic supply system. Hence, experiments which simulated the fine-blanking process could be performed at a comparatively lower set-up cost.

4.2.3 Fine-blanking Die

To perform the fine-blanking process, a special die set known as the fine-blanking die must be designed and built. Fabrications of this high precision fine-blanking die employed advanced fabrication processes, such as electrical-discharge machining (EDM), wire-cutting, optical profile grinding and CNC machining to achieve a close punch and die clearance close to zero as well as high rigidity. Fig.4.3 shows the structure and Fig.4.4 the configurations of this specially designed fine-blanking die.

The major difference between a fine-blanking die and a conventional die is the vee-ring indenter projecting from the guide plate. For a material up to 4.5mm in thickness, it is common to have only one vee-ring on the guide plate.

But when the material thickness is greater than 4.6mm, more than one vee-ring is used, mounted on the guide plate and the die plate (Mukhoty, 1997). The thickness of worked material for this study was 5mm, so two vee-rings were mounted on the guide plate as well as a die plate as shown in Fig.4.4. The vee-ring was pressed into the sheet before blanking to stop material flow from occurring as punch penetrated. The penetration of vee-ring affects not only the sheared edge quality, but also the size of die-roll as well as the dimensional quality. By using an empirical formula in the practical handbook (Dally, 1991), the vee-ring indenter was designed to be located at a distance of 3.0mm from the shearing edge and at a height of 0.7mm, projecting 45 degree upwards from the guide plate and die plate. An ejector (counter punch) with diameter of 30mm and a small die clearance of 0.025mm are two major components of a fine-blanking die. The wider the die clearance, the higher the risk of cracking on the burr side.

4.3 Mesh Selection and Specimen Design

Apart from setting up the equipment as described in the previous paragraphs, design and preparation of the specimens were equally important to obtain accurate results in this study.

4.3.1 Mesh Selection

The first simple idea that comes to mind, for the detection of surface strains in a model, is to install a grid on its surface and to observe the distortion of the grid during loading. This is called the grid method of strain analysis, which is one of the oldest techniques known to most of the experimental stress analyst. Under conditions of large deformation such as plastic deformation related to stress-analysis problems, the grid method is one of the more effective methods known (Dally, 1991). It involves placement of a grid on the surface of the specimen. Next, the grid is carefully photographed before and after deformation, showing distortion of the grid. For rectangular grids, if the initial and final spacing of the grid as well as the change in length of one of the diagonals of the elementary squares are measured, the principle strain and principle direction can be calculated easily by formulae.

Applying the grid method to prepare meshes, there are several kinds of mesh films, such as the square line film and the chessboard pattern one shown in Fig.4.5. Fig.4.5 (a) shows a mesh of grid pattern formed by straight lines. If this mesh is applied and etched on the meridian plane of the specimens, the deformation in fine blanking shearing region will be so severe that the etched line either blurred or broken. As a result, the coordinates of the nodal points in the distorted meshes could not be identified. Fig.4.5(b) shows a mesh of grid pattern formed by "white" and "black" squares, like a chessboard. In large deformation, severe deformation of square grids of chessboard could be seen more easily than that formed by lines. Therefore, the chessboard pattern film shown in Fig.4.5(b) was selected for etching mesh on the specimens due to easy identification of nodal

points in the distorted meshes after deformation.

Since small clearance is one of the distinctive characteristics in fine-blanking, specimens with a thickness of 5.0 mm have been prepared in this researched. The size of square grids in the mesh applied must therefore be as small as possible to reflect the deformation in detail. However, the smaller the grid size, the harder the grid to etch and the more difficult to obtain the deformed grid. Therefore, 0.4mm x 0.4 mm squares were chosen for the mesh grids, as adopted by Chan (1998) and Zheng (2000) (see Fig.4.6).

4.3.2 Specimen Design

Specimens were designed and cut into rectangular blocks of 25mm x 50mm x 5mm as shown in Fig.4.7(a). The meridian plane of each specimen was finished off with a grinding machine, so that the grid pattern would be etched onto the meridian plane for strain analysis. Each specimen was carefully pre-checked to ensure correct dimensions and surface flatness for experiments. Then two symmetrical specimens with meshes were combined to form a large rectangular block of 50mm x 50mm x 5mm, which is shown in Fig.4.7(b). The combined specimens were placed into a special fixture and mounted onto the fine-blanking die. The special fixture was used to centre the specimens during the fine-blanking operation. The drawing of the special fixture is shown in Fig.4.8. Specimens were not prepared as one single piece (50mm x 50mm x 5mm), shown in Fig.4.7(c), because meshes need to be etched on the meridian plane for strain measurement.

4.4 Experimental Procedures

Upon completion of mesh selection and specimen design, the next step to achieve the research objectives was to perform the experiment. The details of meshing steps and the fine-blanking operation will now be introduced in the following sections.

4.4.1 Generation of Mesh by Photochemical Etching Technique

In order to visualize the deformation during processing, mesh must be photo-etched on the specimen before deformation occurs and the distorted mesh will be measured for further analysis. Since this is an axisymmetric problem, mesh formed by square grid pattern should be photo-etched on one of the meridian (sectional) plane. The detailed steps of the mesh etching procedure are as follows:

1. Pre-treatment of specimens: The specimens of 25mm x 50mm x 5mm were cleaned thoroughly by removing oil and dust, then they were dried immediately.
2. Lamination: The pre-treated specimen was laminated with a thin photo-resistant and photo-sensitive material. In this research, KTFR glue and thinner were used to prepare the photo-resistant film, in a ratio of 1:3. The glue was spread evenly on the meridian plane with a brush. A thin layer of photo-resistant material was laminated on the specimen, then it was put into the furnace of about 100°C for 5 minutes to dry the exposition glue.
3. Exposure and development: A mask, which was a chessboard pattern film

with square grids of 0.4mm x 0.4 mm, was placed on top of the laminated specimen. The specimen with mask was exposed under an ultraviolet lamp for about 5 minutes. After exposure, the mask was taken away and the specimen was ready for development. During the development, the unexposed negative working photo-resist (the black square of the mask) was washed away by immersing the laminated portion into the KTFR developer for 2 minutes. The exposed photo-resistant material remained on the specimen, forming a protective layer for etching.

4. Etching and stripping: The specimens were wrapped with tape to prevent corrosion during etching, except the meridian plane, then they were soaked and shaken in a ferric chloride solution for 40-60 seconds. The protective layer and the tape were then stripped away to reveal a final mesh on the meridian plane of the specimens, as shown in Fig.4.9.

4.4.2 Fine-blanking Operations

Having carried out the photochemical etching steps, the specimen with etched mesh on the meridian plane was prepared and ready for the fine-blanking process. Two specimens with etched meshes were held together by a special fixture, and mounted onto the guide plate of a fine-blanking die, which was installed into the tailor-made fine-blanking simulation system. The fixture was used for centring the specimens during fine-blanking process. The fine-blanking operation was then carried out. In order to study the phenomena and effects of the fine-blanking process with different punch penetrations, 20%, 40%, 60% and 80% of material thickness for punch depth were selected and performed accordingly.

After the fine-blanking operation, the specimens were taken from fine-blanking tools cleaned with detergent and the deformed mesh capture for further analysis through the use of Digital Scanning Electron Microscope. Fig.4.10 displays an example of a distorted mesh on the meridian plane of the specimen after fine-blanking operation, with a punch penetration of 20% material thickness.

4.4.3 Post-treatment after Fine-blanking

Cracks might form at the die corner in the subsequent fine-blanking operation due to low formability. It was necessary to increase the formability of the fine-blanked specimens before remeshing. Recrystallization annealing was employed as the post-treatment process to prepare the specimens for further fine-blanking operations.

The annealing process was carried out at temperatures capable of producing a notable reduction in yield strength, without change in the material structure. When heating is done too quickly, there is a danger of forming stress peaks and the specimens may crack. As a result, plastic deformability of the specimen is insufficient. For the same reason, care should be taken to ensure slow rates of cooling.

The annealing operational temperature for recrystallization and stress relief is between 550 – 700 °C and 500 - 600°C shown in Fig.4.11, as directed by Lange (1985). To increase formability and relieve stress for the semi fine-blanked specimens, an annealing operation temperature of 600°C was selected, as shown in Fig.4.11. The fine-blanked specimen was put into the furnace at 600°C for two hours. To ensure a slow rate of cooling specimens were left untouched for

more than 20 hours to cool in room temperature.

4.4.4 Remeshing

When specimens with meshes underwent fine-blanking operation, the nodes or coordinates of distorted meshes were nearly all captured by the Digital Scanning Electron Microscope, as shown in Fig.4.10. When old distorted meshes were removed, new meshes would be prepared for subsequent fine-blanking operation. This step was repeated till the end of the experiment. The procedure for etching new mesh on the meridian plane of the processed specimens is called "Experimental Remeshing". After each mesh was deformed, the meridian plane with deformed mesh was polished clean by either a hand grinder or a universal polisher. When the old meshes (deformed meshes) were removed, new meshes would be etched on the meridian planes by repeating the steps of lamination, exposure and development, etching and stripping. The detailed description could be found in section, 4.4.1. As the new square grid patterns were etched on the meridian plane, the remeshed specimens were ready for fine-blanking with different punch penetrations. To make sure every remesh was etched as close as the old mesh, the top left corner of the meridian plane was regarded as the reference datum.

In order to illustrate all of the experimental procedures, a flow chart summarizing the practical implementation is displayed in Fig.4.12.

4.4.5 Alignment Work

After the remeshing, the prepared specimens were ready for subsequent fine-blanking operation. However, the specimens should be aligned to their previous position, otherwise, the vee-ring could not be pressed exactly at the same location and the fine-blanking operation could not be performed at for the same area of the specimens. To align the specimens properly, the best way was to place the specimens onto a guide plate on the same position as previously located. Vee-ring is an important characteristic of fine-blanking. However, when specimens inside the guide plate were fine-blanked, the vee-ring indentations squeezed the material around itself. As a result, the semi-blanked specimen was slightly larger in area than the original, preventing the specimens from moving backwards onto the guide plate again. To fit the specimens back onto the guide plate for further processing grinding is necessary to remove the extra material flash. Specimens were grounded with a stepwise increment in depth (0.02mm) until they accurately fitted in the guide plate. Then, the ground specimens were ready to be remeshed with new grid patterns.

4.4.6 Strain Measurement

After performing the experiments, the deformed meshes were captured by using a digital camera. This is an important step in measuring the nodal coordinates of the distorted squares. To illustrate the details of strain measurement, Fig.4.13 shows the meridian plane (cross-section) of a specimen before and after fine-blanking. This is an axisymmetric case and the fine-blanked specimen is a circular disk of Ø30mm diameter. The y-axis was

defined as the centre line of the fine-blanked specimen. Before the fine-blanking operation, the location of the centre was defined and it is shown in Fig.4.13. After the fine-blanking operation, the centre was moved downward along the y-axis. It was difficult to locate the exact position of a centre for measuring the deformed nodal coordinates. The origin was therefore not a good choice as a datum or reference point because the datum should be easily located and close to the shearing region. During the fine-blanking operation, only the corners of the specimen were easy to locate. Consequently, the corner at the die side was chosen to be the datum with coordinates (15,0). Despite the change in punch penetration, the datum remains in the same position and it is close to the shearing region. When the datum is defined, the nodal coordinates can be measured with reference to it.

Fig.4.14 shows a picture of a fine-blanked specimen. Software named "WinDig" was used to measure the coordinates for this picture. "WinDig" is a useful complimentary software to generate numerical values from a picture. When file of a picture in bitmap format was opened by "WinDig" and the datum of the picture located, the coordinates could be measured by moving the cursor to the nodal points. As shown in Fig.4.14, it was found that the deformation was highly localized within the shear region. Seven columns of the nodal points within the shear region were therefore selected for strain measurement. The measured coordinates of the selected nodal points were used for calculation of strains.

CHAPTER 5

RESULTS AND DISCUSSION

All the experiments for the strain analysis of fine-blanking were set up and carried out according to the methodology and practical implementation as described in detail in the previous chapters. The results and the findings of the experiments will be presented and discussed in this chapter.

5.1 Experimental Results

5.1.1 Corroboration of Experimental Set Up

For the purpose of this research, a tailor-made fine-blanking simulation system was set up. To ensure proper operation, the fine-blanking simulation system experiments were carried out to corroborate effectiveness of the equipment. Specimens were prepared and fine-blanked by the fine-blanking simulation system. Fig.5.1 presents the experimental sequence whereby a pair of specimens were put into the fine-blanking die and fine-blanked with a punch penetration of 100% of the material thickness. After the operation, the quality of the sheared edge of fine-blanked specimens was checked. The quality was measured in terms of die-roll height, burr height and blanked edge finishing. The measurement of the die-roll height (d) and burr height (h) are presented in Fig.5.2. A summary of the findings of the experiments is shown in Table5.1.

In the fine-blanking process, there is a certain deformation on the die side of each fine-blanked part. This deformation is called a "die-roll", an inherent feature, which is less severe on fine-blanked parts than that of conventionally blanked ones. From the results shown in Table5.1, the die-roll height is 0.35mm. The die-roll height in this experiment did not exceed 10% of the material thickness, which agrees with the

recommendation of Tu (1990). The die-roll height result demonstrates that fine-blanking operation can be performed properly by using fine-blanking simulation system, and this is in agreement with earlier research works.

All blanked parts have burrs located on the opposite side of the die-roll, no matter whether they are produced through conventional blanking or fine-blanking. The generally acceptable burr height of fine-blanked parts is within the range of 0.01-0.08mm and it can be achieved with fine-blanking tool in the best condition; when the burr height is over 0.3mm, regrinding of fine-blanking tool is required (Zhou, 1993). It was found that the burr height of the fine-blanked specimens was 0.021mm, which was within the acceptable range. This showed that the tool is in its good condition. This confirmed the effectiveness of this fine-blanking simulation system.

One of the important advantages of fine-blanking is the excellent shear of blanked edges over the full thickness of the material after production. The percentage of shear on the blanked edge is a common and effective assessment for quality edge finishing of the fine-blanked parts. This percentage is given by the relationship of K value shown in Fig.5.3, which has been defined by Caloska and Lazarev (1996), as

$$K=S_g/S$$

where S_g – thickness of purely shear of blanking edge and

S - thickness of the material

When the K value of the blanked part equals to one, 100% shear of blanked edge is obtained and this represents the highest quality of blanked edge of fine-blanked parts. High values of K therefore indicate a good blanked edge finishing, whilst low values show otherwise, as shown in Fig.5.4, the K value equals to one, which shows a

blanked edge with 100% pure shearing when the specimens were fine-blanked by this fine-blanking simulation system. This illustrates that the best blanked edge finishing of fine-blanked parts could be achieved by using this simulation system.

Apart from the blanked edge quality, strain hardening is also an indicator of fine-blanked parts. A small portion was cut from the circular fine-blanked specimen and mounted in a resin block to test its hardness, measured in terms of Vickers hardness. The Micro Hardness Tester made by Shimadzu Seisakusho Limited was used, applying a load of 200gf, and pressing the diamond indenter into the meridian plane of specimens. Micro-hardness test was carried out with the predetermined testing pattern as shown in Fig.5.5. After diamond indenting, the hardness of the specimens was measured by the image processing systems with the Leica Qwin Standard V2.1 (software). The hardness results are shown in Table 2 and Fig.5.6. It is known that there is a close relationship between the hardening behaviour and the degree of deformation of a deformed material. The blanked edge of a component produced by fine-blanking is hardened because of the severe shearing deformation in the blanking region, where straining effect in terms of the hardness ratio increased by 2.1 times of the original. As seen in Fig.5.6, the hardness ratio decreased to 1.0 with progressive increase in the distance from the blanked edge. Lee et al (1995) obtained similar findings. This shows that the strain hardening effect is extremely localized in shearing region. The phenomenon of metal straining is caused by cold working (Birzer, 1997), resulting in the hardening of the material around the blanked edge after processing. In the fine-blanking process, the hardness around the blanked edge is normally higher than in other areas. This is the work hardening effect of fine-blanking and it can prevent the fine-blanked parts from premature fracture. Consequently, the fine-blanked parts become more durable and this phenomenon

turns later to be a major advantage of fine-blanking. However, it can be eliminated by annealing, i.e. re-crystallization and softening.

5.1.2 Experiments without Remeshing

Specimens with meshes were fine-blanked by different degree of punch penetration, and data of their resultant deformation are shown in Fig.5.7. It clearly shows that the meshes are distorted severely within the shearing regions. But the degree of mesh distortion decreases with a progressive increase in distance from the shearing region. Within the shearing region, mesh distortion increases with an increase in punch penetration. When the punch penetration reaches 20% of the material thickness, the distorted mesh is still recognizable, as shown in Fig.5.7(a). When the punch penetration is increased to 40% of the material thickness, the distorted mesh is still clear but the deformed grid pattern is hardly distinguishable (Fig.5.7(b)). As the punch penetration reaches to 60% or 80% of the material thickness, the distorted mesh is blurred, and the deformed grid pattern fuses together into an indiscernible mass. Strain analysis cannot be performed then, as quantification of deformity becomes impossible with the blurred grid patterns.

In order to observe the metallurgical features of fine-blanking, the fine-blanked specimen was prepared in the laboratory. To minimize unexpected damage and the thermal effect caused by electrical wire cutting, the specimen was sectioned by manual sawing. The sectioned specimen was mounted in the resin block. The exposed surface of each sample in the resin block was polished and lapped to mirror fine. Then the specimen was rinsed with alcohol in order to ensure the cleanliness of the exposed surface. Fig.5.8 shows a well-prepared specimen ready for metallurgical examination. The microstructures of the specimens were examined by

using an optical microscope. Metallographic inspection around the shear zone on the meridian plane of the fine-blanked specimen revealed several salient macroscopic features. When punch penetration was less than 20% of the material thickness, shear localization was not noticeable. With an increase of punch penetration, it was found that the shear localization developed gradually. Fig.5.9 shows the severe shear localization around the narrow shearing region, when the punch penetration was 50% of the material thickness. Fig.5.10 shows an enlargement of the shear region near the die edge when the punch penetration was 50% of the material thickness. It also shows particles that have been elongated due to the severe shearing. Close observation reveals highly elongated and rotated grains extending in the direction of shear. The material is therefore involved in shearing deformation and localized deformation around the clearance zone. The localized deformation can be characterized by a high degree of rotation and elongation of grains within the shear zone.

After performing the experiments without remeshing, the deformation of grids was explained, and the experimental remeshing strategy was defined. Clearly deformed grids could be found at punch penetration of 20% of the material thickness, and severe blur deformed grids at 40% or above. It was therefore appropriate to perform remeshing at various steps of the punch penetration. In other words, remeshing could be performed at each increment of punch penetration by 20% of the material thickness.

5.1.3 Experiments with Remeshing

Before presenting and discussing the experimental results of remeshing, the stages of the experiments are to be described first as follows:

Experimental Stages,

First Stage: Specimens with meshes were fine-blanked for 20% of the material thickness and the distorted meshes were captured for strain measurement.

Second Stage: Specimens obtained from the first stage were remeshed with new grid patterns and fine-blanked for a punch penetration of a further 20% of the material thickness, by which specimens were fine-blanked for punch penetrations of 20% to 40% of the material thickness.

Third Stage: Specimens processed at the second stage were remeshed with new grid patterns and fine-blanked with a punch penetration of another 20% of the material thickness, by which specimens were fine-blanked for punch penetrations of 40% to 60% of the material thickness.

Fourth Stage: This is the final stage of the experiment, in which specimens with 60% punch penetration obtained from the previous stage were remeshed with new grid patterns and then fine-blanked with punch penetrations of 60% to 80% of the material thickness.

In the first stage, specimens with square grid meshes were fine-blanked for a punch penetration of 20% of the material thickness, and the distorted meshes were photographed, one of which is shown in Fig.5.11. The distorted meshes can be clearly seen, and the grid patterns easily measured. Fig.5.11(a) shows the mesh distorted within and around the shearing region, and no deformed grid can be found to the left of the shearing region. Fig.5.11(b) shows an enlarged section of the shearing

region, in which the square grids of the distorted mesh were transformed into quadrilaterals. The strain could then be obtained by measuring the nodal coordinates of the deformed grids. However, the square grids near the vee-ring indented area were also deformed, as shown in Fig.5.11(a). Since the study mainly focuses on the deformation of the shearing region, the effect of the vee-ring is not considered. In order to measure the strain, the distorted mesh was captured and the coordinates of the square grids of the distorted mesh were measured for strain analysis. Thereafter, the semi fine-blanked specimens were prepared for further processing. The distorted meshes were erased and new grid patterns were remeshed onto the meridian plan of the semi fine-blanked specimens.

In the second stage, within the punch penetration of 20%-40% of the material thickness, cracks were seen when the semi fine-blanked specimens obtained in first stage were fine-blanked again for another 20% of punch penetration of the material thickness. Therefore, in the second stage, a post-processing procedure was carried out before remeshing, involving putting the specimens obtained from the first stage into a furnace to relieve stress through annealing. The annealed specimens were cleaned and etched with a new mesh of square grids. Fig.5.12 shows a remeshed semi fine-blanked specimen after punch penetration of 0%-20% of the material thickness. The remeshed specimens were then further fine-blanked with a punch penetration of 20% to 40% of the material thickness. After fine-blanking, the distorted meshes were captured, and one sample is shown in Fig.5.13. From the enlarged picture of the distorted mesh shown in Fig.5.13 (b), it can be seen that the square grids are deformed into quadrilaterals. In Fig.5.13, the deformed grid pattern can be seen clearly and the measurement of strain is made possible.

Semi fine-blanked specimens obtained from the second stage underwent a

post-processing of annealing. Then, new meshes were etched with square grid pattern on meridian plane. Fig.5.14 shows a post-processed specimen with a new mesh of square grids ready for another fine-blanking operation. The remeshed specimens were put into a fixture mounted onto the fine-blanking tool. In the third stage, the remeshed specimens were fine-blanked with punch penetration between 40% to 60% of the material thickness. The fine-blanked specimens were removed from the fixture, and the distorted meshes were captured as shown in Fig.5.15. The deformed squares were found to be quadrilaterals as shown in Fig.5.15(b), in which part of the shearing region is enlarged for easy observation. The strain measurement is practically possible if the deformed grid patterns can be identified. The strains could therefore be measured through a picture of the distorted mesh.

In the fourth stage, the specimens with a punch penetration of 60% of the material thickness were post-processed by annealing. Then, new square grid patterns were remeshed onto the meridian plane of the specimens through photo-chemical etching. A sample of a remeshed specimen is shown in Fig.5.16. The remeshed specimens were mounted onto the fine-blanking tool and further fine-blanked with a punch penetration equalled to 80% of the material thickness. Fig.5.17 shows the distorted mesh obtained from this last fine-blanking operation with 80% punch penetration. In addition, the deformed grids, which are found to be quadrilaterals in the enlarged picture shown in Fig.5.17(b), could be easily recognized.

The experimental remeshing for fine-blanking has been carried out successfully throughout the above-mentioned four stages. The captured images of the distorted meshes at each stage are very important for strain analysis of the fine-blanking process. The sequence of deformation and remeshing processes is summarized in

Fig. 5.18.

5.2 Strain Analysis of Fine-blanking

Using distorted meshes from the experimental remeshing procedures, strain analysis of fine-blanking could be accomplished by measuring strains calculated from the deformed grid patterns. The strains of each remeshing step could be established by measuring the nodal coordinates of the deformed grids of the distorted meshes. Once all nodal coordinates of grids from each experimental stage were known, they were transformed into a delegated coordinate system to find out the overall deformation. With known overall deformation, overall strains for each fine-blanking stage could be worked out. Three successful fine-blanking tests were carried out. The variation of the effective strain for punch penetrations at various percentages of material thickness is averaged to be around 8%. Details for strain analysis of the experimental results are presented in this section.

5.2.1 Strain Measurement of Distorted Meshes

In order to carry out strain analysis for the fine-blanking operation by the approach of experiments, strain measurement is necessary. The distorted meshes obtained from each experimental stage with various percentages of punch penetration were used for strain measurement. Nodal coordinates of the deformed grids were measured first. Fig.5.19 displays a coordinate plane for the measurement of the nodal coordinates. The x-axis represents the radius, in millimetres, of the meridian plane of the specimen, while y-axis represents the height. Since this is an axisymmetric case, strain distributions on the left hand side are the same as those on the right hand side. The right hand side of the specimen was therefore chosen for the strain analysis. As seen

from Figs.5.11 to 5.17, the deformation of grids is highly localized in the shearing region. Seven columns of nodal points covering the shearing region were therefore selected for the strain measurement.

The nodal coordinates of the distorted meshes were measured with the aid of "WinDig", software. Then, the measured nodal coordinates of an individual distorted mesh were plotted (as shown in Fig.5.20) to check whether the nodal coordinates reflected the distorted meshes properly and completely. Fig.5.20(a) shows the distorted mesh plotted by the coordinates and measured at a punch penetration of 20% of the material thickness. The graph would appear to be nearly the same as the picture of the distorted mesh shown in Fig.5.11. Furthermore, when comparing the plotted graphs Fig.5.20(b), Fig.5.20(c), and Fig.5.20(d) with the pictures of the distorted meshes shown in Figs.5.13, 5.15 and 5.17 respectively, it was found that the former were able to represent the distorted meshes at various percentages of punch penetration. Therefore, the measured nodal coordinates of the deformed grids were valid for the strain measurement. The effective strain values were calculated by inputting the nodal coordinates of the deformed grids into the computation programme. Table5.3 shows the calculated effective strain values of punch tip, die corner and the centre of the shearing region during the fine-blanking operation at each stage.

5.2.2 Effective Strains of Each Remeshing Stage

Effective strain values of each individual remeshing stage were calculated by inputting nodal coordinates of the distorted meshes into the computation programme. As shown in Table5.3, the effective strain values at punch tip for the original distorted meshes at punch penetrations of 20%, 40%, 60% and 80% are 1.19, 1.19, 1.13 and 1.16 respectively. The calculated effective strain values at the die corner for punch

penetrations of 0%, 20%, 40%, 60% and 80% are 1.14, 1.08, 1.03 and 1.13 respectively. It was found that the effective strain values at the die corner are very close to but slightly less than that at the punch tip. The effective strain values at the centre of the shearing region in the original distorted meshes for punch penetrations of 0%, 20%, 40%, 60% and 80% are 0.67, 0.63, 0.60 and 0.65 respectively.

For better understanding, the U.S.A. computing software known as "SURFER" was employed to demonstrate the results of strain distributions. Effective strain distributions over the meridian plane of the specimens were obtained by inputting the effective strain values into "SURFER". The 2-Dimensional and 3-Dimensional contour maps of the effective strain distribution of various punch penetrations were obtained from the software. Some outputs of the 2-Dimensional and 3-Dimensional contour maps are shown from Fig.5.21 to Fig.5.24.

Strain distributions, at a punch penetration of 20% of the material thickness, show that the strain is highly localized at the punch tip and the die corner (Fig.5.21), resembling two hills. This means that in the fine-blanking process, severe deformation takes place in the areas of punch tip and die corner, and the peak value of strain is found at the punch tip. This difference can be explained by the fabrication of the fine-blanking tool. In practice, before the tool is mounted onto the fine-blanking press, the edge of the die aperture and the piercing form of the punches must be lightly rounded. The rounded dimension is known as the nose radius, which improves the conditions of the material flow. The size of the nose radius depends on the material quality and thickness. Rotter (1990) has suggested that when blanking parts, the nose radius of the fine-blanking punch could be near zero. However, when piercing holes, the nose radius of the fine-blanking die could be zero. In this research, the nose radius of punch and die are 0.05 and 0.10mm respectively. In addition, the strain distribution

at the centre of the shearing region are relatively smaller than that at the punch tip and die corner, nearly half in value. This phenomenon corresponds with the distorted mesh. In the distorted meshes, the grid deformation at the shearing region is not as vigorous as that at the punch tip and die corner. The small deformation of the grids at the shearing region results in small strain values.

The effective strain values at punch tip and centre of the shearing region were plotted against the percentage of punch penetration, as shown in Fig.5.25. This shows a zigzagged path in which every fall of the effective strain indicates remeshing. During remeshing, the old distorted mesh was replaced by a new mesh. The effective strain returned to zero after a new mesh was etched onto the meridian plane. The effective strain values at the punch tip of 20% of punch penetration, as shown in Fig.5.25, were consistently found to be about 1.1 at each incremental stage. This shows that the deformation is consistent and reliable at each stage. However, it only illustrates an independent remeshing status and is insufficient for understanding the overall deformation process of fine-blanking, unless the total effective strains at 80% of punch penetration are found.

5.2.3 Effective Strains of Total Punch Penetration

To have a better understanding of fine-blanking, the effective strains of the total punch penetration of the whole deformation should be found. However, it is impossible to measure the effective strain values at 100% punch penetration through an experimental approach, because no deformed grid pattern remains in the shearing region. By using the experimental remeshing technique at each remeshing stage, distorted meshes of 0%, 20%, 40%, 60% and 80% punch penetration were obtained. Therefore, it is possible to find the effective strains of the total punch penetration of

80% by means of transforming nodal coordinates of the individual distorted meshes into an overall distorted mesh. Deformed nodal coordinates of each remeshing stage could be transferred to the designed coordinates system by using the linear interpolation technique, as shown in Fig.5.26. Since the deformation in fine-blanking is highly localized within the shearing region, the designed coordinate system to be used mainly covers the major deformation area of configuration in Fig.4.13. After the transformation by linear interpolation technique, the overall distorted meshes at punch penetrations of 0%-40%, 0%-60% and 0%-80% could be generated. After the nodal coordinates of the distorted meshes were transferred into the designed coordinates system, the data obtained is plotted and shown in Fig.5.27. Fig.5.27 shows that the total deformation of the distorted meshes in fine-blanking could be represented by the designed coordinates system. Each graph in Fig.5.27 confirms the feasibility of the specimen being directly fine-blanked with a maximum total punch penetration of 80% of the material thickness. For instance, Fig.5.27(d) shows the specimen fine-blanked directly from 0% to 80% punch penetration of the material thickness. Thus, nodal coordinates of the distorted meshes for the total punch penetrations of 40%, 60% and 80% could be deduced by using experimental remeshing technique. Since the graphs of the distorted meshes with various percentages of punch penetration displayed in Fig.5.27 are similar to those in Fig.5.20(a), but with a larger deformation of grids, the effective strain values for the total punch penetrations of over 20% could be found by using the transferred nodal coordinates. Hence, by inputting transferred nodal coordinates into the strain calculation program, effective strain values of the overall distorted meshes could be calculated. With the application of "SURFER", the effective strain values were used for generating 2-Dimensional and 3-Dimensional contour maps. The effective strain

distributions on meridian plane of the specimens are shown from Fig.5.28 to Fig.5.30, associating with punch penetrations of 0%-40%, 0%-60% and 0%-80% of the material thickness.

The contour maps shown in Figs.5.28 to 5.30 display strain distributions of the experimental remeshing results. These effective strain distributions were all obtained from the experiments performed under the same specified conditions, but with varied depths of punch penetrations. It can be seen clearly that the effective strains become more intensively localized at the punch tip and the die corner with an increase of punch penetration. The closer the position to shearing region, the greater the value of the associated effective strain. Moreover, the deeper the punch penetration, the greater the value of effective strains accumulated within the shearing region. Figs.5.28, 5.29 and 5.30, display an "U" shaped effective strain distributions. These phenomena indicate that the strain is highly localized at the punch tip and the die corner. Higher effective strain values are found at the blanking line of the sheared region. This points to a very severe deformation at the centre line of the sheared region. Therefore, the strain is concentrated and localized in the sheared region, which may initiate cracks and cause failure of material plasticity.

The effective strain values with the total punch penetrations of 0%, 20%, 40%, 60% and 80% at the punch tip, the die corner and the shearing region were summarized and reported in Table5.4. At the punch tip, the effective strain values are 1.19, 2.90, 6.77 and 11.78 respectively. At the die corner, they were 1.14, 2.83, 5.68 and 11.28 respectively. It was found that the total effective strains at punch tip and the die corner were very close to each other with a difference less than 4.5%. The effective strain values at the centre of shearing regions were found to be 0.70, 1.30, 2.89 and 6.24 with the total punch penetrations of 20%, 40%, 60% and 80% of the material

thickness respectively. Whilst, the effective strain values at the centre of the shearing region were nearly half of that of the punch tip. The same phenomenon was found in every individual remeshing stage. The total effective strain values at the punch tip, the die corner and the centre of the shearing region were plotted and shown in Fig.5.31. In Fig.5.31, the three curves show that the increase of the total punch penetration leads to an increase in the total effective strain. It was found that the three curves seemed to behave exponentially. Since the effective strains were highly localized at the punch tip and the die corner, the values of the punch tip were chosen as the representatives for discussion and comparison. At the punch tip, the effective strain values increased from 1.19 to 11.78 as the percentage of the total punch penetrations increased from 20% to 80% of the material thickness. Effective strain at the punch tip was increased by nearly ten times, increasing the possibility of cracks formation and fractures when the total punch penetration exceeded 80% of material thickness. At the centre of the shearing region, the effective strain value increased from 0.70 to 6.24 as the total punch penetration increased from 20% to 80%. The increase of the effective strain value at the centre of the shearing region was nearly nine times. This result hence shows that though the total punch penetration increased four times from 20% to 80% of the material thickness, the ratio of increase of effective strain values to the percentage of punch penetration are unequal. On the other hand, the effective strain at the punch tip of 80% of punch penetration was 11.78, a much higher value than the summation of the effective strains 4.67 (=1.19 + 1.19 + 1.13 + 1.16) of an individual distorted mesh. Hence, the total effective strain value could not be found by simply adding values of each individual remeshing stage.

5.2.4 Comparison Between FEM and Experimental Findings

The numerical simulation of material forming processes is a discipline which has been growing in popularity and undergoing continuous development over the past twenty years. The finite element method is one of the numerical simulations which gives an approximate solution to differential equations that model problems arising in the metal forming industry. Chen (2002) developed the FEM process model of fine-blanking by using a thermo-mechanical coupling method. The effective strain distribution of the total punch penetration between 0%-60% of the material thickness, obtained by Chen through FEM, is shown in Fig.5.32. A comparison between Fig.5.32 and Fig.5.29 shows that the effective strains obtained from FEM and the experiment has similar distributions. In both cases, effective strain distributions were highly localized at the punch tip and the die corner with different punch penetrations. The effective strain values at punch tip found by FEM are summarized in Table5.5. At punch tip, they were 3.94, 6.72, 9.65 and 11.50 for the total punch penetrations of 20%, 40%, 60% and 80% of material thickness respectively. The effective strain values derived by FEM were greater than those by experimental remeshing with the total punch penetrations of 20%, 40% and 60%. The difference between effective strain values of FEM and the experimental remeshing were 2.75, 3.82 and 2.88 with the total punch penetrations of 20%, 40% and 60% respectively. But the effective strain value with 80% of the total punch penetration found by the experimental remeshing was slightly higher by 0.28 than that of FEM.

A comparison between the effective strain values, obtained from the experimental remeshing and FEM, is shown in Fig.5.33. Also in Fig.5.33, according to Chan (1998), the values of effective strain at punch tip can only be obtained from the experiment (without remeshing) up to a total punch penetration of 30% of material

thickness. Whilst, experimental remeshing is able to acquire the effective strain value up to 80% of the total punch penetration. Moreover, both curves of effective strains obtained from FEM and the experimental remeshing showed a tendency of increase with the increasing values of the total punch penetration. The effective strain values of FEM increased steadily from 3.94 up to 11.50 as the total punch penetrations increased from 20% to 80%. The values of every increment of the punch penetration were 2.78, 2.93 and 1.85 as shown in Fig.5.34. However, in Fig.5.33, the experimental remeshing showed another type of trend of effective strain distributions, i.e. from 1.19 to 11.78, when the total punch penetrations increased from 20% to 80%. The increments of effective strain, as shown in Fig.5.34, are 1.71, 3.87 and 5.01 with every 20% increase in the total punch penetration. From the experimental remeshing, it was found that the severity of deformation augmented the values of effective strain with the increase of the total punch penetration, especially over 40% of material thickness. Each increment shown in the experimental findings illustrated a trend of increase in their values of effective strain, while the increment shown by the FEM declined slightly as the total punch penetration increased.

On the other hand, the variations between the findings of FEM and the experimental remeshing are shown in Fig.5.33. Findings obtained form the experimental remeshing process usually revealed a more realistic deformation of fine-blanking compared with the FEM, a predictive method. The effective strain values found at the punch tip by FEM with the total punch penetrations of 20%, 40% and 60% seemed to be over-estimated. The experiment for validation of the remeshing technique (as described in Chapter 3) showed that the increase in effective strain was not proportional to the increase of elongation. Therefore, in a real situation, the deformations in the initial stages are gentler than that deformations

predicted by FEM. A perfect FE simulation model should include all the parameters of the fine-blanking process, such as the nose radii of the punch and the die, punch and die clearance, lubrication and operation forces. In practice, the nose radii of the punch and the die are fabricated manually by a grinding stone. As a result, uneven nose radii could found on the punch and the die, which are hard to be simulated by FEM. Small punch and die clearance is one of the major characteristics of fine-blanking. In the manufacturing of a fine-blanking tool, the tolerance of nose radii would be accepted and this is not easy to be simulated. Chen (2002) applied thermo-mechanical coupling to model fine-blanking, where the thermal boundary condition was assumed to be a thin layer of lubricant at the interface, and the constant convection coefficient was taken from experimental results for solving the deep drawing problem. The result showed the limitations of FEM modelling.

Furthermore, there is another reason for the discrepancies between the effective strains obtained by the experimental remeshing technique and that by the corresponding of FE simulation. Fig.5.35 shows the stepwise of the punch penetrations from 20% to 80% of the material thickness, in which, $\bar{\varepsilon}_{FE}$ of shaded region and $\bar{\varepsilon}_{EX}$ of rectangular bounded region are supposed to be the average effective strain values obtained from FEM and the experiment at punch tip respectively. In FE simulation, the effective strains at the punch tip were highly localized within the tiny finite element mesh. However, the grid size (0.4mm x 0.4mm) using in the experiment was much larger than the element size of FEM, whereas the corresponding average effective strains were obtained from that rectangular bounded region. Therefore, the $\bar{\varepsilon}_{FE}$ values were usually greater than that of $\bar{\varepsilon}_{EX}$ as shown in Figs.5.35 (a) and (b). However, as the percentage of the

total punch penetration increased, the strain distributions obtained from the FEM and the experiment should become more and more close because the average effective strain values, $\bar{\varepsilon}_{FE}$ and $\bar{\varepsilon}_{EX}$, approached the same strain distribution, as shown in Fig.5.35 (c). Therefore, $\bar{\varepsilon}_{FE}$ and $\bar{\varepsilon}_{EX}$ values of the total punch penetration of 80% of the material thickness were almost the same. As a result, greater effective strain values of FEM were obtained with the total punch penetration of 20%, 40% and 60% of the material thickness, and whilst, nearly same effective strain values were obtained by FEM and experimental remehing when the total punch penetration reached 80% of the material thickness.

5.3 Difficulties and Limitations

In this research, the fine-blanking process was studied by large strain analysis and with the application of an experimental remeshing technique. Since this was an experimental investigation, there were limitations, difficulties and unexpected problems, such as mesh etching, alignment accuracy and formation of cracks, which needed to be solved and overcome.

5.3.1 Mesh Etching and Remeshing

The grid method was employed for the strain measurement in this research. It was used to apply a mesh with grid pattern onto the meridian plane of specimens before carrying out experiments. There are various methods to apply a mesh to a specimen. These methods can be broadly classified into two groups, temporary and permanent. Ink printing is one of the temporary methods, which marks the mesh onto the specimen with ink. This is probably the most common method because ink could be easily removed and marked on again if the mesh was misprinted. Although

ink printing is easy to use, it is not suitable for this research. When the specimens with ink printed meshes were put together for fine-blanking, the meshes were easily rubbed off. The metal etching technique is more suitable for this research because the mesh can be etched on the specimen permanently. It was however very difficult to control the etching process, and poorly etched meshes may result, if the etching time was either too short or too long. However, the etching time depends on the lamination of thin photo-resistant and material. It was difficult to control the quality of the photo-resistant lamination because this manual work is highly dependent on experience. Fig.5.36 shows a sample specimen with mesh which is useless because some grids were over etched, and some were not etched at all. This was mainly due to poor lamination of the photo-resistant. The mesh on the specimen shown in Fig.5.36 had to be removed and the etching process had to be repeated.

During experimental remeshing, distorted meshes were removed and new ones were etched on, and the process of removal was carried out manually with sand paper. It was hard to erase the permanently distorted mesh by polishing the meridian plane evenly. Some areas, like the edge, would have been polished too much, and the sharp edge became round. As a result, photo-resistant was hard to laminate, and grids were not etched on the over polished area. The lower part of the remeshed specimen shown in Fig.5.37 was one of the failed samples. The idea of experimental remeshing seems to be very simple and easy to handle. However, in practice, it is not easy to etch mesh onto the specimens, and remeshing is even more difficult. Plenty of time, effort and patience are essential for success.

5.3.2 Alignment Work

As discussed in Chapter 4, specimen alignment is very important for this series of fine-blanking operation in the remeshing experiments. This is because an accurate alignment can ensure accurate punch locations from previous fine-blanking positions, and deformation can be induced to localize in the same shearing region each time during the whole remeshing experiment.

Although a guide plate had already been designed to ensure precise specimen location for fine-blanking after remeshing, misalignments still occurred sometimes. The result of misalignment was shown in Fig.5.38. The specimen in Fig.5.38(a) gave a good example of an accurate alignment for a semi fine-blanked specimen of a punch penetration equals to 20%-40% of the material thickness. However, in Fig.5.38(b), a specimen of punch penetration equals to 20%-40% of the material thickness has two vee-ring indentations due to misalignment. Two shearing regions were formed after the subsequent fine-blanking operation, and remeshing was pointless in such a case. Thus, the effective strain values of the 20 - 40% punch penetration would be inaccurate even though they were measured precisely.

The main reason for misalignment was that the pair of specimen was either over-ground or ground in an unbalanced way. As mentioned in Chapter 4, to fix a pair of specimen into the guide plate, re-grinding is necessary after previous fine-blanking and remeshing. However, over-grinding will make a large clearance between the specimen and the guide plate, while unbalanced grinding will cause translocation of the centre of the specimens. As this grinding process was done by hand, the above errors were unavoidable. Luckily, misalignment did not occur frequently in the experimental remeshing process, and all specimens were rejected due to misalignment.

5.3.3 Crack Formation Without Post-treatment

A pair of fine-blanked specimens, with a punch penetration of 20% of the material thickness, was re-meshed using new grid patterns, and then subjected to a further punch penetration of 20% of the material thickness. When the specimens were fine-blanked with the punch penetration of a further 20% of the material thickness (20%-40%), a crack was found in the shearing region at the corner at the die side, as shown in Fig.5.39. An optical micrograph showing the crack after removing the etched grid pattern is displayed in Fig.5.40. The crack about 0.8mm in length was located at the die side within the shearing region. There was an initial separation between the blanked part and the slug starting at the crack. However, 100% shearing is the main characteristic of the fine-blanking process, and that means no crack would be formed during the process. The appearance of a crack indicated that post-process treatment was necessary in the second stage. Since the distorted mesh was broken by the crack, the square grids on the left hand side of the crack remained undeformed. As a result, strain could not be measured and the distorted mesh could not be used for strain analysis.

When the remeshed specimens without post-process treatment undergo secondary fine-blanking with another 20% of punch penetration, cracks will be formed due to locking up of dislocations in the structure during cold working of the material (Dally, 1991). As a result, the internal or the residual stresses were concentrated within the shearing region and thus reduced the formability of the material. The formation of cracks prevents the specimens from being further processed, and experimental remeshing cannot be carried out when ductility is lost and formability reduced. In order to overcome this obstacle, annealing is a necessary post-treatment process before remeshing.

5.3.4 Limitations

A maximum punch penetration of 80% of the material thickness was analysed in this research. It was the upper limit designed by the research. Thickness of the specimens used in this research was 5mm. If a specimen had been fine-blanked with a punch penetration of 90% of the material thickness, the remaining un-blanked thickness would have been 0.5mm, and the total height (overall thickness) would have become 9.5mm. The un-blanked thickness would not be sufficient for strain measurement. The grid size adopted in this research was 0.4mm x 0.4mm. During 90% punch penetration, there would be one deformed grid remaining in the un-blanked thickness. To perform strain analysis with 90% punch penetration for fine-blanking, a smaller grid size, such as 0.2mm x 0.2mm, may be more appropriate.

In this research, strain measurement was carried out by grid method. The grid size is important for strain analysis. The grid in the mesh should not be too large, in spite of it being easier to measure, as it will be unable to reveal details of the deformation. However, small (fine) grid is good for strain analysis, although it is difficult to inscribe and etch onto specimens. The grid size used in this research was 0.4mm x 0.4mm, the same as those used by Chan (1998) and Zheng (2000) in their research on fine-blanking. In order to achieve a better strain analysis with a smaller grid size of 0.2mm x 0.2mm was first adopted in this research. A successful mesh of smaller grid was etched onto meridian plane of the specimen after many trials, as shown in Fig.5.41. The mesh of the smaller grid can be seen clearly. The specimen was then fine-blanked with a punch penetration of 10% of the material thickness. Unfortunately, the deformed grids in the shearing region were blurred and could not be identified. Fig.5.42 shows a fine-blanked specimen of the punch penetration of 10% of the material thickness. It was found that the deformed grids were fused

together due to severe deformation, even with a punch penetration as low as 10% of the material thickness. Hence, a grid size of 0.4mm x 0.4mm was adopted in this research. Since the grid size could not be smaller than 0.4mm x 0.4mm, the maximum strain analysis of fine-blanking was limited to 80% of the punch penetration. This research was successful because strain analysis of fine-blanking up to 80% the punch penetration was achieved.

CHAPTER 6

CONCLUSIONS

This project aims at contributing a better understanding of fine-blanking by means of strain analysis with the application of a new approach of experimental remeshing. The reported work in this thesis is the first attempt to apply experimental remeshing technique to solve practical severe deformation problem.

After performing the experimental work, strain analysis of fine-blanking for a total punch penetration of up to 80% of the material thickness has been successfully carried out. It was found that as the percentage of punch penetration increased, an increasing trend in the effective strain values was displayed. The effective strain values at the punch tip were 1.19, 2.90, 6.77and 11.78 for a total punch penetration of 20%, 40%, 60% and 80% of the material thickness respectively. However, when the punch penetration is increased from 20% to 80% of material thickness, the increasing ratio of the effective strain values does not equal to that of the percentage of punch penetration. The effective strain values have been found to increase exponentially with an increase in total punch penetration. By the application of experimental remeshing technique, the effective strain value at punch tip, maximum for a total punch penetration of up to 80% of the material thickness, was found to be 11.78. Although the effective strain values for a total punch penetration of over 80% of the material thickness could not be measured due to experimental limitations, the effective strain value at punch tip for a total punch penetration of 80% of the material thickness should be over 11.78. Since a 100% shearing edge is a major characteristic of fine-blanked parts, fine-blanking is a crack free metal forming process. Therefore, despite an effective strain value as high as 11.78, no cracks could form in the fine-blanking.

Comparing the predictive effective strains found by Chen (2002) using FEM with those from experimental remeshing, both values have shown a trend to increase as the total punch penetration is increased. But there were two different incremental styles. In FEM approximation, the effective strains increased gradually, while an increase in experimental remeshing was observed like an exponential curve. Prior to this research, predictive FEM models of fine-blanking were evaluated only by experiments of total punch penetrations of less than 28% of the material thickness. In fact, the effective strain values obtained by experimental remeshing reflected the actual deformation mechanism of fine-blanking. This is an important finding for future development of FEM models of fine-blanking.

Measurement of large strain values, using this newly developed remeshing technique, will no longer be hindered or limited by severe deformation of grid patterns often occur in fine-blanking. This experimental approach permits a stepwise strain measurement process and the findings of this research therefore satisfy the proposed objectives. Through this study, a better understanding of fine-blanking process can be achieved in a more practical way. This study demonstrates that a more intensive strain analysis of fine-blanking can be achieved with the aid of this new technique. The success of this research could be extremely useful in future investigation and application of fine-blanking in the design of dies and products beneficial to related industries.

CHAPTER 7

SUGGESTIONS OF FUTURE WORK

Although fine-blanking has been widely applied in the sheet metal forming industry as an advanced sheet metal working process, academic research on this technique has just begun in the last decade. Therefore, more extensive investigation on fine-blanking can be carried out. The following areas are suggested for further investigation:

1. In the fine-blanking industry, over 90% of all fine-blanked parts are made of mild steel, and this is the main reason for the selection of mild steel SS400 for this research. In addition, due to limitation of time, only mild steel was studied in this research. Whilst about 8% of fine-blanked parts are made of aluminium alloy and 2% of copper alloy and other materials. Other materials such as stainless steel and alloys of aluminium and copper should be further studied in other similar research. Since different materials have different properties, it may be interested to know whether other materials will yield the same result.
2. In the distorted mesh obtained from the experiments, deformation of the grid pattern also found in vee-ring regions. Since the main focus of this study was on the deformation of sheared regions, the effect of the vee-ring is not included in detail. The vee-ring is one of the major characteristics of the fine-blanking process. In order to have a more in-depth understanding of the fine-blanking process, a strain analysis of the vee-ring should be performed. It is suggested that an analysis of vee-ring should be included in further studies of fine-blanking.

3. Due to the occurrence of severe deformation in the very narrow sheared region in fine blanking, a mesh with larger grids cannot reveal deformation in detail. Moreover, if the grids in the mesh are too small, they will be seriously blurred and unidentifiable by the severe deformation in the shearing zone. For this reason, the grid size for the mesh adopted in this research was 0.4mm x 0.4mm, which was easy to handle. The use of this grid size was effective in this new approach but other sizes should be tested too. Even though a smaller grid size of 0.2mm x 0.2mm was used in the initial stage of the research, it was found that 0.2mm x 0.2mm was too small to allow analysis of the deformed grids under punch penetration of 10% of material thickness. To increase the accuracy of strain analysis by improving grid size, 0.4mm x 0.4mm grids were etched onto the specimens. In the strain measurement, each side of a grid was divided by its midpoint to form an eight-node quadrilateral, turning a 0.4mm x 0.4mm grid into a 0.2mm x 0.2mm one. However, this is no longer a linear case, but a quadratic problem.

4. The practical application of fine-blanking in the sheet metal forming industry is important and there are demands to promote the use of fine-blanking technology. Reduction in production cost is worth studying. However, a high operational cost, expensive tools required for fine-blanking operation and severe rate of tool wear are the common and significant problems which obstruct the application of fine-blanking. As far as the latter problem is concerned, more theoretical research on the cyclic loading and the interfacial hydraulic-solid coupling effect on the wear and failure of tools in fine-blanking should be conducted in the future. The low set-up

cost of this fine-blanking simulation system has now been corroborated. With the aim of arousing an interest in fine-blanking technology in the sheet metal forming industry of Hong Kong, promotion of this fine-blanking simulation system should be launched as soon as possible.

5. According to the results of experimental remeshing, the effective strains were highly localized at the punch tip and the die corner. However, there was a small difference between the obtained effective strain values and the value at punch tip, which was greater than that at the die corner. The difference could be explained by the small variation of nose radii. During the application of fine-blanking process in mass production, wear of the fine-blanking tool is unavoidable. This damage changes the geometry and the form of a tool, so there is an increase in the nose radii of punch and die. As a result, this reduces the quality of fine-blanked parts. Minimizing wear on a fine-blanking tool is an important issue to lower operational cost and increase productivity in application of the fine-blanking technology. Future research on the relationship between nose radius and product quality is necessary.

6. The success of the application of this experimental remeshing in fine-blanking process is only at its infancy. Therefore, as a consequence in the future, this experimental approach is expected to be applied and valuable to many other metal forming processes, such as forging, drawing, extrusion, etc.

CHAPTER 8

CONTRIBUTION TO KNOWLEDGE

This is one of the attempts to study fine-blanking process with a total punch penetration of up to 80% of the material thickness through an experimental approach. In the area of conventional research on fine-blanking, FEM is the most common approach for simulating deformation mechanism of fine-banking. All the FEM simulation models are evaluated by tentative experiments. Since the deformation of fine-blanking is very large, large strain analysis is an important technique for validation of simulation models. However, all of these reported tentative experiments for validation have only been performed with limited punch penetrations of no more than 28% of the material thickness. It is because strain analysis could not be executed directly for a total punch penetration of more than 28% of the material thickness. As a result, these simulations are only valid for the total punch penetration within 28% of the material thickness, on the assumption that the predictive results of simulations for a total punch penetration more than 28% of the material thickness are true. Without knowing the actual deformation mechanism, it is hard to claim that these simulation results are valid for a total punch penetration of up to 80% of the material thickness. Moreover, experimental studies of fine-blanking for a total punch penetration between 28% and 80% is rarely reported.

With intention of studying the actual deformation mechanism of fine-blanking, a new approach, the experimental remeshing technique, has been proposed and evaluated in this research. Because of large deformation of

fine-blanking, large strain technique cannot directly analyse the fine-blanking operation for large total punch penetrations. Adopting the insight gained from the remeshing technique of FEM, large strain analysis of fine-blanking for large punch penetration is feasible. In this research, experimental remeshing for fine-blanking was carried out successfully. The deformation mechanism of fine-blanking up to 80% of a total punch penetration of the material thickness was revealed. The experimental remeshing technique was used for the first time in this kind of empirical research. This is a pilot application of a new experimental remeshing technique to overcome the difficulties of large deformation problems. Its contribution is important to future experimental and predictive research using simulations.

REFERENCES

Al-sened, A. A. K., Hartley, P., Sturgess, C. E. N. and Rowe, G. W., "Forming Sequences in Axi-symmetric Cold Forging", *Proceedings of 12th North American Manufacturing Research Conference*, Houghton, pp.151-158 (1984)

Andersen K, Helsch R., "Calculation of grating co-ordinates using correlation Filter techniques", Optik, Vol 80, pp.76-9 (1988)

Backofen, Walter A., "Deformation processing", Reading, Mass.: Addison-Wesley, (1972)

Badawy, A., Oh, S. I. and Altan, T., "A Remeshing Technique for the FEM Simulation of Metal Forming Processes", *Proceedings of International Computer Engineer Conference*, ASME, Chicago, IL., pp.143 (1983)

Bell, J.F., "Determination of Dynamic Plastic Strain Through the Use of Diffraction Gratings", *Journal of Applied Physics*, Vol. 27 No.10, pp.1109-1113 (1956)

Birzer, F., "Materials for a New Generation of Parts", *International Feintool Fineblanking Symposium*, May 1984, pp. 13-20 (1984)

Birzer, F., *Forming and Fineblanking: cost-effective manufacture of accurate sheetmetal parts*, Landsberg/Lech: Verlag Moderne Industries, (1997)

Bremand F, Lagarde A., "Bidimensional spectral-analysis of a crossed lines grating - application to the determination of large and small deformations", *Comptes Rendus de l'Acad Sci Ser ii*, Vol. 307 No. 7, pp.683-688 (1988)

Brokken D., Brekelmans W.A.M. and Baaijens F.P.T., "Numerical modelling of the metal blanking process", *Journal of Materials Processing Technology*, Vol.83, Issues 1-3, pp.192-199 (1998)

Buchar Z., "Circle grid analysis applied to the production problems of the car body panel", *Journal of Materials Processing Technology*, Vol.60, pp.205-208 (1996)

Caloska J. and Lazarev J., "Fine Blanking of Steel and Nonferrous Plates", *Advanced manufacturing systems and technology*, Wien ; New York : Springer, pp.761-767 (1996)

Chan, L. C., Process Modelling of Fine-blanking, PhD Thesis, *The Hong Kong Polytechnic University,* Hong Kong, 1998

Chen, Z. H., Process Modeling of Fine-Blanking Using Thermo-Mechanical Coupling Method, PhD Thesis, *The Hong Kong Polytechnic University,* Hong Kong, 2002

Cheng, J. H. and Kikuchi, N., "A Mesh Re-zoning Technique for Finite Element Simulations of Metal Forming Processes", *International Journal of Numerical Mechanical Engineering*, Vol.23, pp.219-228 (1986)

Clough, R. W. "The Finite Element Method in Plane Stress Analysis", *Proceedings of 2nd Conference in Electronic Computations*, ASCE, Pittsburgh, Pa., pp 345-378 (1960)

Colin, A. W, "A historical review of moiré interferometry", *Experimental Mechanics*, Vol. 34, No.1, pp.281-299 (1994)

Dally, J. W., *Experimental stress analysis*, 3rd ed., McGraw-Hill, New York, (1991)

Danckert, J. and Wanheim, T., J., Mechanical Working Technology, Vol.3, No.1, pp.5 (1979)

Dong Hongzhi and Lin Zhongqin, " Investigation of sheet metal forming by numerical simulation and experiment", *Journal of Materials Processing Technology*, Vol. 103, pp.404-410 (2000)

Durelli A. J., Parks V. J. and Feng H., "Experimental methods of large strain analysis", *International Journal of Non-Linear Mechanics*, Vol. 2, Issue 4, pp.387-404 (1967)

Durelli A.J. and Parks V.J., *Moiré Analysis of Strain*, Prentice Hall, Upper Saddle River, N.J., (1970)

Fail R.W. and Taylor C.E., "An application of pattern mapping to plant motion", *Experimental Mechanics,* December 1990, pp.404-410 (1990)

Feorrer, F. Schiess, *Gaschichle desersien Feinschnitt-stanzwerkes Schiess*, Fritz Schiess U. Co. Lichtenseig, (1970)

Frauchiger, P., *Beyond Fine Blanking*, Manufacturing Engineering, August, pp.100-102 (1997)

Garc, C., *Effective Applications of the Fine Blanking Technique, Part II*, Sheet Metal Industries, February 1982, pp.158-161 (1982)

Gelten, C. J. M. and Jong, J. E. De, "A Method to Redefine a Finite Element Mesh and its Application to Metal Forming and Crack Growth Analysis", ed. by IKOSS Gmbh, *Proceedings of the International FEM-Congress at Baden-Baden*, Germany, (1981)

Gelten, C. J. M. and Konter, A. W. A., "Application of Mesh-Rezoning in the Updated Langrangian Method to Metal Forming Analysis", *Numerical Methods in Industrial Forming Processes*, pp.511-521 (1982)

Goldrein HT, Palmer SJP, Huntley JM., "Automated Fine grid technique for measurement of large-strain deformation maps", *Optics and Lasers in Engineering*, Vol.23, pp.305-18 (1995)

Gonzalez R.C. and Woods R.E., *Digital Image Processing*, Addison-Wesley Publishing, London, (1992)

Grimm, W., "Tooling Systems and Types of Tooling Used in Fineblanking Technology", *International Feintool Fineblanking Symposium*, May 1984, pp.3542 (1984)

Gunasekera, J. S., and Hobbs, R. M., "Stable Shear Separation in Fine Blanking", *Proceedings of the Fourth Tewkesbury Symposium*, Melbourne, pp.10.1-10.17 (1979).

Haack, J. and Birzer, F., *Fine-Blanking Practical Handbook*, Feintool AG Lyss, Switzerland, Revised Edition (1984)

Haack, J., "Extending the Limitations of Part Design, Dimensional and Profile Tolerances and Surface Finish", *International Feintool Fineblanking Symposium*, May 1984, pp.21-34 (1984)

Habraken A.M. and Cescotto S., "An automatic remeshing technique for finite element simulation of forming processes", *International Journal of Numerical Mechanical Engineering*, Vol. 30, pp.1503-1525 (1990)

Holister, G. S. and Luxmoore, "A. R.", *Experimental Mechanics*, Vol.8 No.5, 210 (1968)

Hsü, T. C., "A Study of Large Deformations by Matrix Algebra", *Journal of Strain Analysis*, Vol.1 No.4 (1966), p313-320.

Huang S. and Khan A.S., "On the Use of Electrical-resistance Metallic Foil Strain Gauges for Measuring Large Dynamic Plastic Deformation", *Experimental Mechanics*, Vol.31, pp122-125 (1991)

Im, Y. T., Finite Element Modeling of Plastic Deformation of Porous Materials, *PhD Dissertation*, University of California, Berkeley, (1985)

Im, Y. T. and Kobayashi, S., "Analysis of Axisymmetric Forging of Porous Materials by the Finite Element Method", *Advanced Manufacturing Processes*, Marcel Dekker, Vol.1 No. 3&4, pp.473-499 (1986)

Jana, S. and Ong, N.S., "Effect of punch clearance in the high speed blanking of thick metals using our accelerator designed for a mechanical", *Journal of Mechanical Working Technology*, Vol.19, pp.55-72 (1989)

Jayadevan, K. R. and Narasimhan, R., "Finite Element Simulation of wedge Indentation", *Computers & Structures*, Vol. 57, No.5, pp.915-927 (1995)

Johnson, W. and Slater, R.A.C., "Survey of slow and fast blanking of metals at ambient and high temperatures", *Proceedings of the International Conference in Manufacturing Technology, Michigan, CIRP-ASTME*, pp.825-851 (1967)

Johnston, R., Fogg, B. and Chisholm, A. W. J., "An Investigation into the Fine Blanking Process", *Proceedings of the 96th Machine Tool Design and Research Conference*, Birmingham, pp.397-410 (1968)

Karnes C.H. and Ripperger E.A., "Strain Rate Effects in Cold Worked High-purity Aluminum", *Journal of the mechanics and physics of solids*, Vol.14, pp.75-88 (1966)

Khan A.S. and Hsiao C., "On the Use of Electrical-resistance Foil Strain Gauges for Plastic-wave Studies in Solids", *Experimental Mechanics*, Vol.28, pp.254-258 (1988)

Khan, Akhtar S. and Wang, Xinwei, *Strain measurements and stress analysis*,

Upper Saddle River, N.J. : Prentice Hall, (2001)

Koni, W., Rotter, F., and Krapoth, A., "Feinschneiden Dicker Bleche – Experiment and Theories", *Industries – Anzeiger*, Vol.106, pp.24-28 (1984).

Lackner, R. and Mang, H. A., "Mesh generation and mesh refinement procedures for the analysis of concrete shells", *Advances in Engineering Software*, 33, pp. 389–402 (2002)

Lange, Kurt, *Handbook of Metal Forming*, New York: McGraw-Hill, (1985)

Lee N.S., Bathe K.J., "Error indicators and adaptive remeshing in large deformation finite element analysis", *Finite Elements in Analysis and Design*, Vol.16, pp.99–139 (1994)

Lee, T. C. and Chan, L. C., "The Mechanism and Application of Fine Blanking Process", *Asian Industrial Technology Congress '93*, pp.72-76 (1993)

Lee, T. C. and Chan, L. C. and Wu, B. J., "Straining Behaviour in Blanking Process - Fine Blanking Vs Conventional Blanking", *Journal of Materials Processing Technology*, Vol. 48, pp.105-111 (1995)

Lee, T. C. and Chan, L. C. and Zheng, P. F., "Application of the Finite-Element Method in the Fine Blanking Process", *Journal of Materials Processing Technology*, Vol.63, pp.744-749 (1997)

Lee, T. C. and Chan, L. C. and Wu, B. J., "Further Investigation of the Fine Blanking Process Employing Large Deformation Theory", *Journal of Materials Processing Technology*, Vol. 66, pp.258-263 (1997)

Maeda, T. and Nakagawa, T., "Experimental Investigation on Fine Blanking", *Scientific Papers of the Institute of Physical and Chemical Research*, Vol.62 No.2, pp.65-80 (1968)

Mukhoty, A., Birzer, F., Singer, H. and Lange, K., *Cold forming and fineblanking : a handbook on cold processing material properties component design*, Edelstahlwerke Buderus AG, (1997)

Oh, S. I., Tang, J. P. and Badawy, A., "Finite Element Mesh Rezoning and its Applications to Metal Forming Analysis", *Proceeding of 1st International Conference on Technology of Plastics*, Tokyo, pp.1051-1058 (1984)

Parks V.J., "Strain measurement using grids", *Optical Engineering*, Vol.21, No.4, pp.633-639 (1982)

PavanaChand Ch. and KrishnaKumar R., "Remeshing issues in the finite element analysis of metal forming problems", *Journal of Materials Processing Technology*, Vol.75, Issues 1-3, pp. 63-74 (1998)

Rae P.J., Goldrein H.T., Bourne N.K., Proud W.G., Forde L.C. and Liljekvist M., "Measurement of dynamic large-strain deformation maps using an automated fine grid technique", *Optics and Lasers in Engineering*, Vol.31, Issue 2, pp.113-122 (1999)

Ragab, Abdel-Rahman A. F., *Engineering solid mechanics : fundamentals and applications*, Boca Raton, Fla. : CRC Press (1999)

Rotter, F., *Feinschneiden Dicker Bleche*, Tag Der Mündlichen Prüfung: Chinese Version (1990).

Rouche, P. J. *Computational Fluid Mechanics Albuquerque*, N .M.: Hermosa Publishers (1972)

Schuler GmbH, *Metal forming handbook*, Berlin ; New York : Springer-Verlag (1998)

Sciammarella Cesar A., The Moire Method - A Review, Experimental Mechanics, pp 418-433, (1982)

Sevenhuijsen P.J., "The photonical , pure grid method", *Optics and Lasers in Engineering*, Vol.18, pp.173-194 (1993)

Sevenhuijsen PJ, Sirkis JS, Bremand F., "Current trends in obtaining deformation data from grids". *Experimental techniques*, Vol.17 No.3, pp.22-26 (1993)

Sharpe Jr., W.N., "Dynamic Plastic Response of Foil Gauges", *Experimental Mechanics*, Vol.10, pp.408-414 (1974)

Sirkis JS., "System response to automated grid methods". *Optical Engineering*, Vol. 29 No. 12, pp.1485-1493 (1990)

Smith JA, Burger CP, "Spectral analysis of natural grid features for surfaces analysis of compositeplates", *Proceedings of SEM Fall Conference on*

Experimental mechanics, Keystone, pp.173-176 (1986)

Sun L.B., Cheng B.Y. and Zhou Z.M., "Theoretical Analysis on Fine Blanking Deformation Process", *Metal Forming Technology*, Vol.3, pp.15-21. (in Chinese) (1990)

Taupin, A., Breitling, J., Wu, W. T. and Altan, T., "Materials fracture and burr formation in blanking: results of FEM simulations and comparision with experiments", *Journal of Materials Processing Technology*, Vol.59, pp.68-78 (1996)

Thomson, P. F. and Gunasekera, J. S., "The Mechanics of Conventional and Fine Blanking", *International Conference on Manufacturing Engineering, Melbourne*, August 1980 pp.75-79 (1980)

Tu, G. Q., *Fine Blanking Technology*, Machinery Industrial Press, Beijing, (Chinese Version) (1990)

Tu, G. Q., Zheng, P. F., Li, R. H, Niu, J. W. and Zhang, X. G., "Recent Development of Fineblanking Technology in China", *Advanced Technology of Plasticity 1993 — Proceedings of the Fourth International Conference on Technology of Plasticity*, Beijing, China (1993)

Zheng, P. F., Finite Element Analysis of the Combined Fine Blanking and Extrusion Process, PhD Thesis, The Hong Kong Polytechnic University, Hong Kong, 2000

Zhou Kai-hua, Yao Ting-guang, Qi Xiang-xian bian, *Jian ming jing chong shou ce*, Bei-jing, Guo fang gong ye chu ban she (1993)

Zhou, K. H., Yao, T. X. and Qi, X. X., *Brief Handbook for Fine Blanking*, Defence Industrial Press, Beijing, (Chinese Version) (1993)

Zhu Y. Y., Zacharia T. and Cescotto S., "Application of fully automatic remeshing to complex metal-forming analyses", *Computers & Structures*, Vol.62, Issue 3, pp.417-427 (1997)

Yang, H. T. Y., Heinstein, M. and Shih, J. M., "Adaptive 2D Finite Element Simulation of Metal Forming Processes", *International Journal of Numerical Mechanical Engineering*, Vol.28 , pp.1409-1428 (1989)

Tables and Figures

Poisson's Ratio	Young's Modulus	Chemical Composition (%)			
		Carbon C	Manganese Mn	Phosphorus P	Sulphur S
0.33	206 GPa	0.04	0.02	0.013	0.008

Table 3.1 Properties and Chemical Composition (%) of SPCC

	Peak Load (kN)	Peak Stress (Mpa)	Elongation at Break (mm)	% Strain at Break (%)	Off Yield Stress (Mpa)	Modulus (Gpa)
Mean	2.07	334.41	3.70	26.12	249.4	193.75

Table 3.2 Experimental Result of Tension Test

Tensile Strength (N/mm^2)	Hardness (HV)	Chemical Composition (%)				
		Carbon C	Manganese Mn	Phosphorus P	Sulphur S	Silicon Si
~ 455	~170	0.09	0.55	0.026	0.014	0.14

Table 4.1 Properties and Chemical Composition (%) of Work Material

Die-Roll Height (d) (mm)	Die-Roll Height / Thickness	Burr Height (mm)	K-Value
0.35	8.4%	0.021	1.00

Table5.1 Summary of Experimental Findings

Location	Hardness (HV)	Hardness Ratio
1	362	2.1
2	340	2.0
3	294	1.7
4	266	1.6
5	250	1.5
6	231	1.4
7	170	1.0

Table5.2 Hardness Distributions

Punch Penetration (In Terms of % of Material Thickness)	Effective Strain Values		
	Punch Tip	Die Corner	Central of Shearing Region
0-20%	1.19	1.14	0.67
20-40%	1.19	1.08	0.63
40-60%	1.13	1.03	0.60
60-80%	1.16	1.13	0.65

Table5.3 Effective Strain Values of Individual Remeshing Stage

Total Punch Penetration (In Terms of % of Material Thickness)	Effective Strain Values		
	Punch Tip	Die Corner	Central of Shearing Region
0-20%	1.19	1.14	0.70
0-40%	2.90	2.83	1.30
0-60%	6.77	6.68	2.89
0-80%	11.78	11.07	6.24

Table5.4 Effective Strain Values of Total Punch Penetration

Total Punch Penetration (In Terms of % of Material Thickness)	Effective Strain Values
	Punch Tip
0-20%	3.94
0-40%	6.72
0-60%	9.65
0-80%	11.50

Table5.5 Effective Strain Obtained by FEM (Chen, 2002)

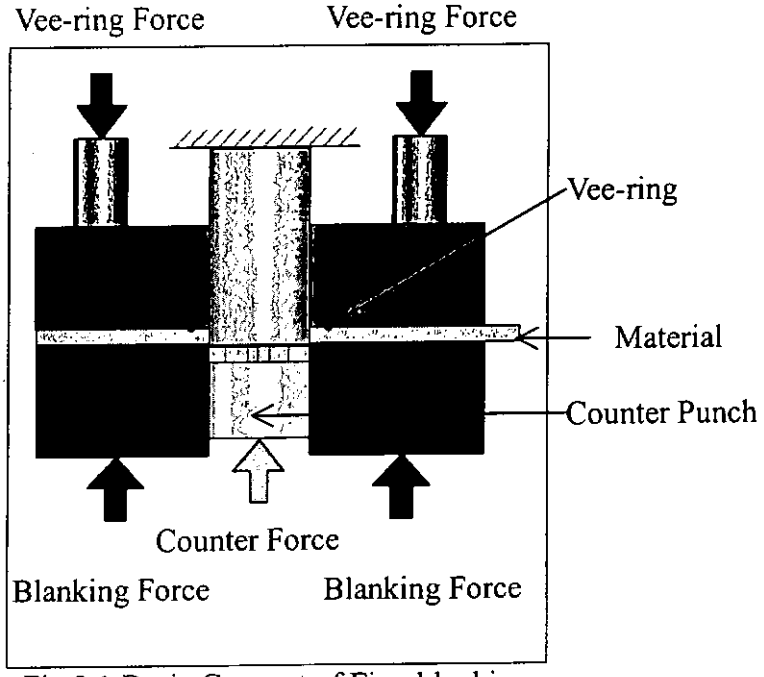

Fig.2.1 Basic Concept of Fine-blanking

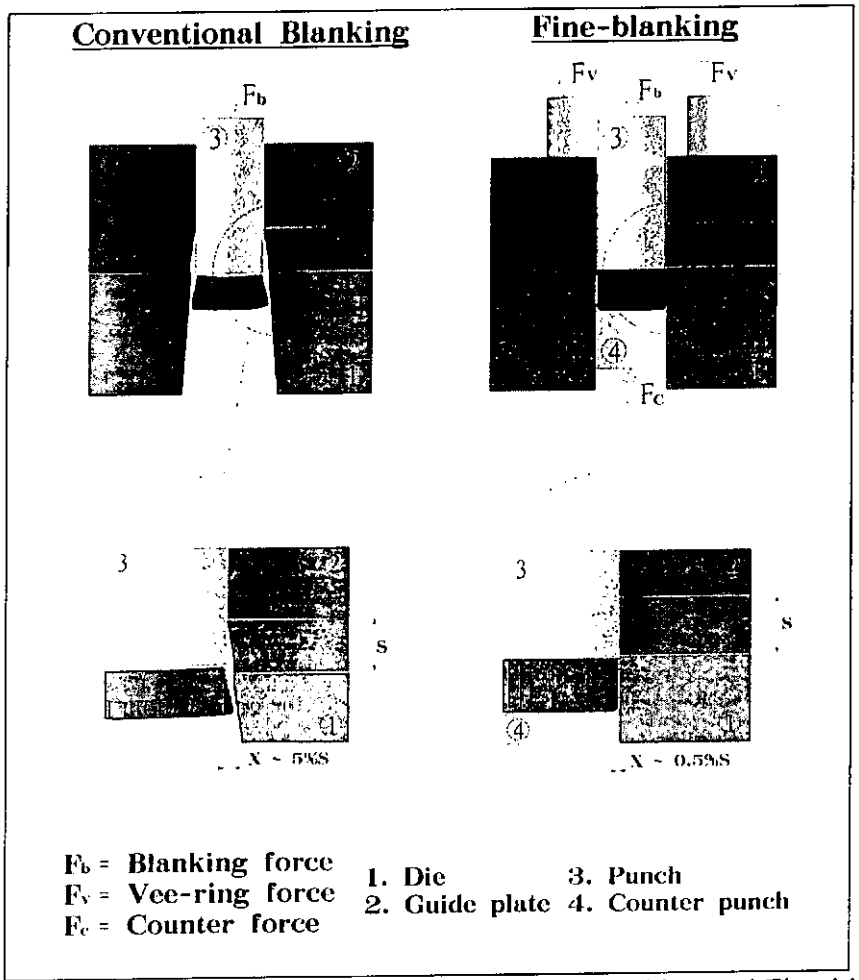

Fig.2.2 Main Differences Between Conventional Blanking and Fine-blanking

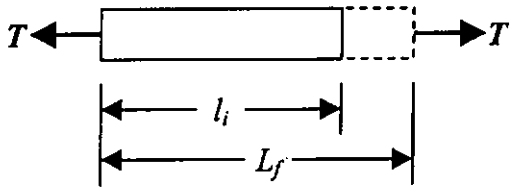

Fig.2.3 Deformation on a Tensile Bar

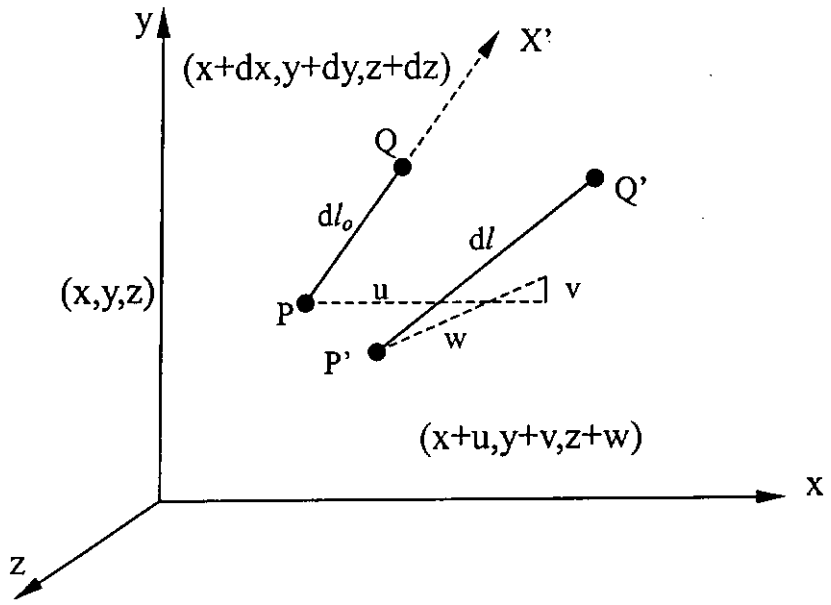

Fig.2.4 Transformation of linear strain

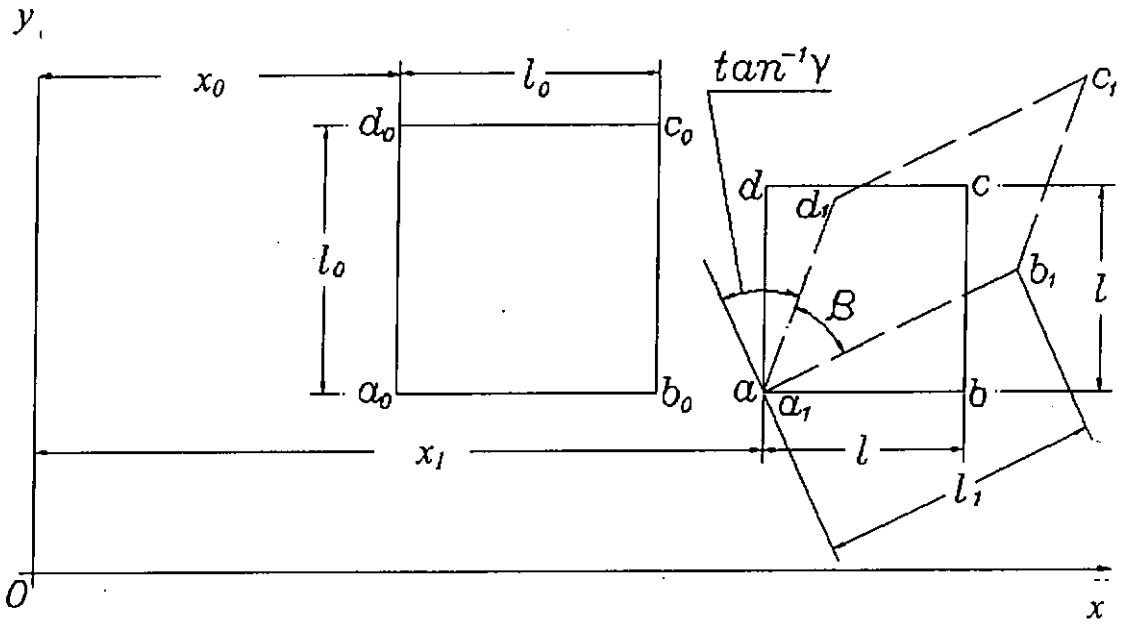

Fig.2.5 Large Strain Analysis – Homogenous Case

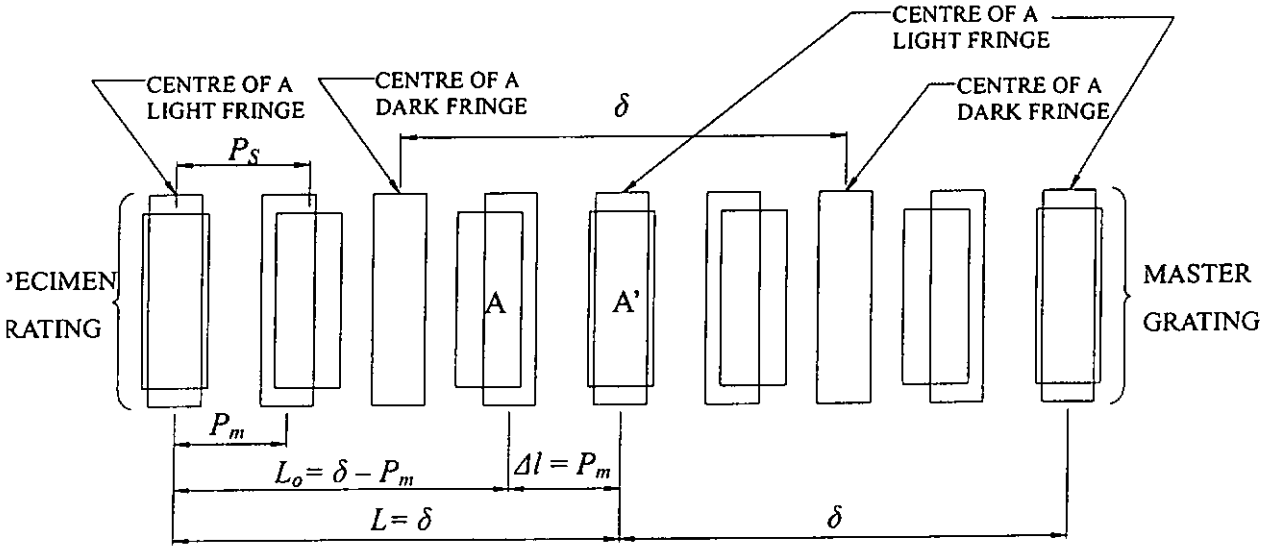

Fig.2.6 Formation of Moiré Fringes Due To a Difference in Pitch

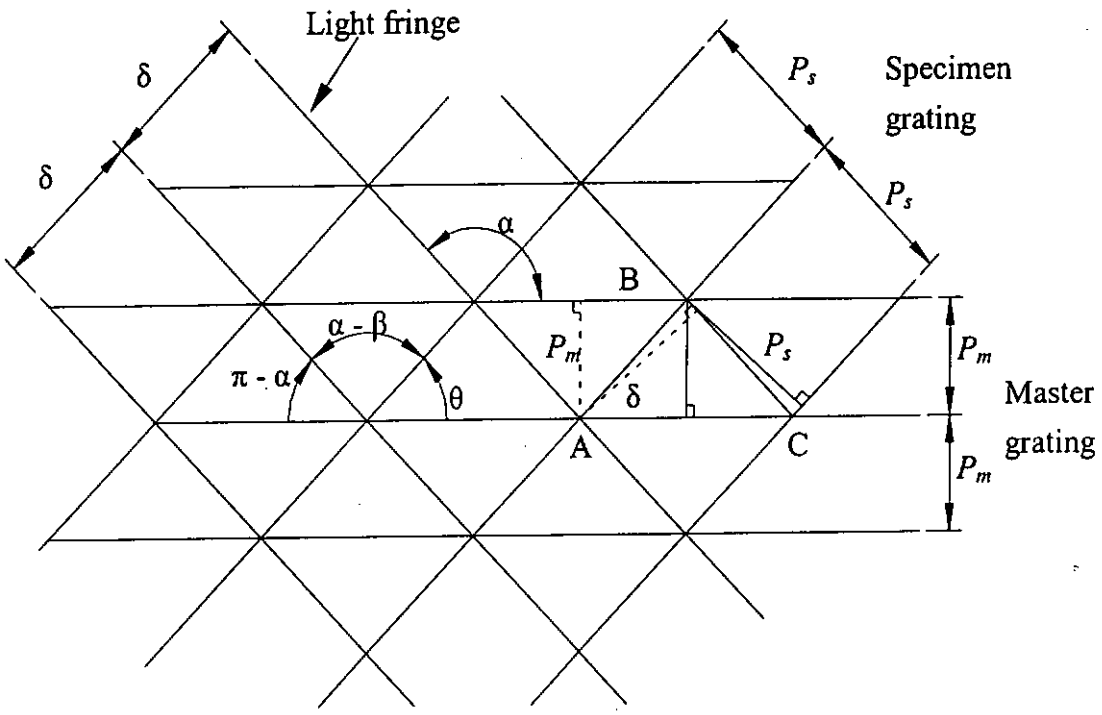

Fig.2.7 Moiré fringes of combination of different pitches and rotations

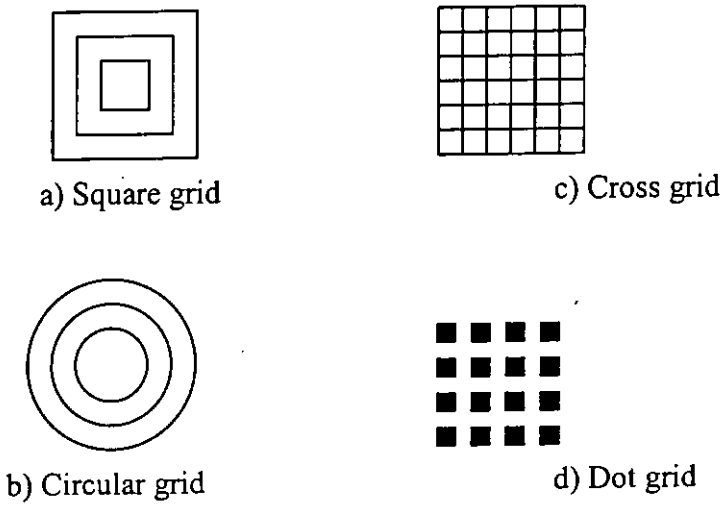

Fig.2.8 Various Types of Grids

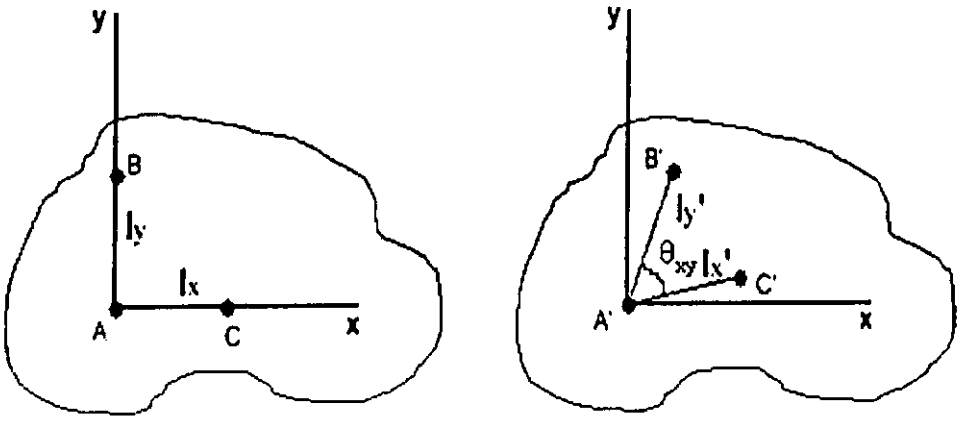

Fig.2.9 2-D Measurement of Strain

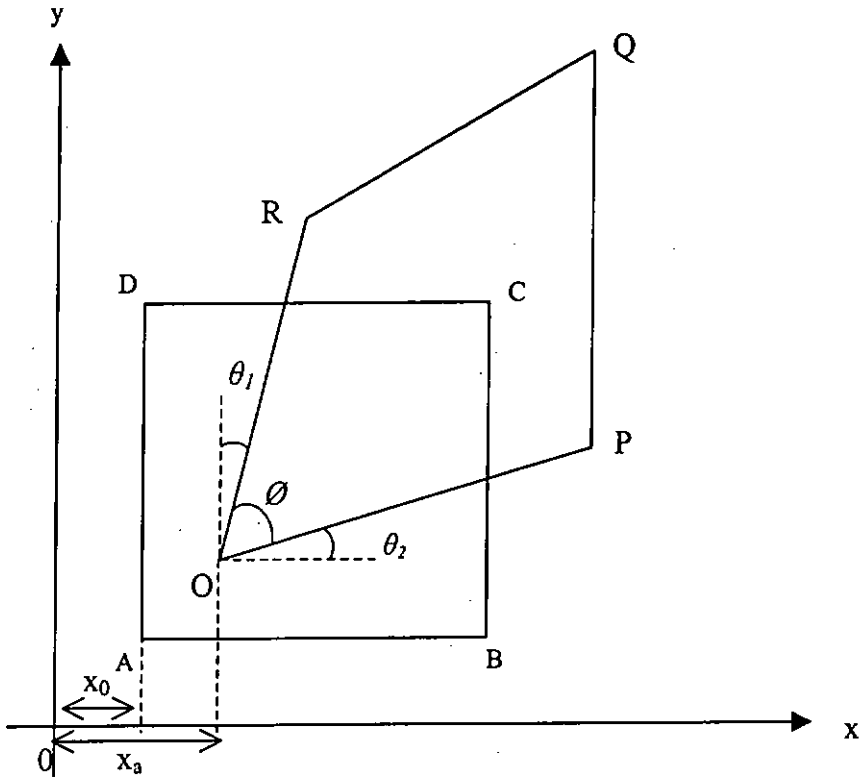

Fig.3.1 Two-dimensional Displacement Components in Cartesian Coordinates

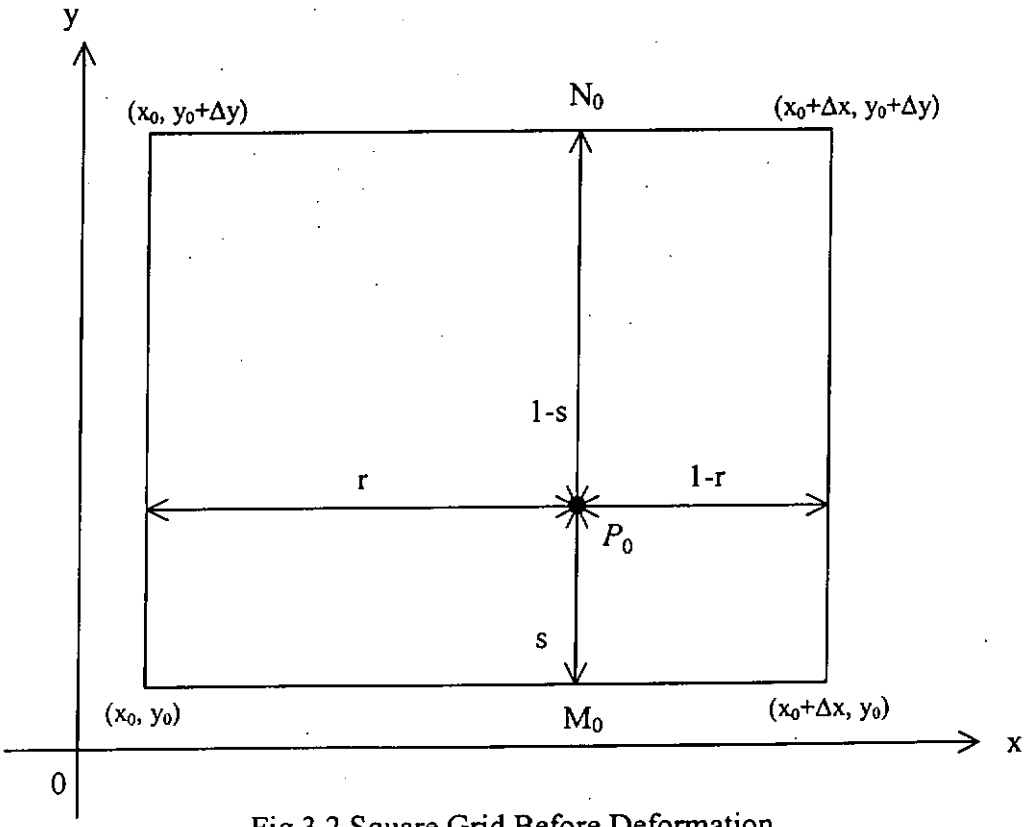

Fig.3.2 Square Grid Before Deformation

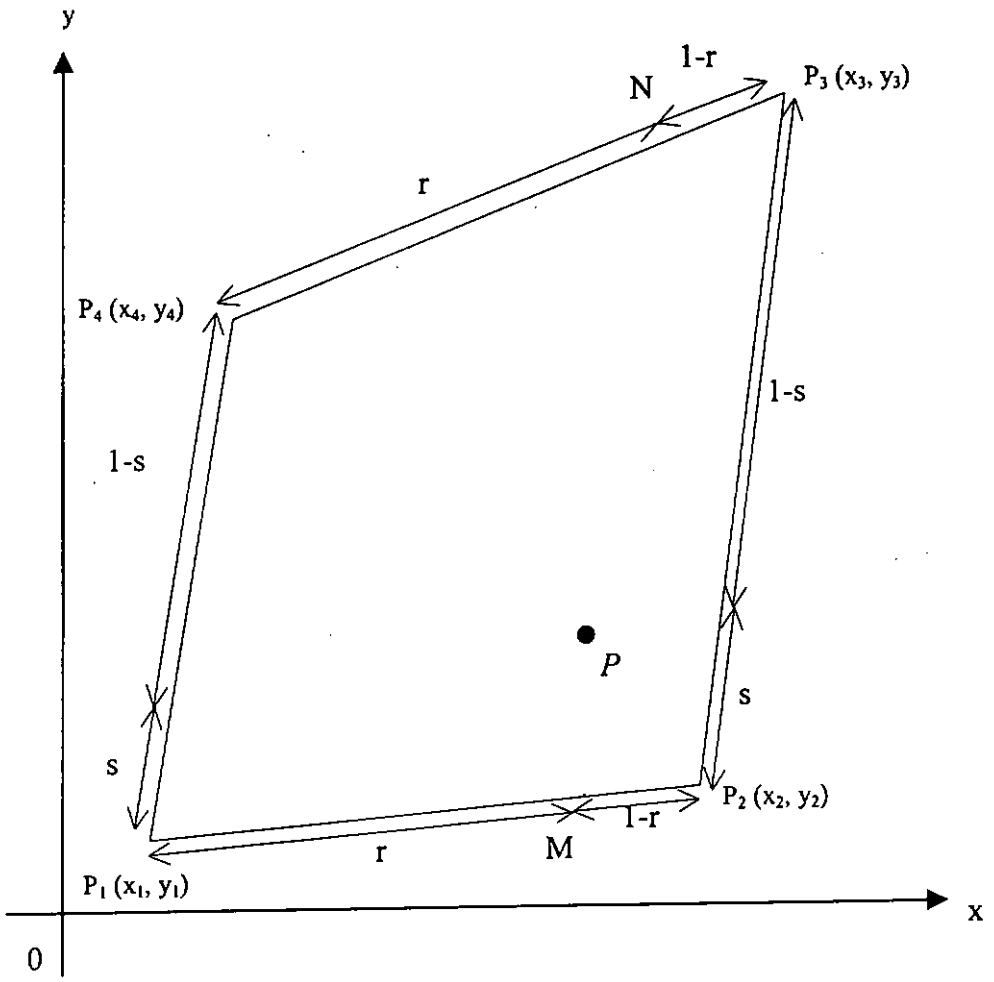

Fig.3.3 Square Grid after Deformation

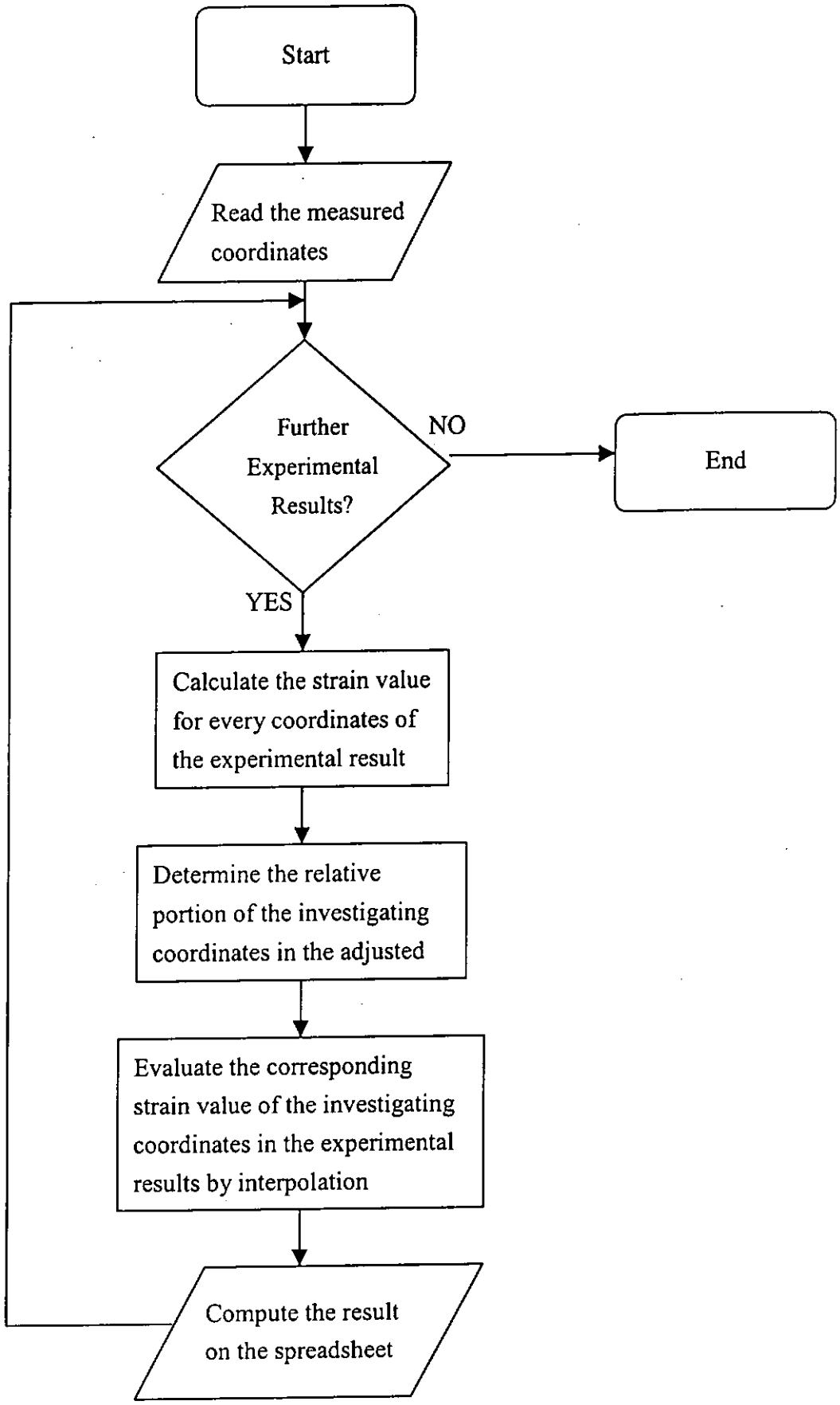

Fig.3.4 The Flow Chart of Developed Program

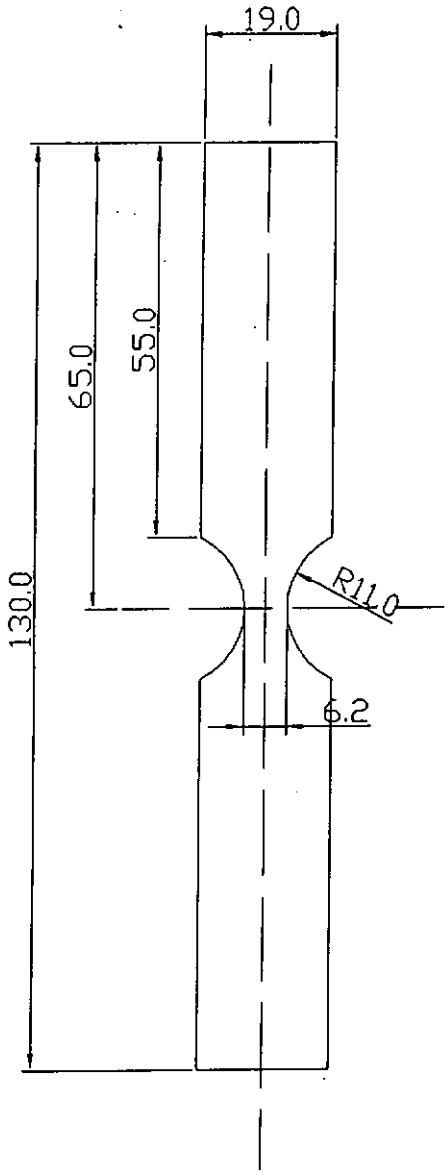

Fig.3.5 Specimen Design for Testing

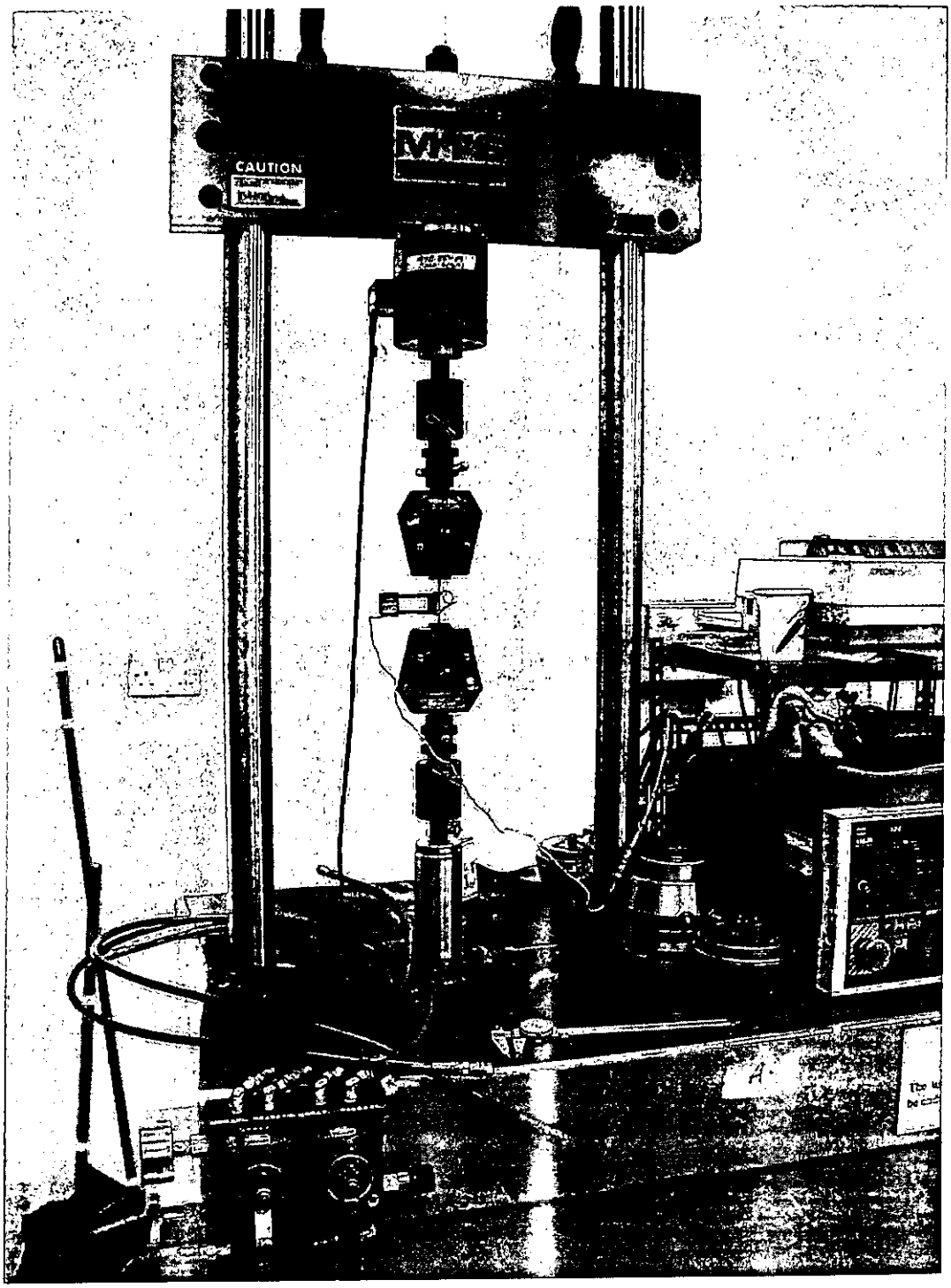

Fig.3.6 MTS Tension Test Machine

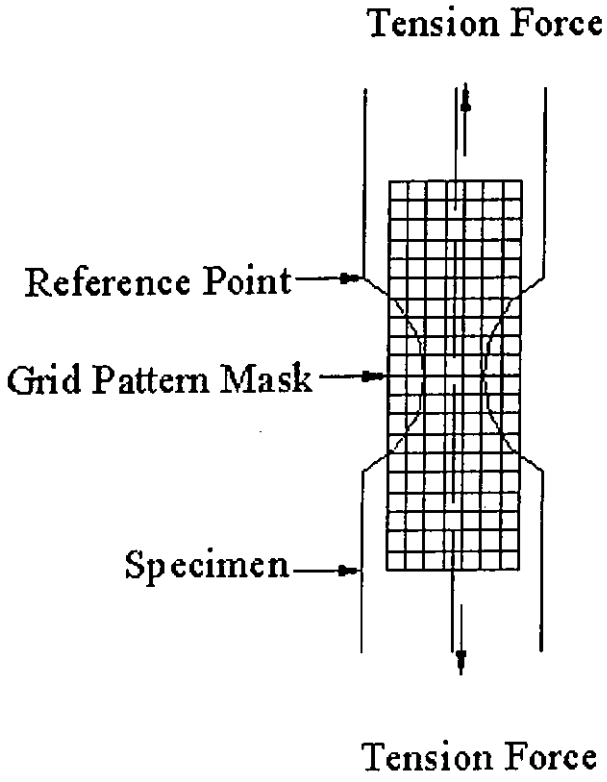

Fig.3.7 Specimen With Printed Grids

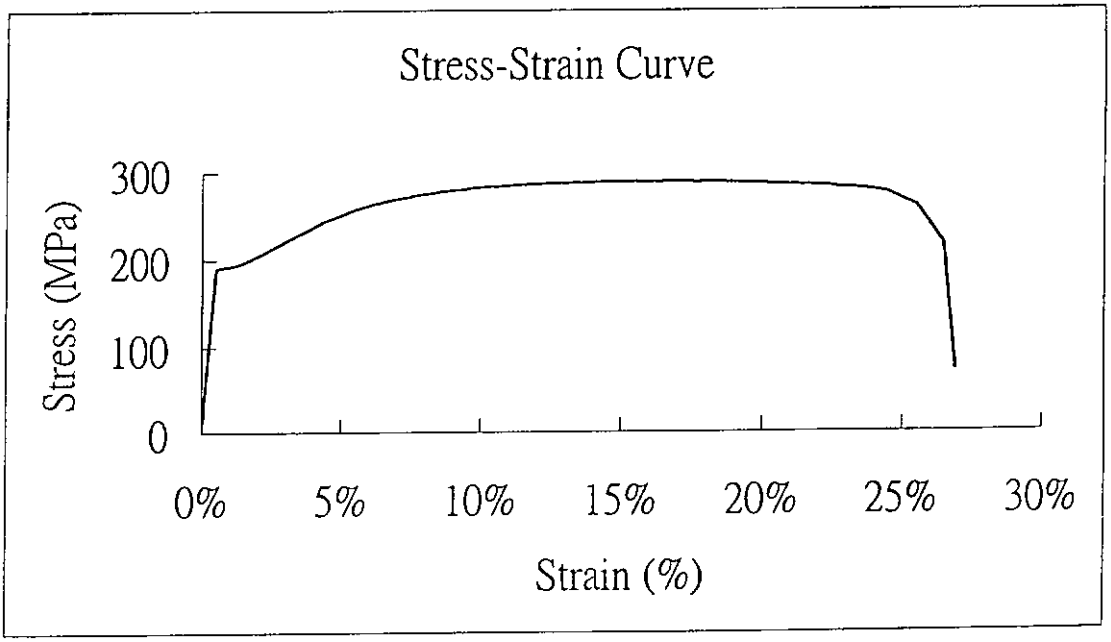

Fig.3.8 Stress-Strain Curve of SPCC from Trial Test

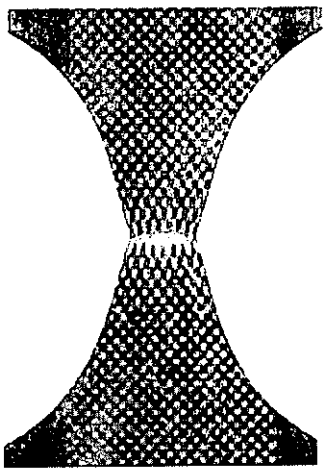

Fig.3.9 Ruptured Specimen

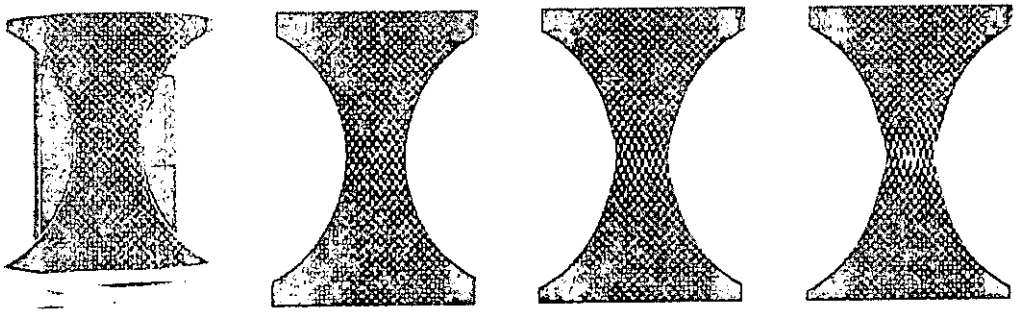

(a) (b) (c) (d)

Elongation=1.0mm Elongation=2.0mm Elongation=3.0mm Elongation=3.5mm

Fig.3.10 Sequence of Grids Deformation before Point of Rupture

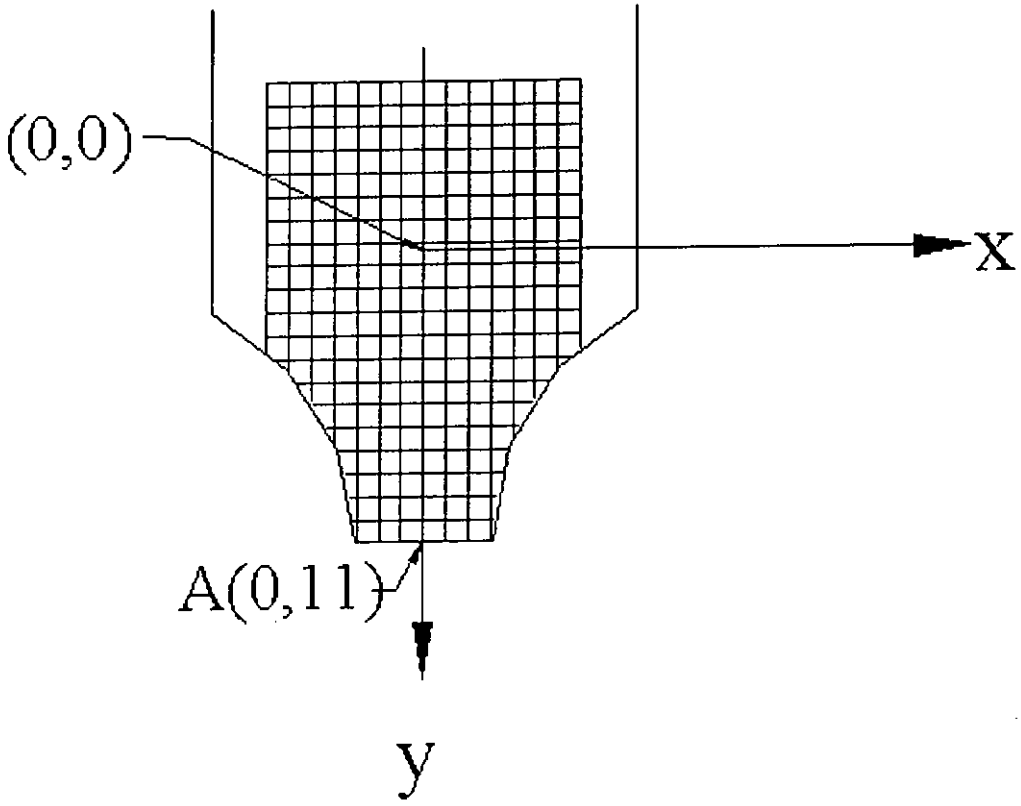

Fig.3.11 Coordinate System for Plotting Contour Maps

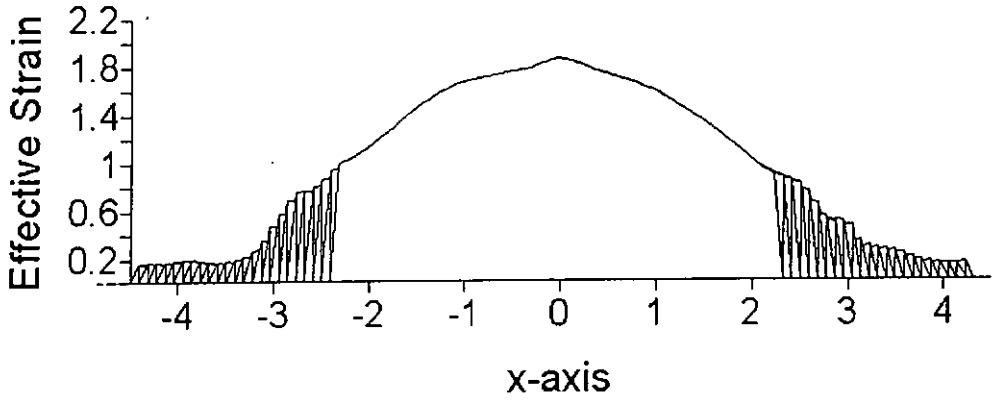

(a) 2-D Contour Map

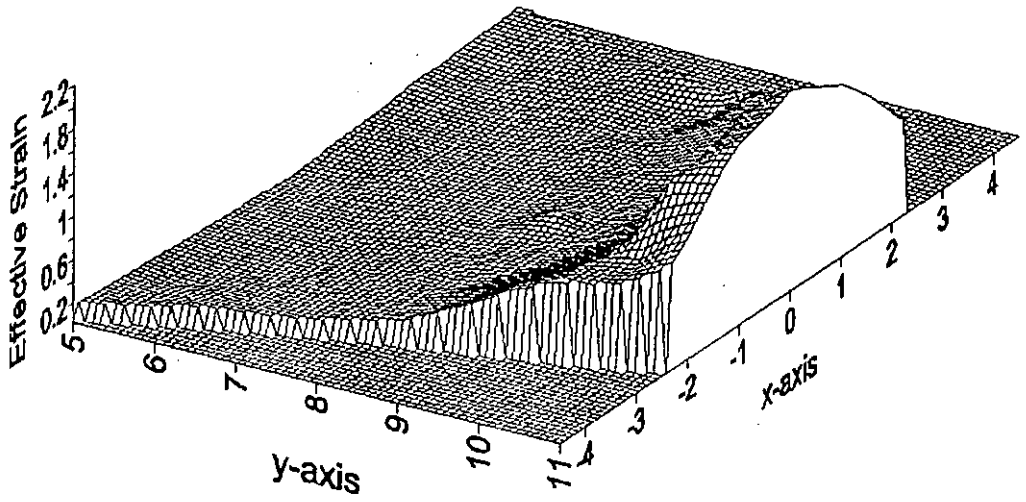

(b) 3-D Contour Map

Fig.3.12 Contour of Strain Values of Tension Test (Elongation = 3.5mm)

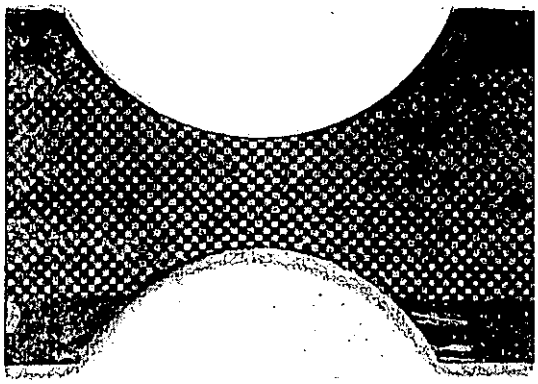

Fig.3.13 Deformed Grid Pattern of 2.0mm Elongation

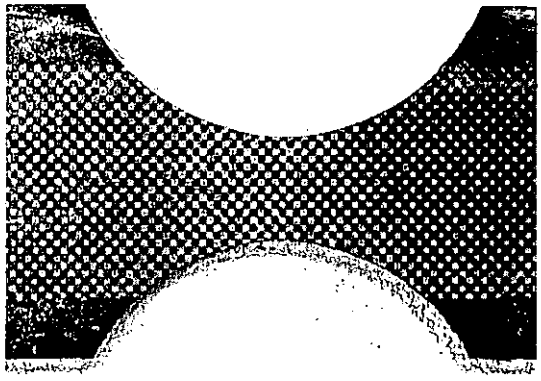

Fig.3.14 Specimen with Remeshed New Grid Pattern

Fig.3.15 Deformed Remeshed Grid Pattern After 2nd Tension Test

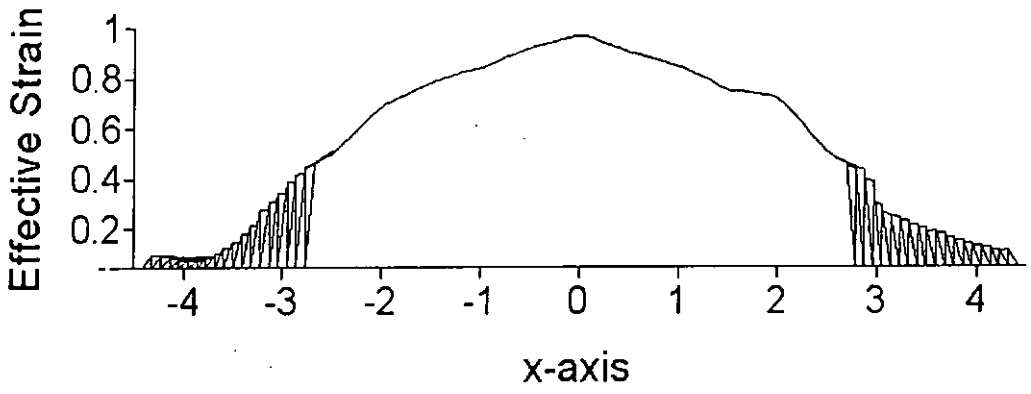

(a) 2-D Contour Map

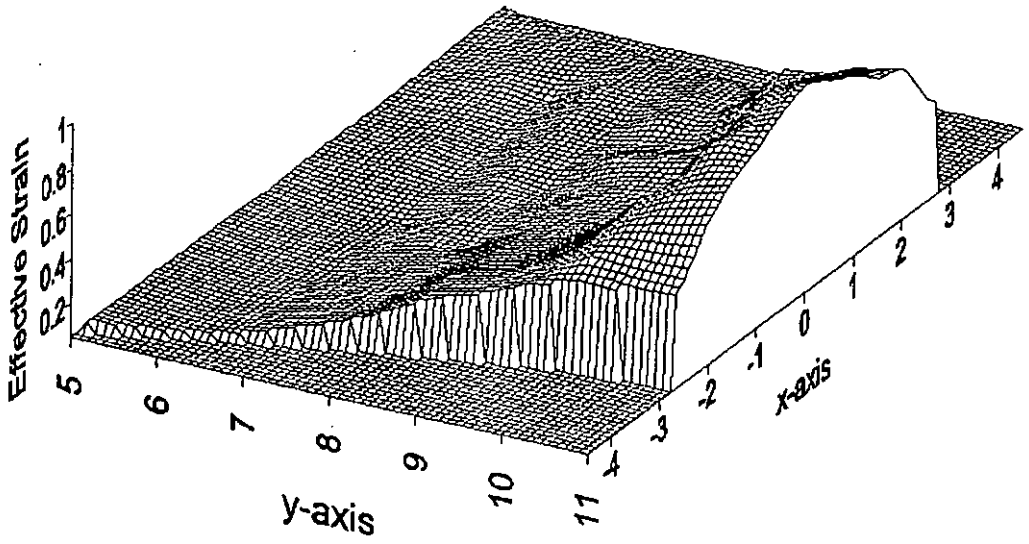

(b) 3-D Contour Map

Fig.3.16 Contour of Strain Distribution of 1st Tension Test (Elongation = 2.0mm)

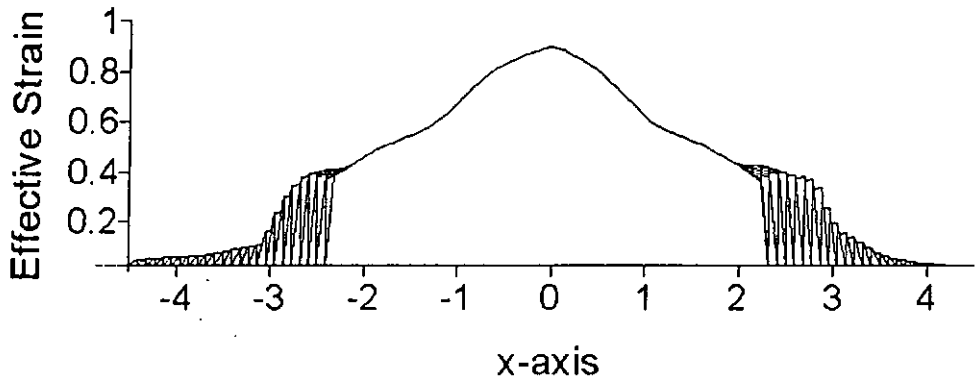

(a) 2-D Contour Map

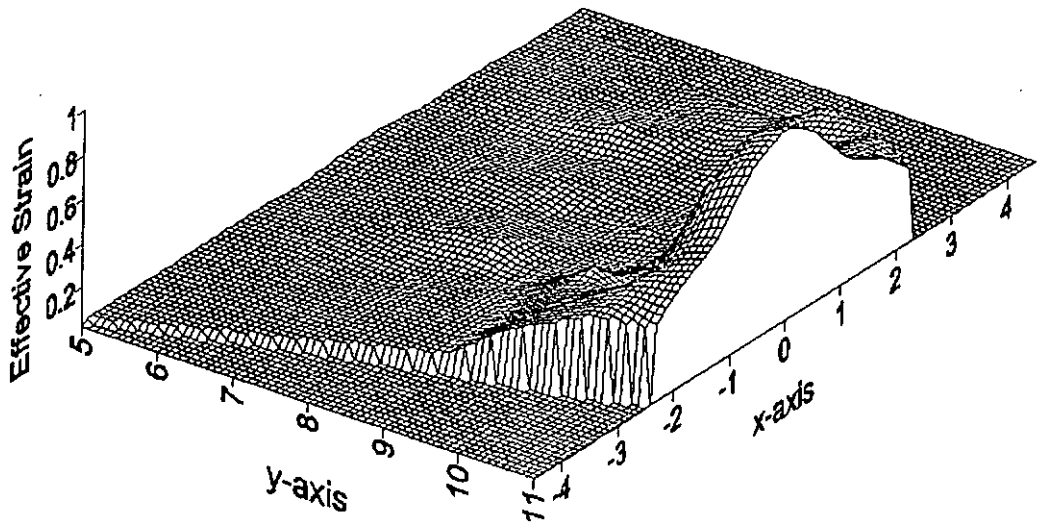

(b) 3-D Contour Map

Fig.3.17 Contour of Strain Distribution of 2nd Tension Test (Elongation = 1.5mm)

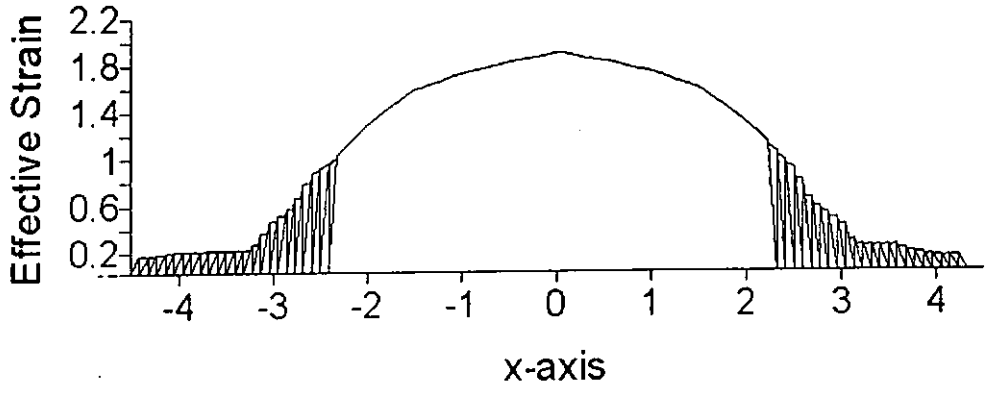

(a) 2-D Contour Map

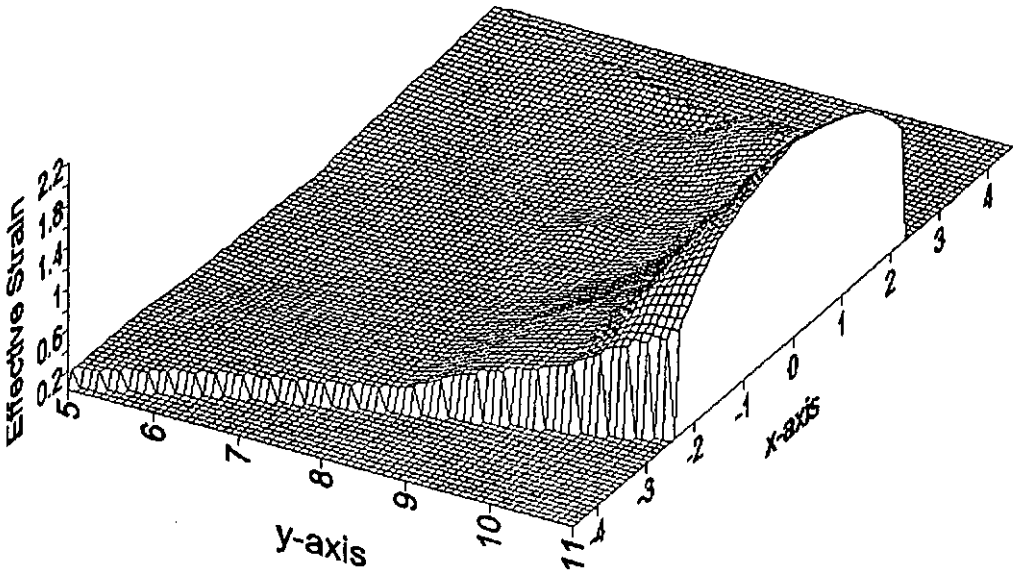

(b) 3-D Contour Map

Fig.3.18 Contour of Overall Strain Distribution After Remeshing

(Total Elongation = 3.5mm)

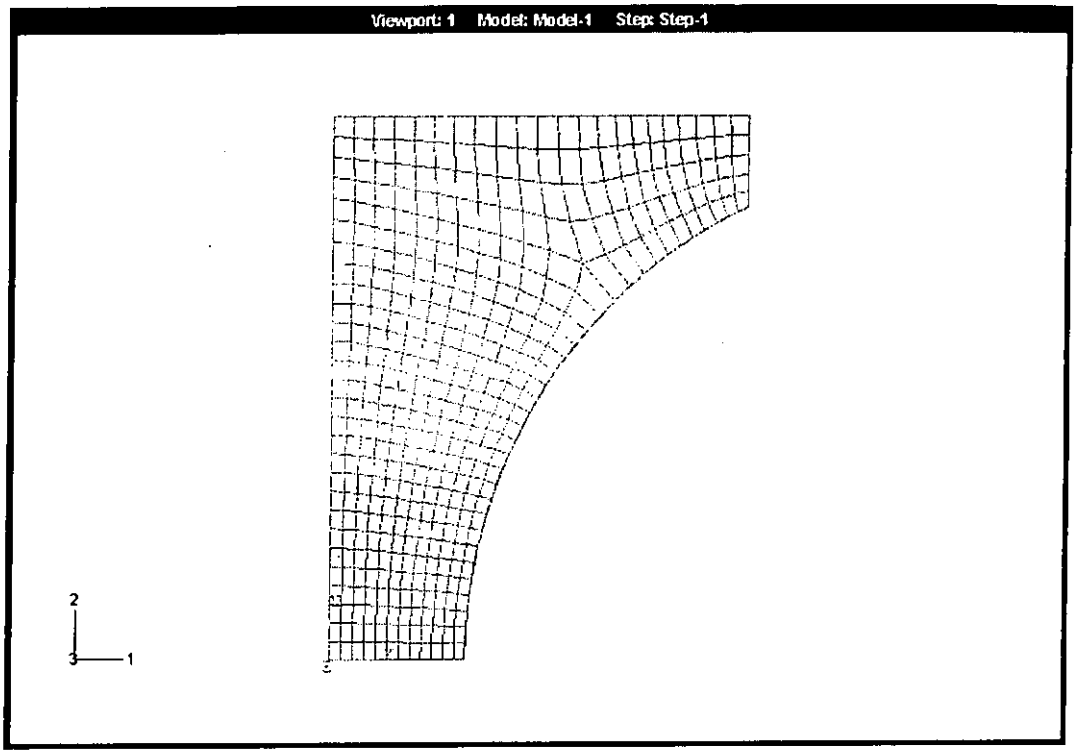

Fig.3.19 Finite Element Mesh of a Quarter of the Symmetrical Specimen under a Tension Test

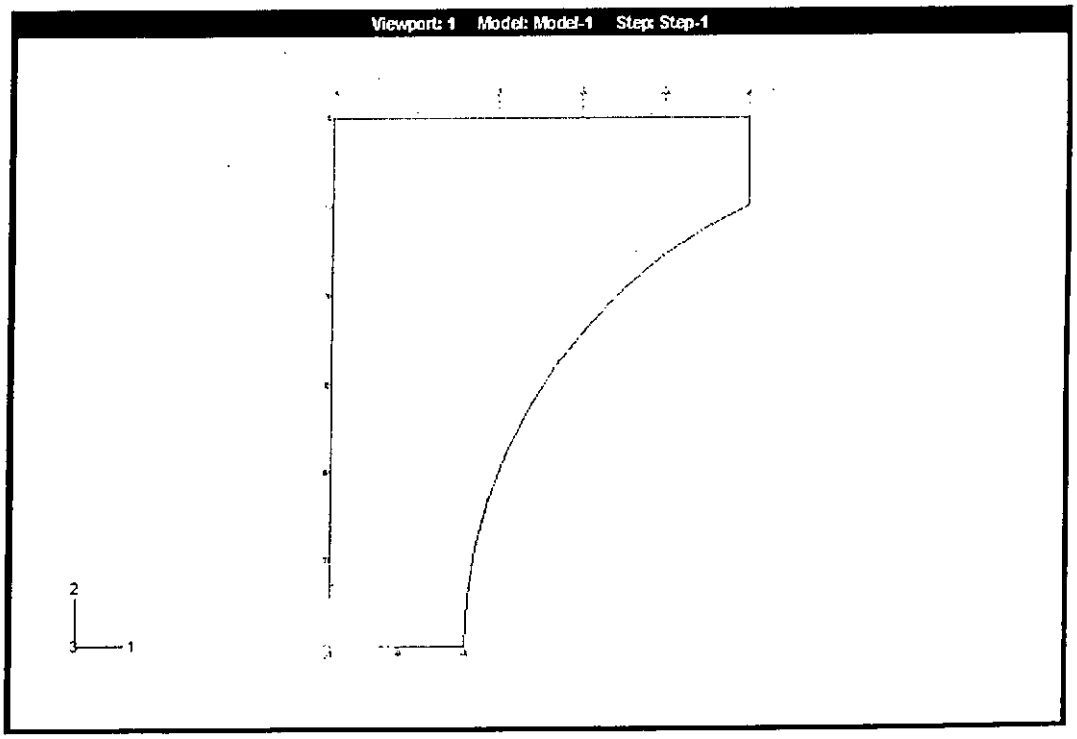

Fig.3.20 Boundary Conditions of a Quarter of the Symmetrical Specimen under a Tension Test

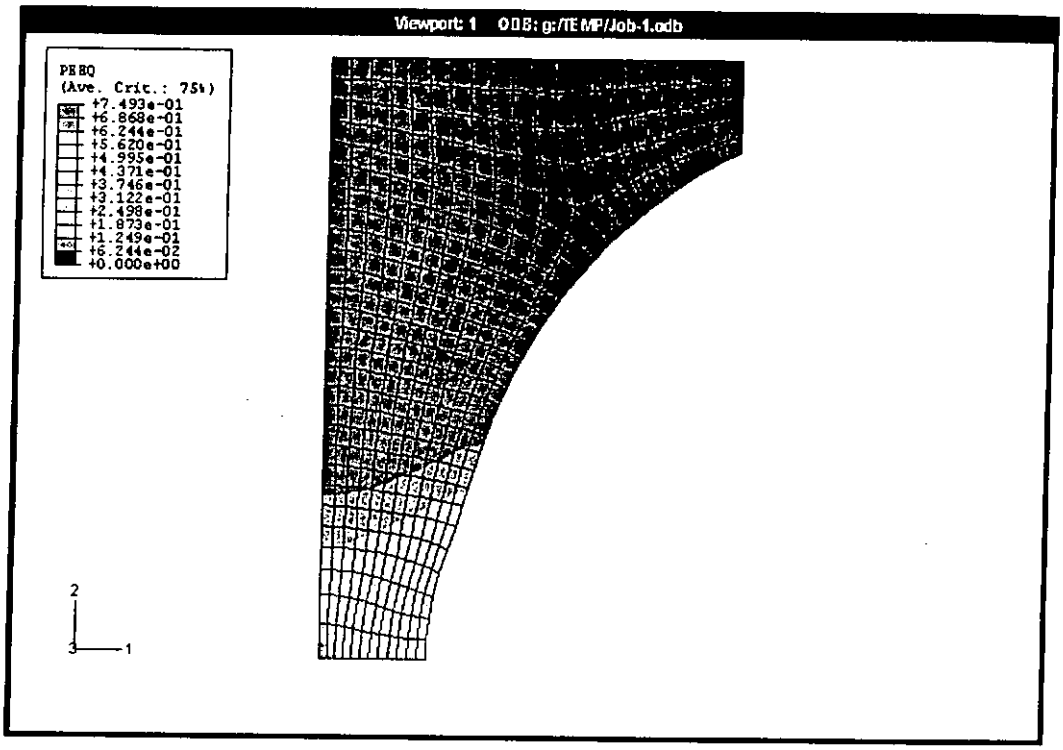

(a) Displacement = 2.0mm

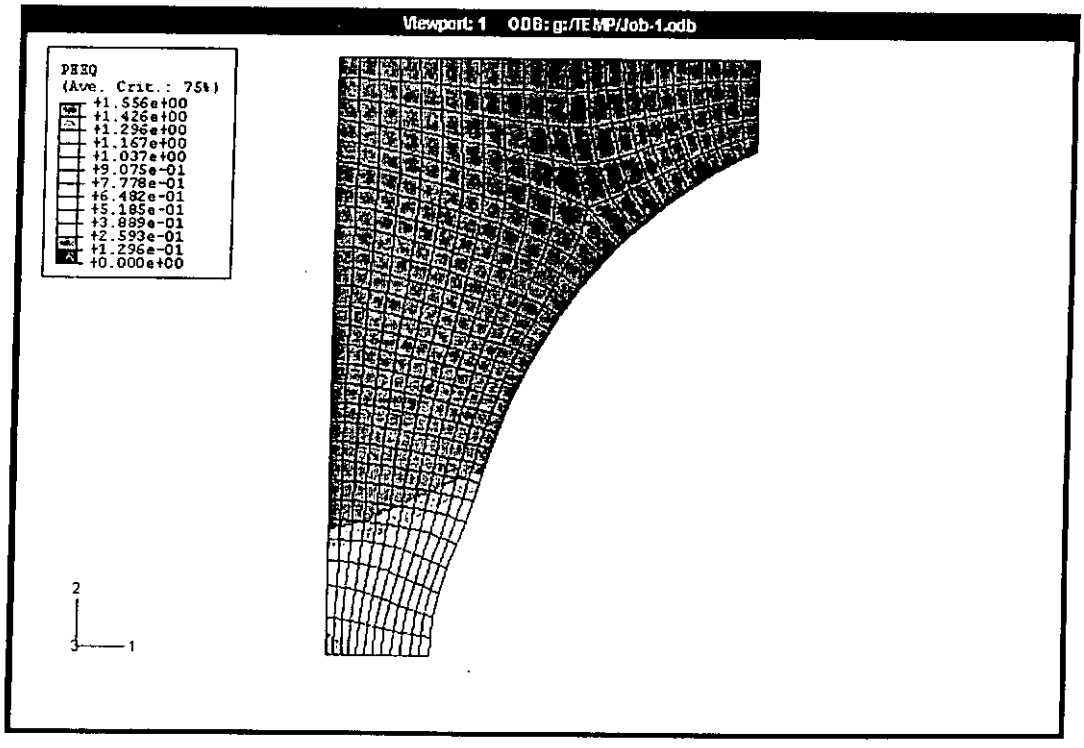

(b) Displacement = 3.5mm

Fig.3.21 Predicted Maximum Effective Strain Values

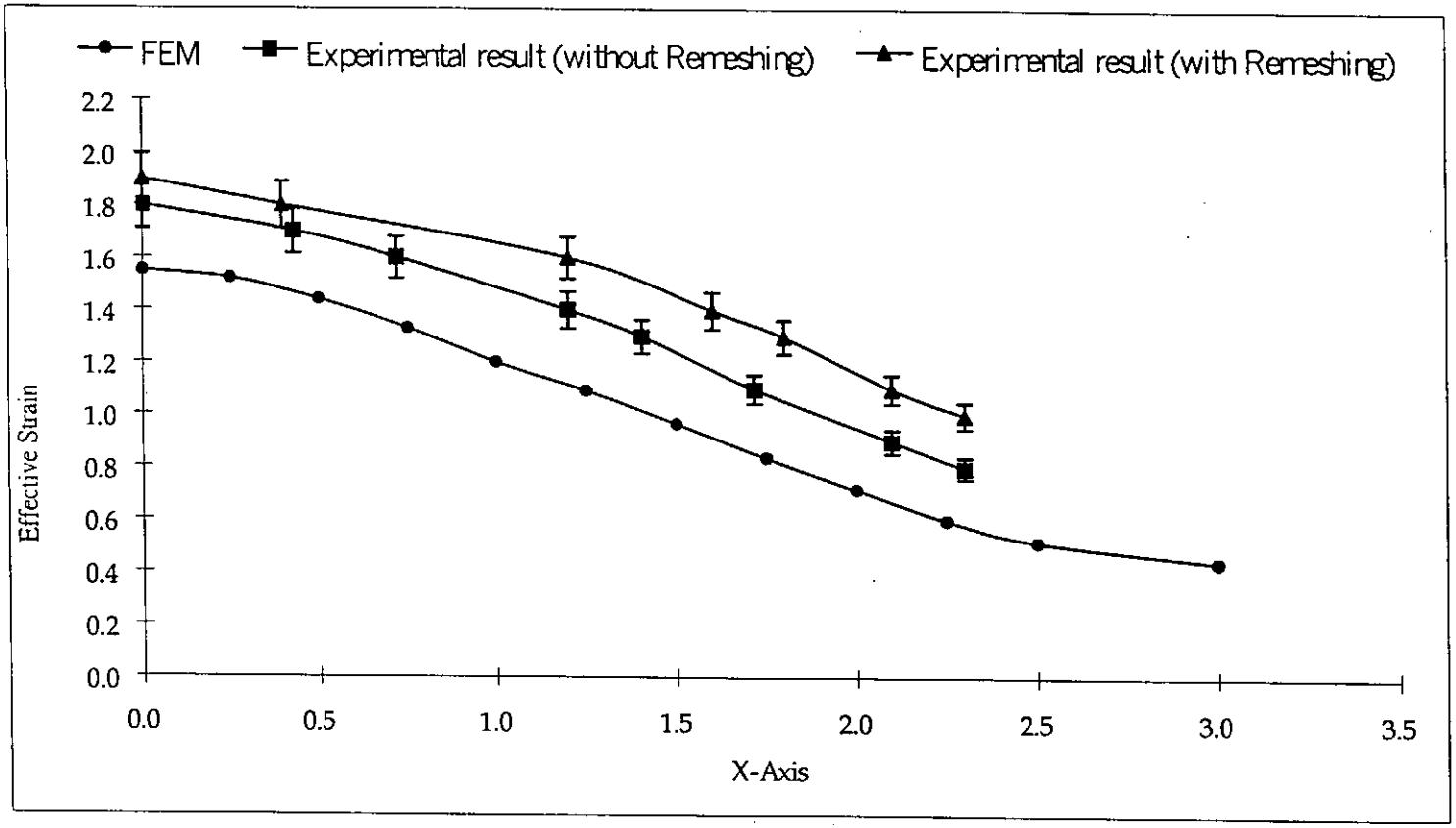

Fig.3.22 Summary of Validation Results

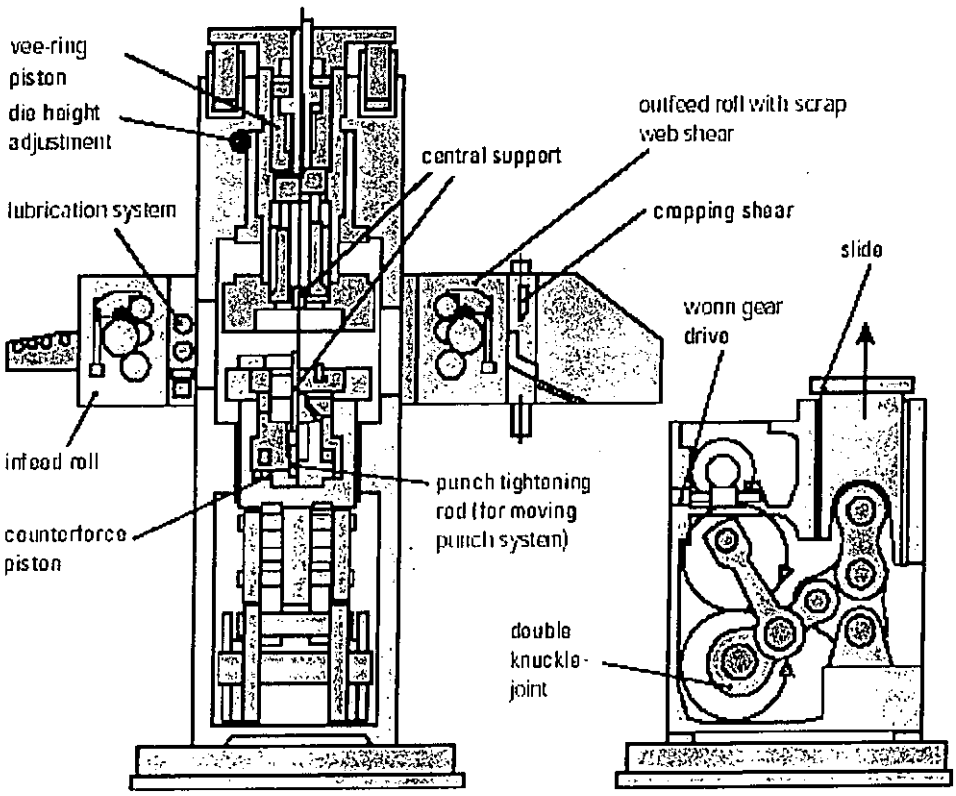

Fig.4.1 Schematic Layout of a Mechanical Fine-blanking Press (Schuler, 1998)

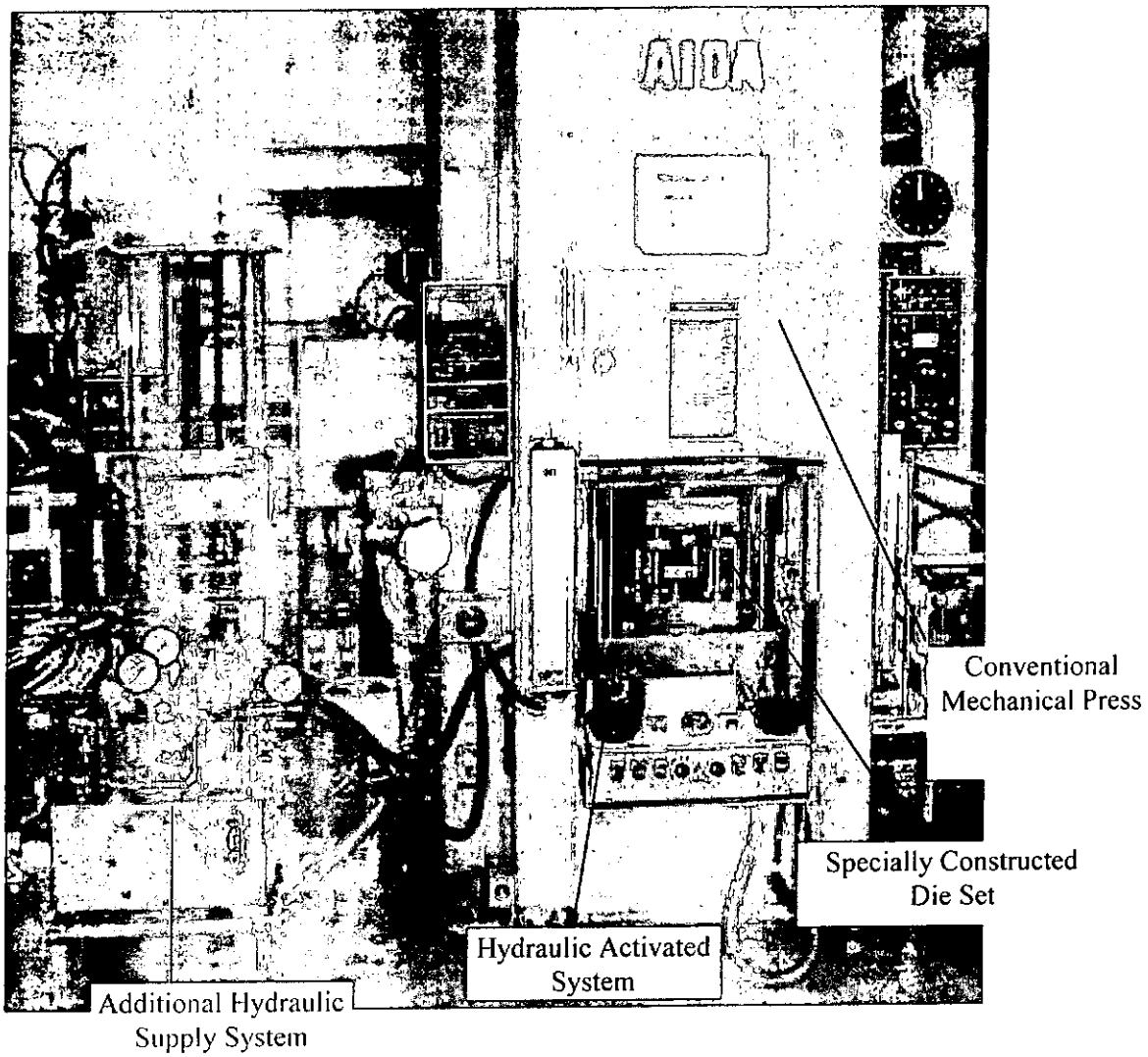

Fig.4.2 Construction of a Fine-blanking Simulation System for Experiment

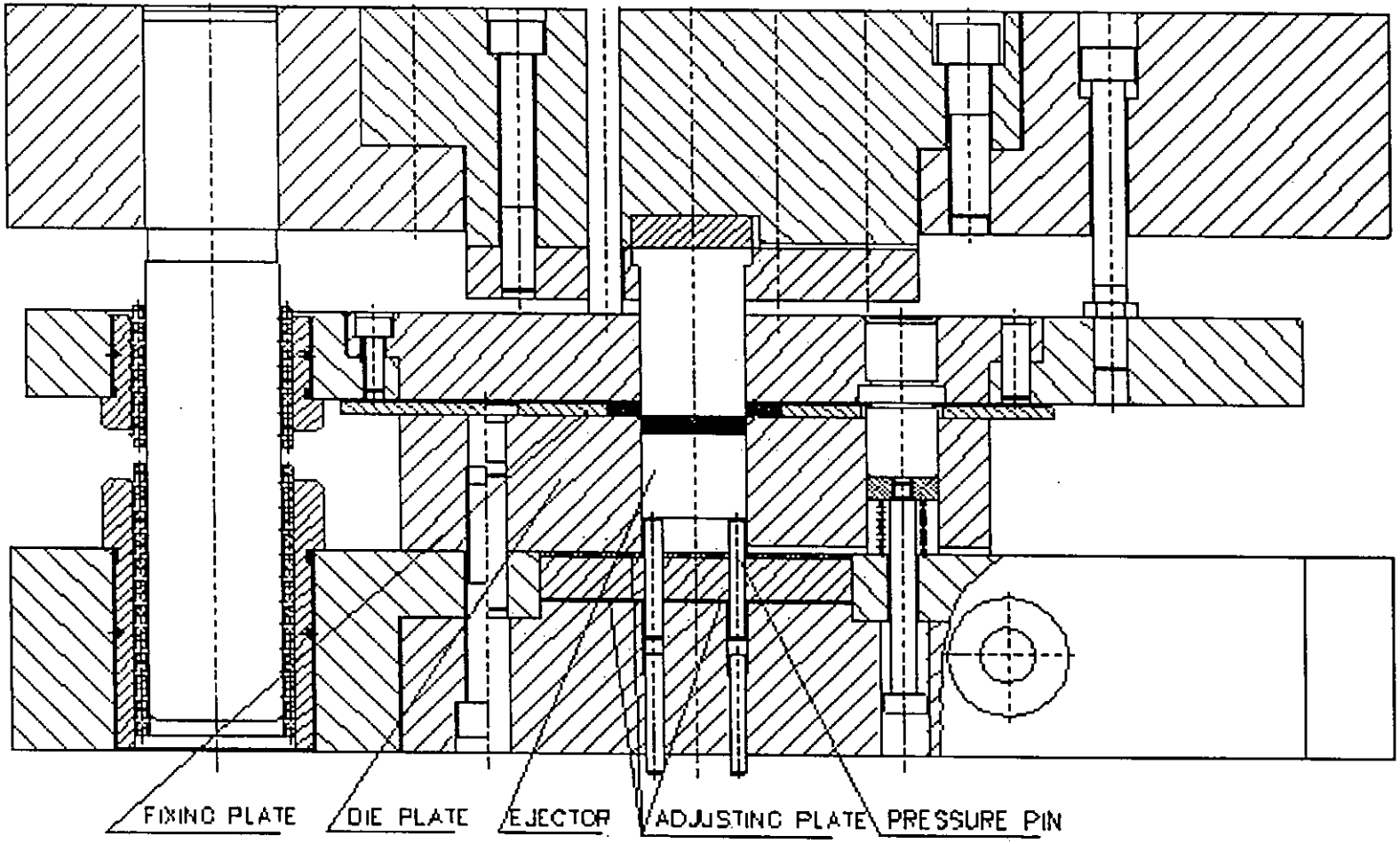

Fig.4.3 Structure of the Special Die Set for Fine Blanking

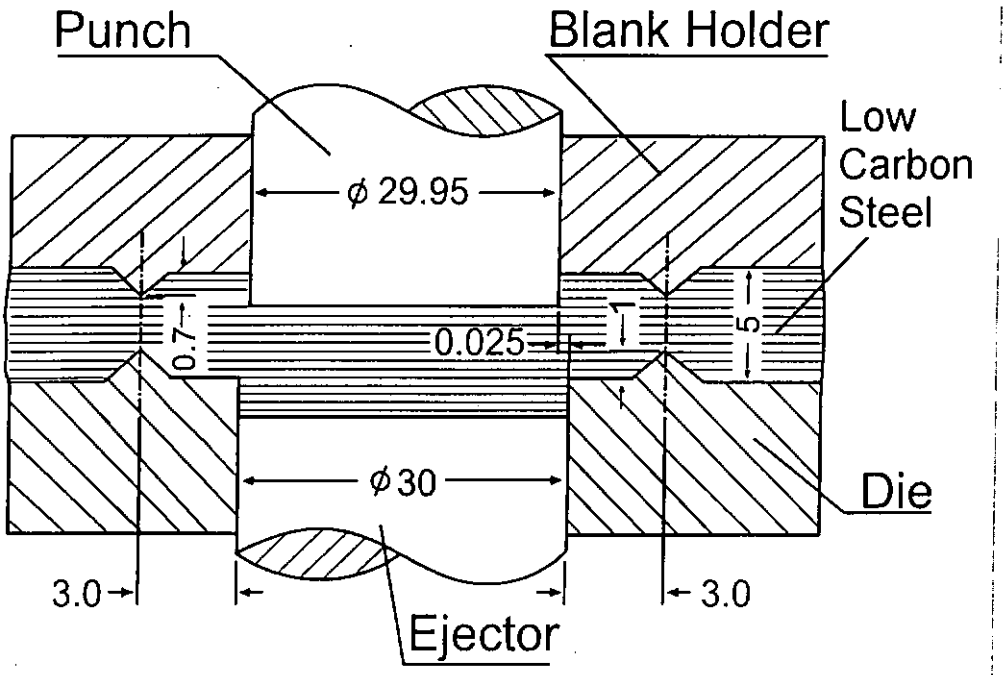

Fig.4.4 Configuration of Fine-blanking Die (units in mm)

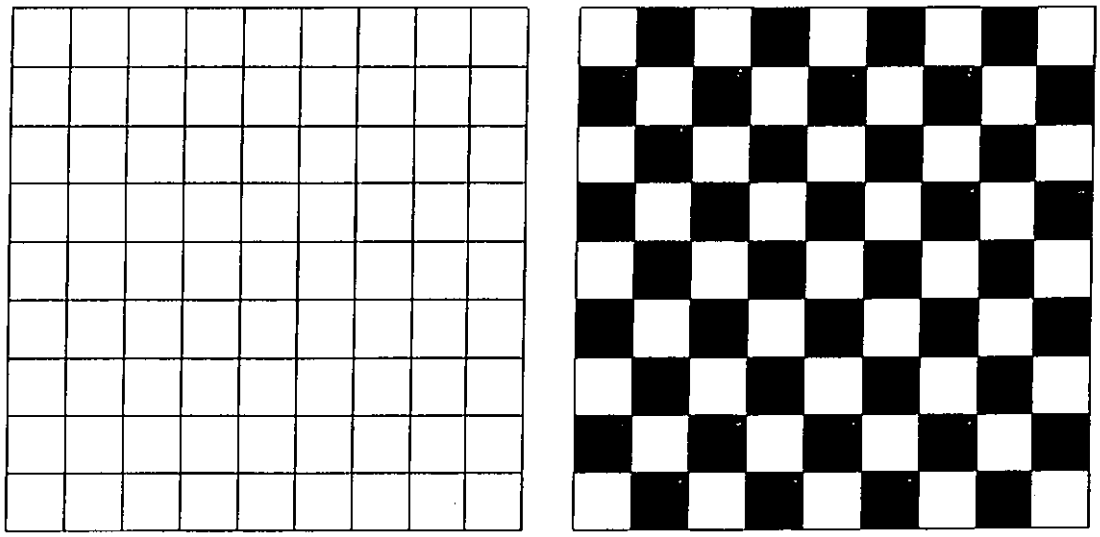

(a) The Square Line Film (b) The Chessboard Pattern Film

Fig.4.5 Two Types of Mesh

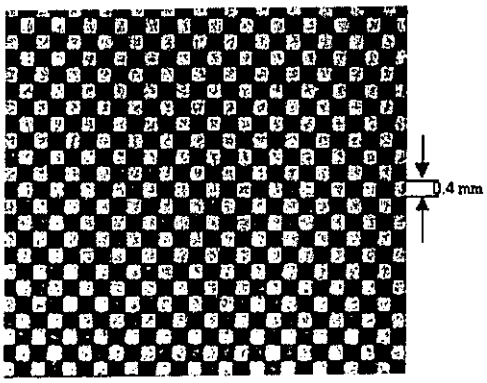

Fig.4.6 Photochemical Etched 0.4mm x 0.4mm Grid Patterns

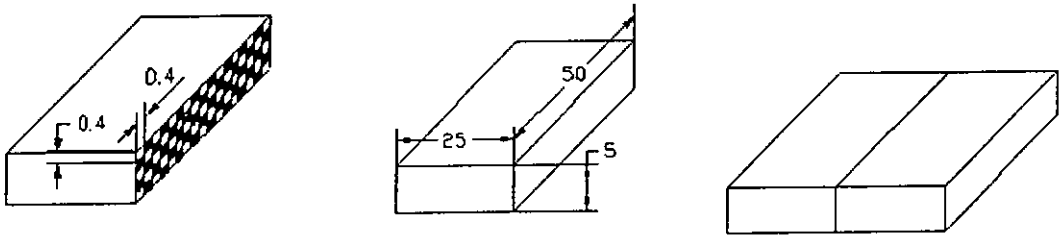

(a) Specimen with Mesh (b) Dimensions of Specimen (c) Combined Specimens

Fig.4.7 Specimens Design

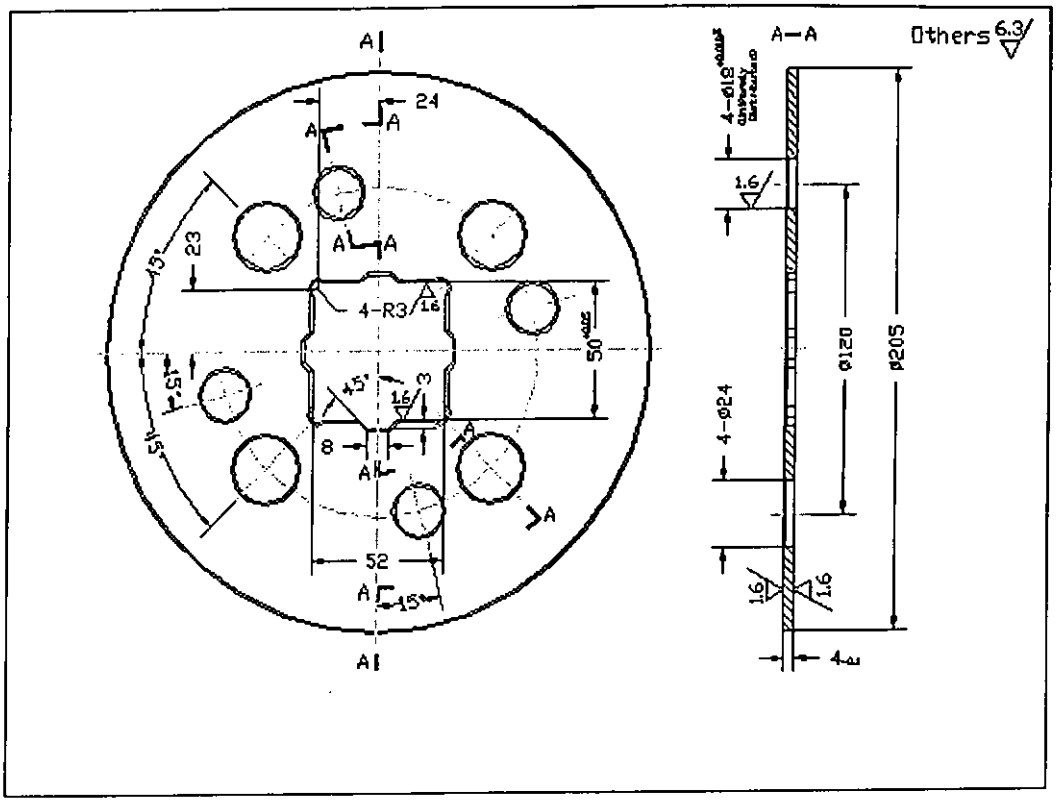

Fig.4.8 The Fixture for Holding Specimens

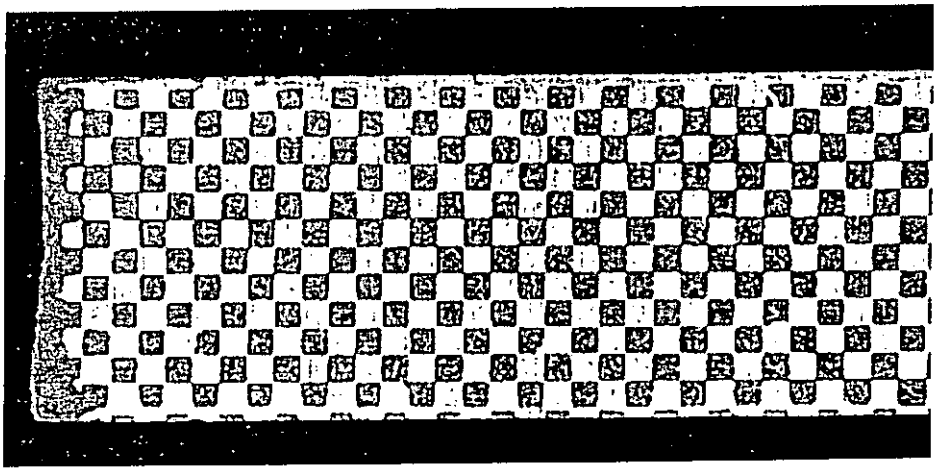

Fig.4.9 A Photochemically Etched Specimen

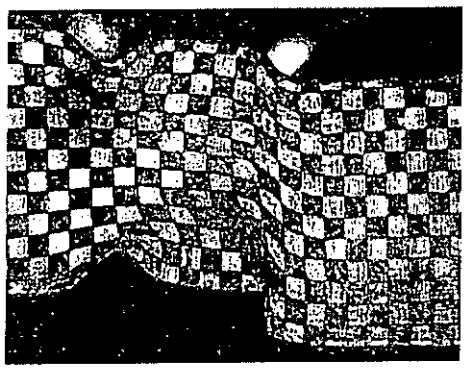

Fig.4.10 An Example of Distorted Mesh of 20% Punch Penetration

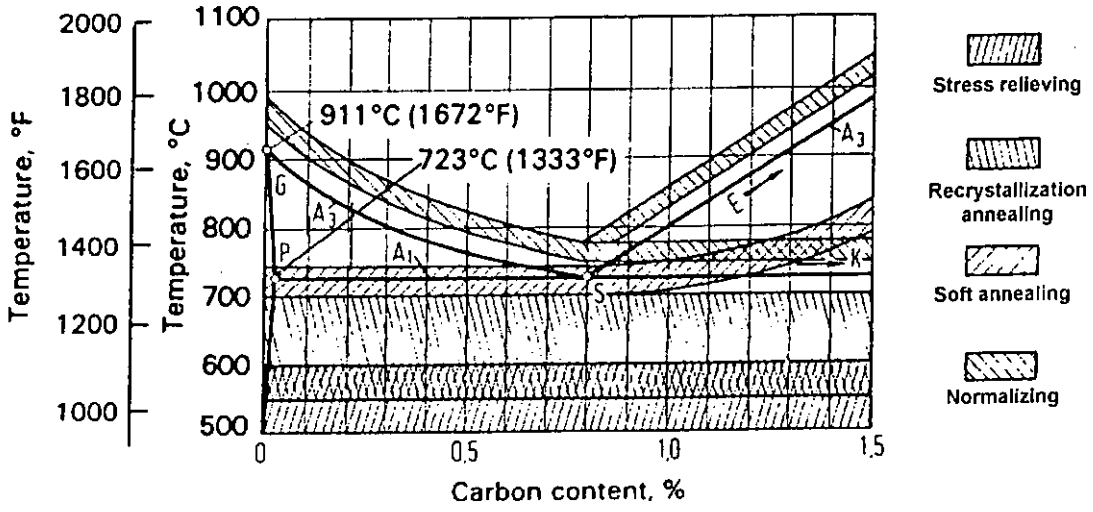

Fig.4.11 Iron-carbon Diagram of Annealing temperature (Lange, 1985)

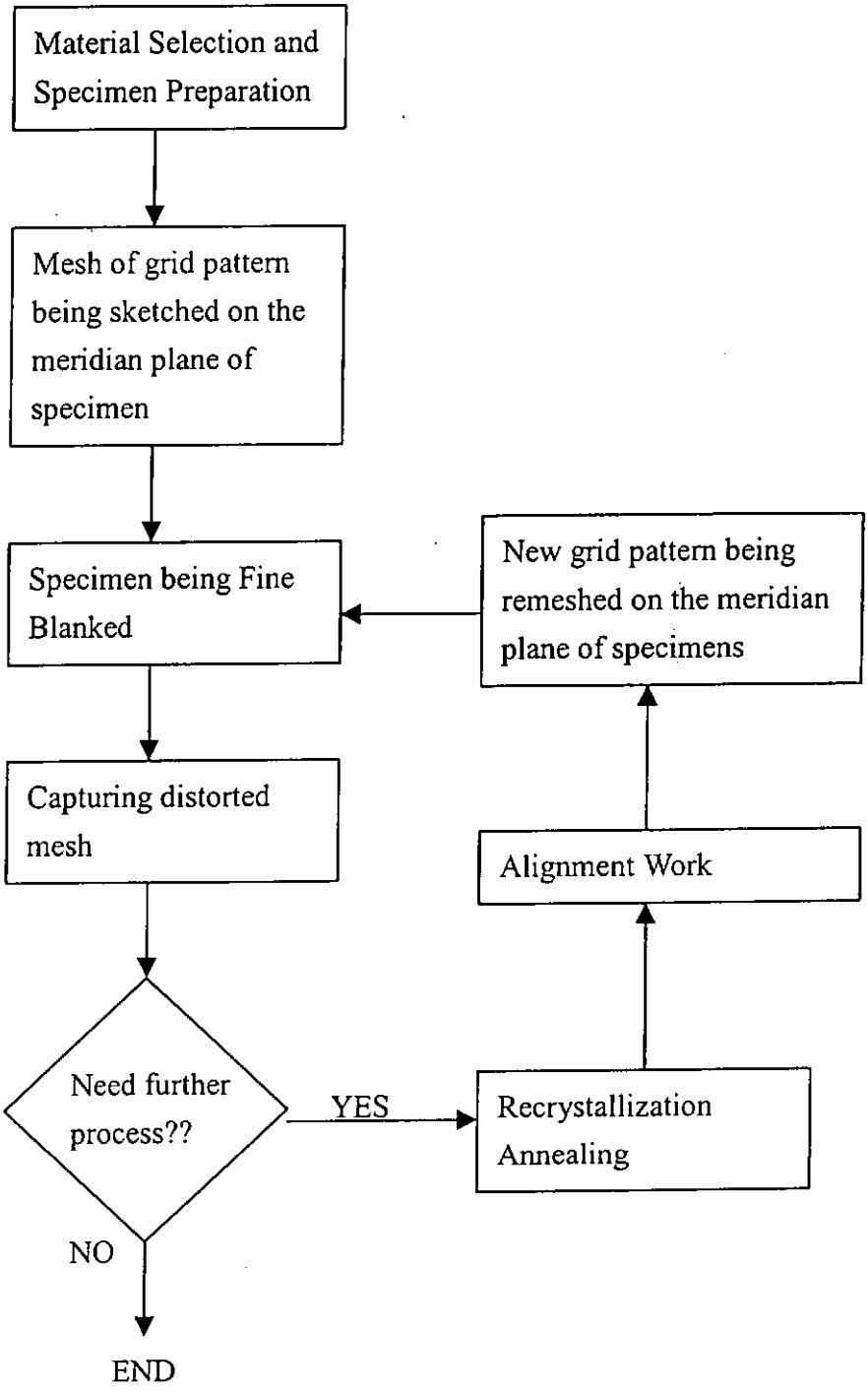

Fig.4.12 A Flow Chart Summarizing the Practical Implementation

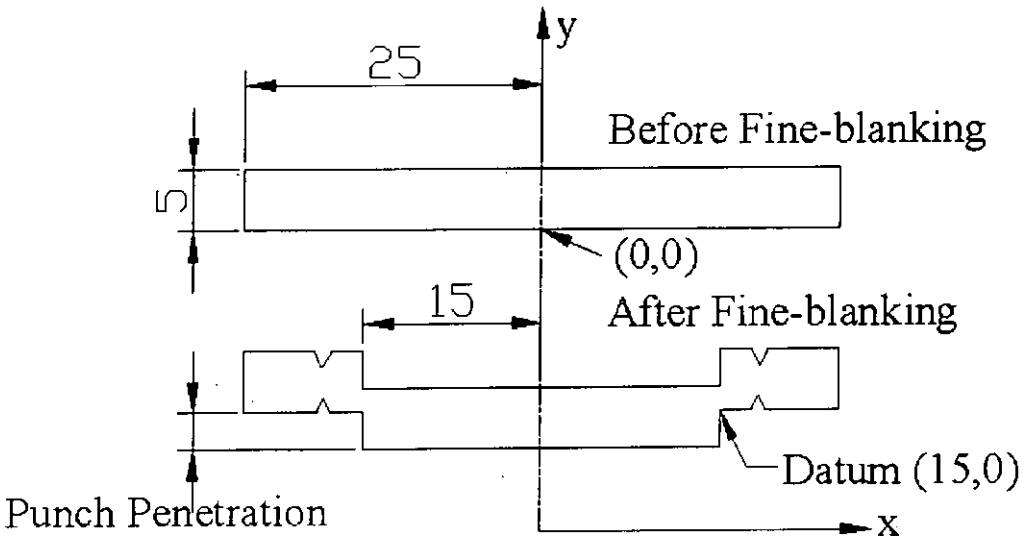

Fig.4.13 Illustration of Strain Measurement (Graphically)

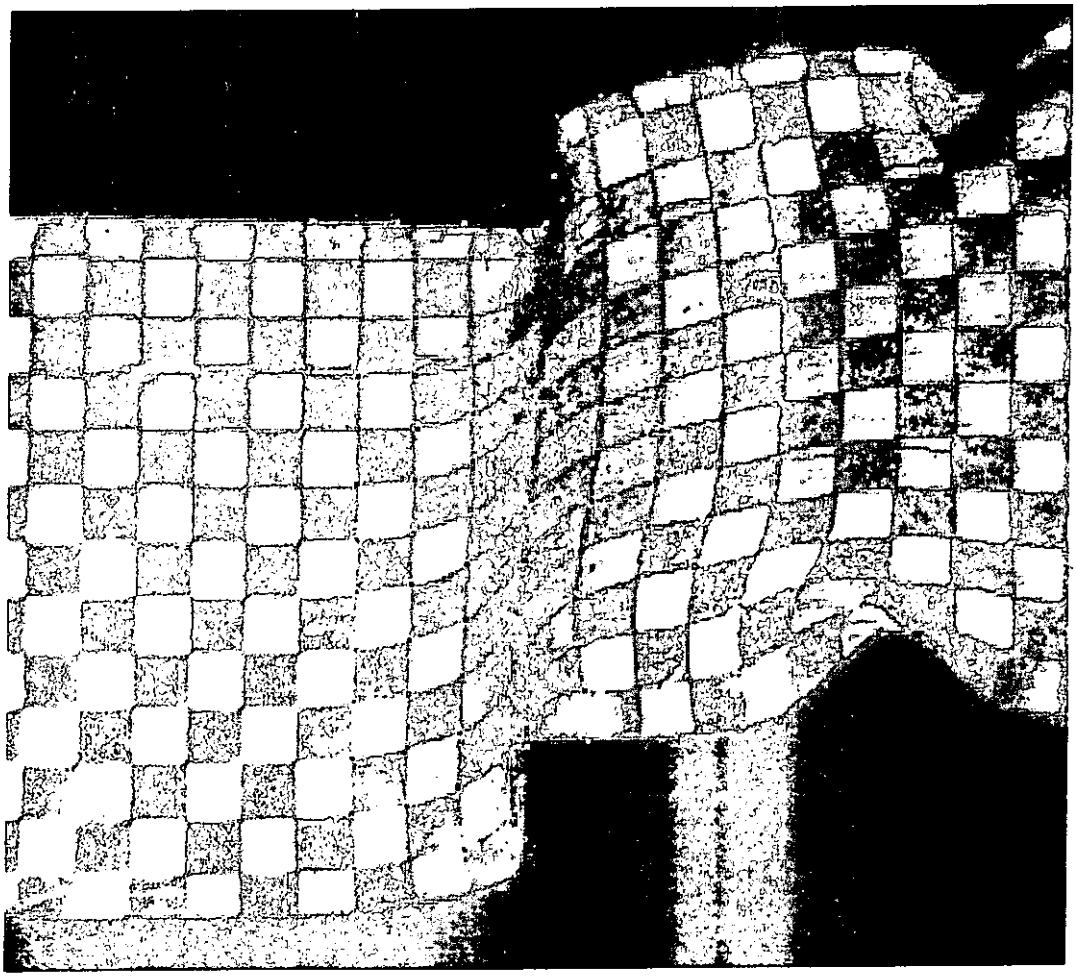

Fig.4.14 Illustration of Strain Measurement (Practically)

Start

End

Fig.5.1 The Experimental Sequence

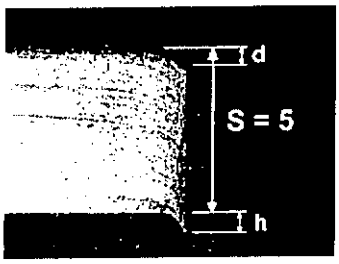

Fig.5.2 Die-roll Height and Burr Height of the Blanked product

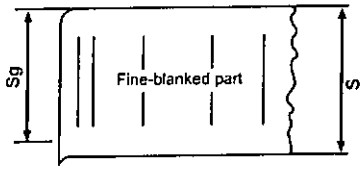

Fig.5.3 Fine-blanked Edge Quality Relation

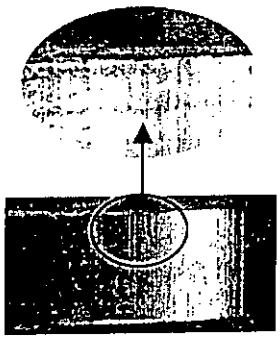

K=1.00

Fig.5.4 Blanked Edge Finishing

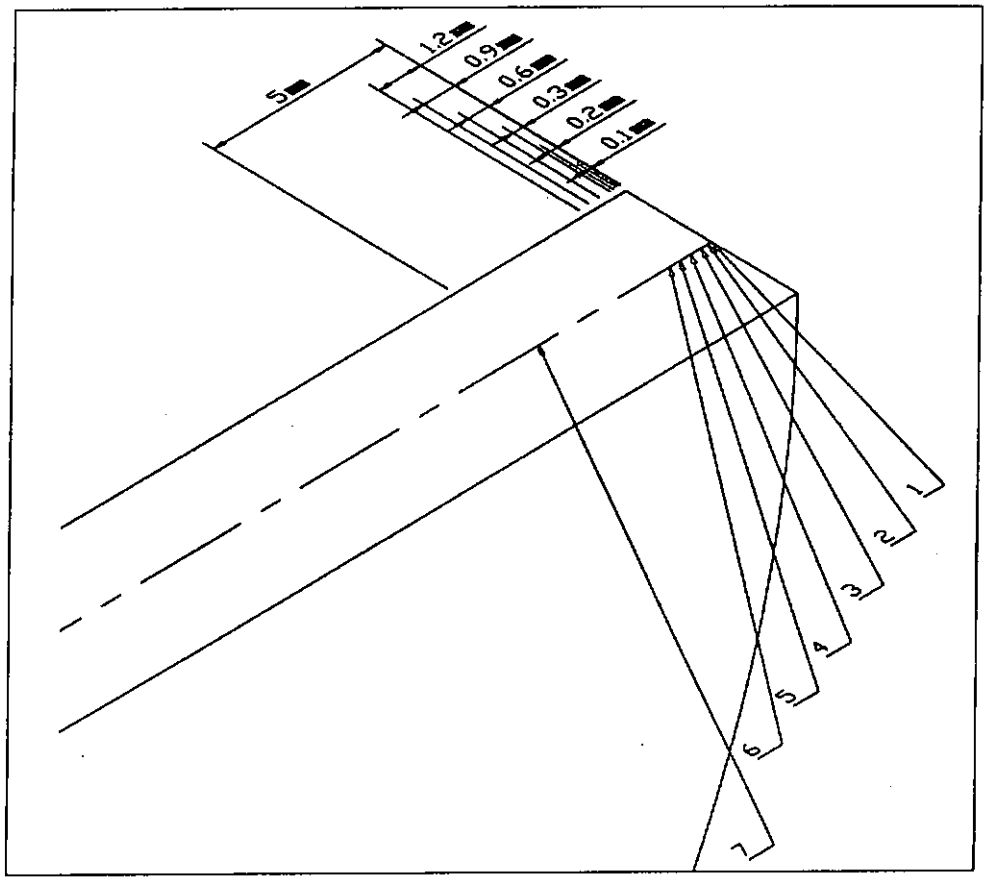

Fig.5.5 The predetermined testing pattern on the Fine-blanked specimen

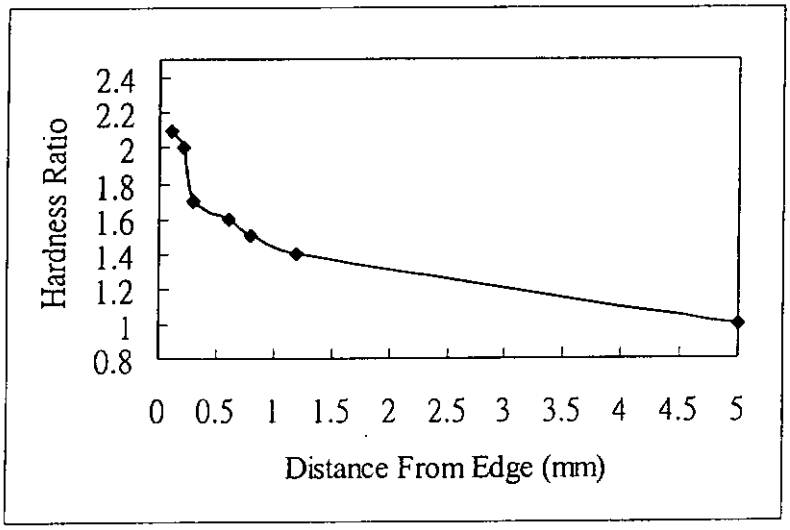

Fig.5.6 Hardness Ratio

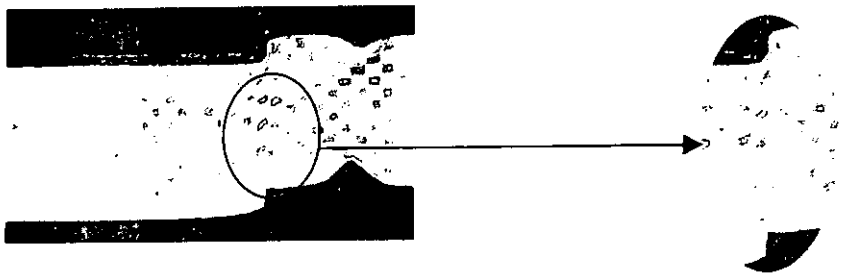

(a) Punch Penetration: 20% of material thickness being Fine-blanked

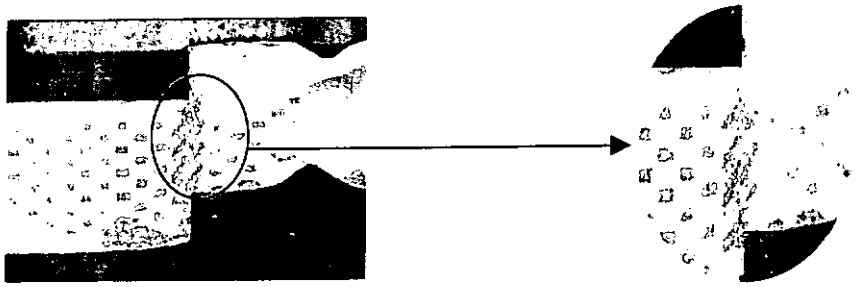

(b) Punch Penetration: 40% of the Material Thickness being Fine-blanked

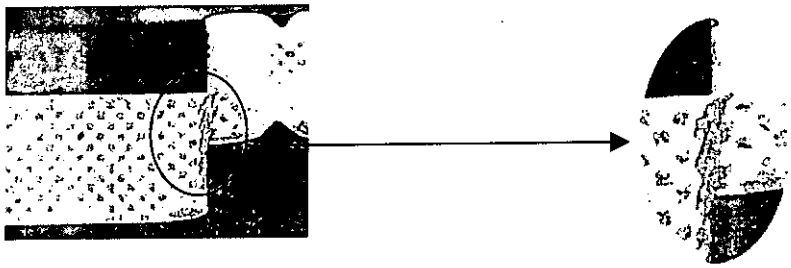

(c) Punch Penetration: 60% of the Material Thickness being Fine-blanked

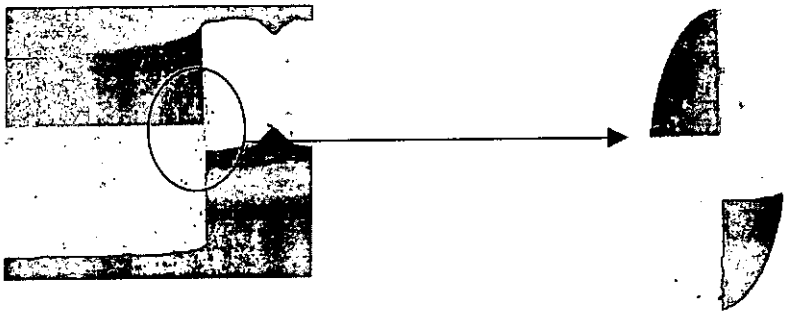

(d) Punch Penetration: 80% of material thickness being Fine-blanked

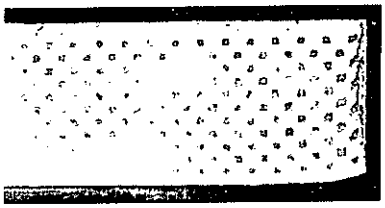

(e) Punch Penetration: 100% of material thickness being Fine-blanked (Final part)

Fig.5.7 The Distorted Meshes at Different Punch Penetrations

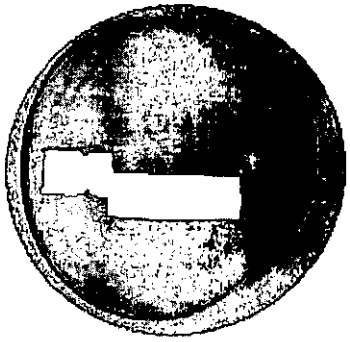

Fig.5.8 Sectioned and Polished Specimen for Further Examination

Fig.5.9 Micrograph of Shear Zone with Punch Penetration of 50% of Material Thickness

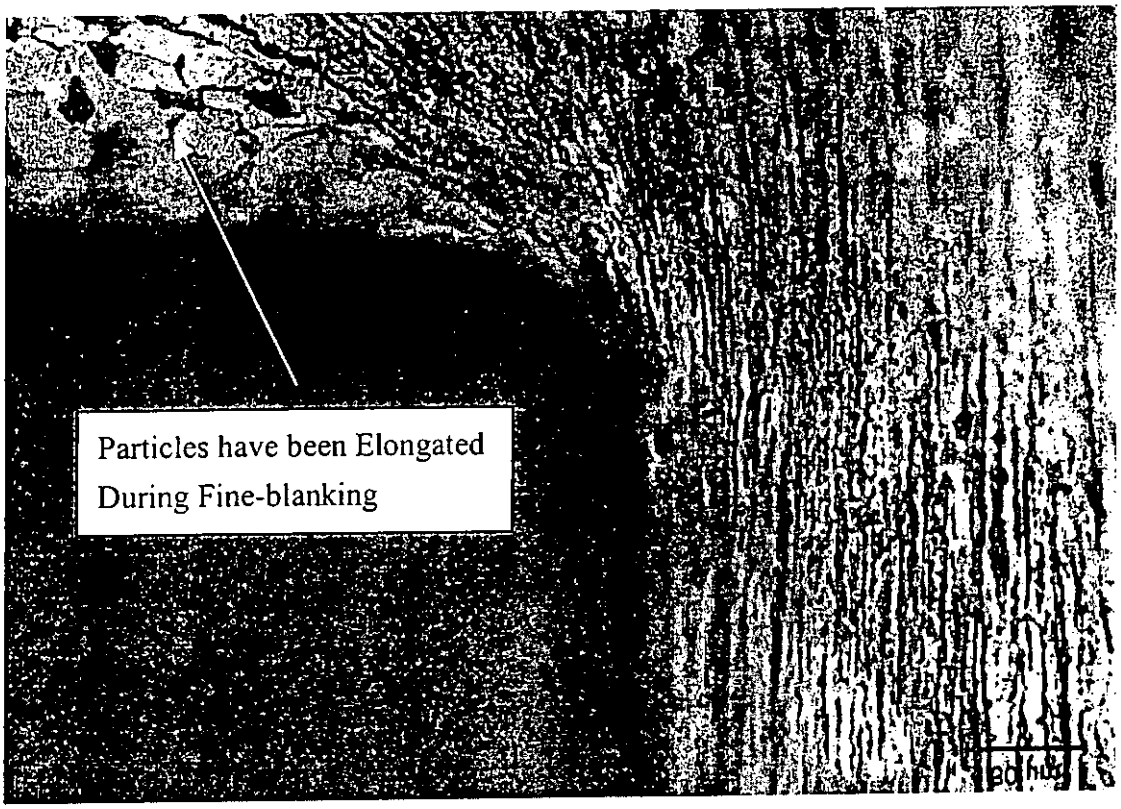

Fig.5.10 Enlargement of Severe Shear Localization Region of 50% Punch Penetration

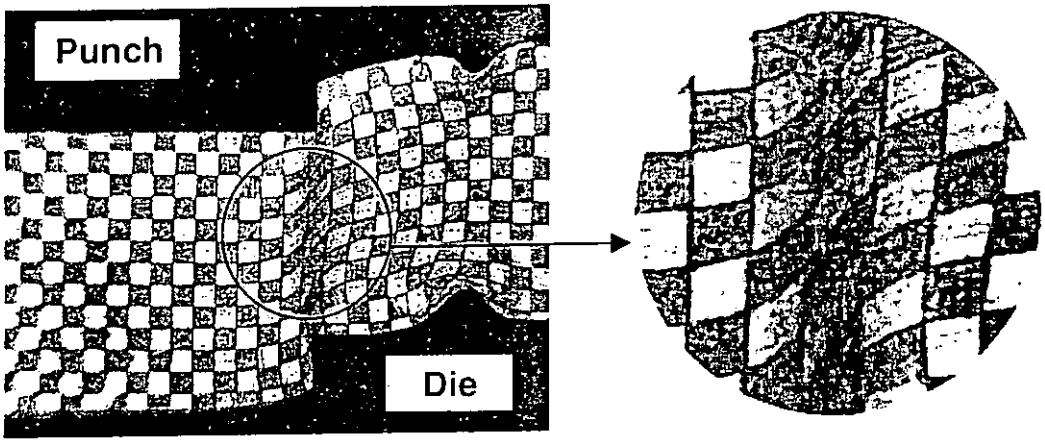

(a) (b)

Fig.5.11 Distorted Mesh obtained from 20% Material Thickness of Punch Penetration

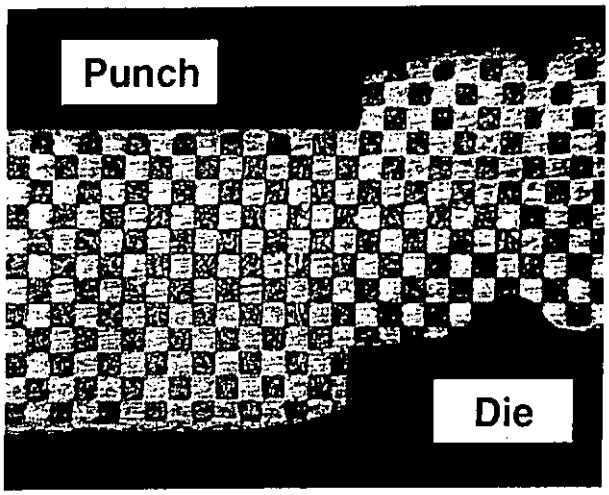

Fig.5.12 Remeshed Fine-blanked Specimen after Punch Penetration 0-20%

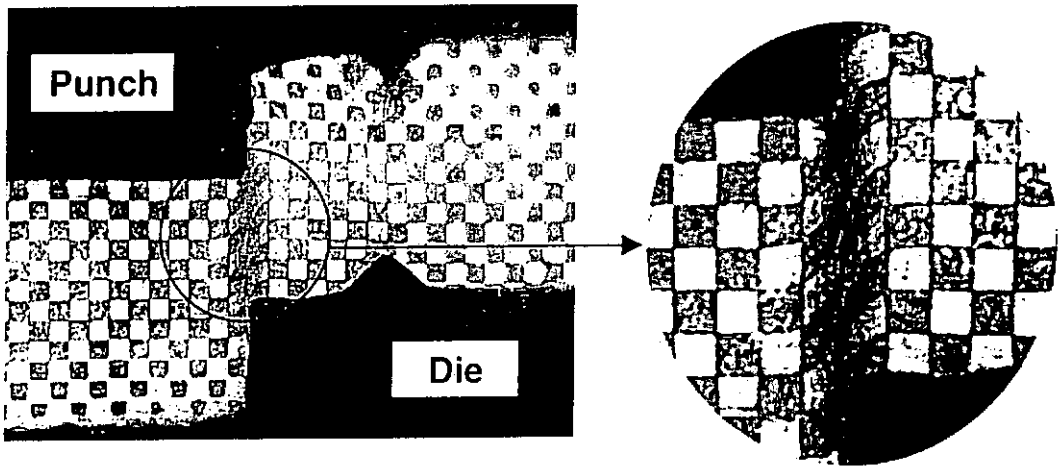

(a) (b)

Fig.5.13 Distorted Mesh after Remeshing in second stage

(Punch Penetration: From 20% to 40%)

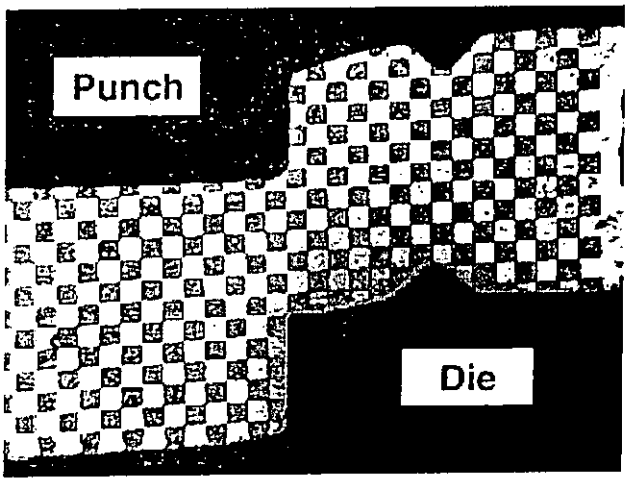

Fig.5.14 Remeshed Fine-blanked Specimen after Punch Penetration 20-40%

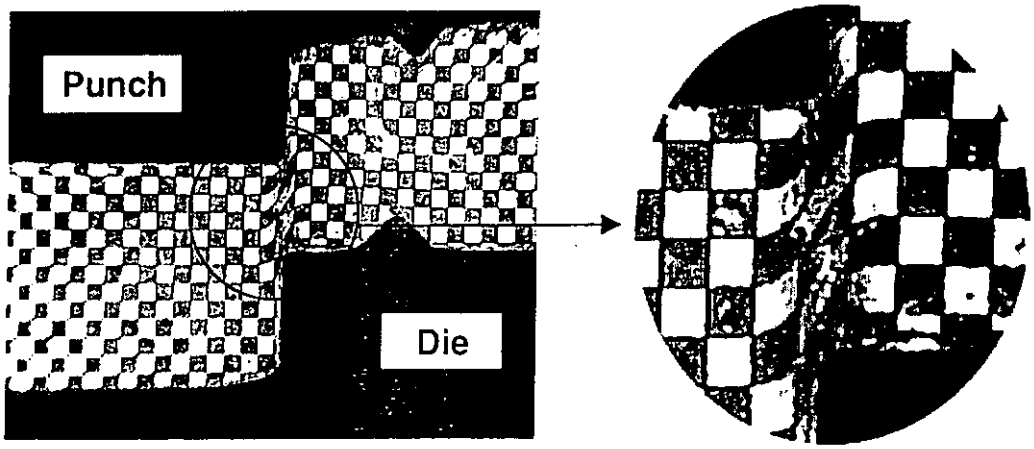

(a) (b)

Fig.5.15 Distorted Mesh after Remeshing in third stage

(Punch Penetration: From 40% to 60%)

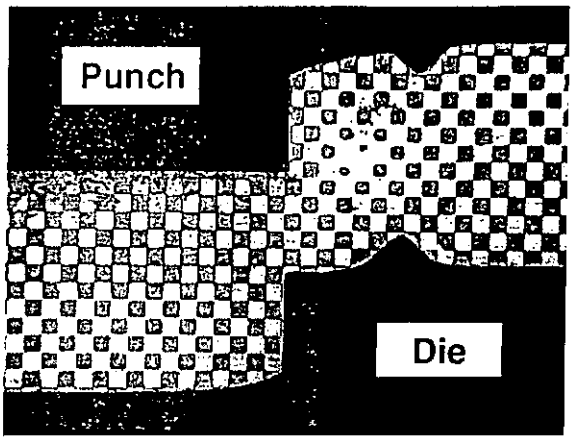

Fig.5.16 Remeshed Fine-blanked Specimen after Punch Penetration of 40-60%

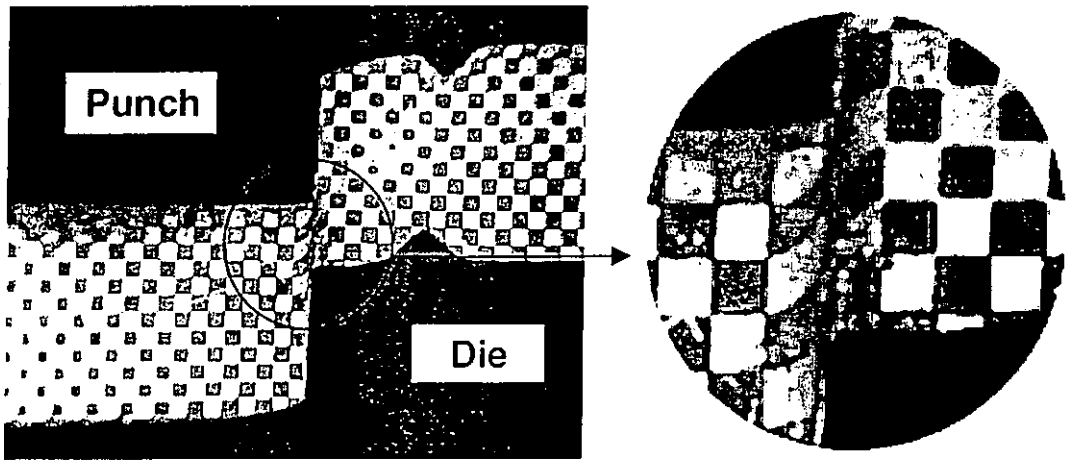

(a) (b)

Fig.5.17 Distorted Mesh after Remeshing in fourth stage

(Punch Penetration: From 60% to 80%)

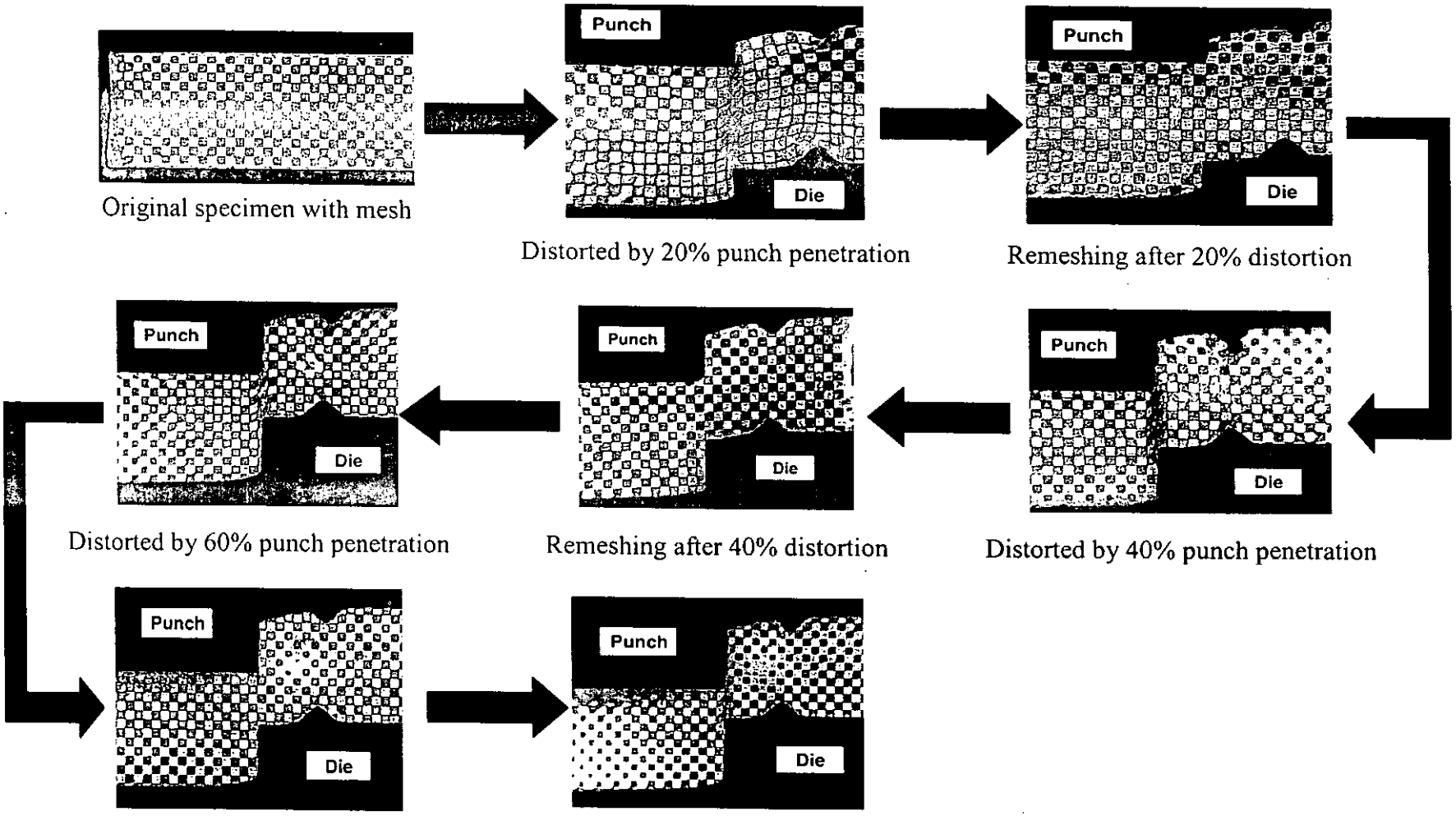

Fig. 5.18 Sequence of Deformations and Remeshing Processes

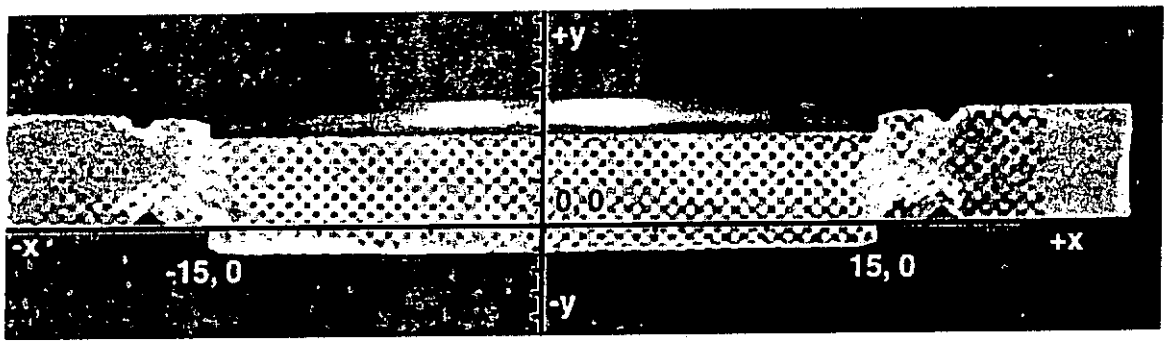

Fig.5.19 The Coordinate Plane for Measurement

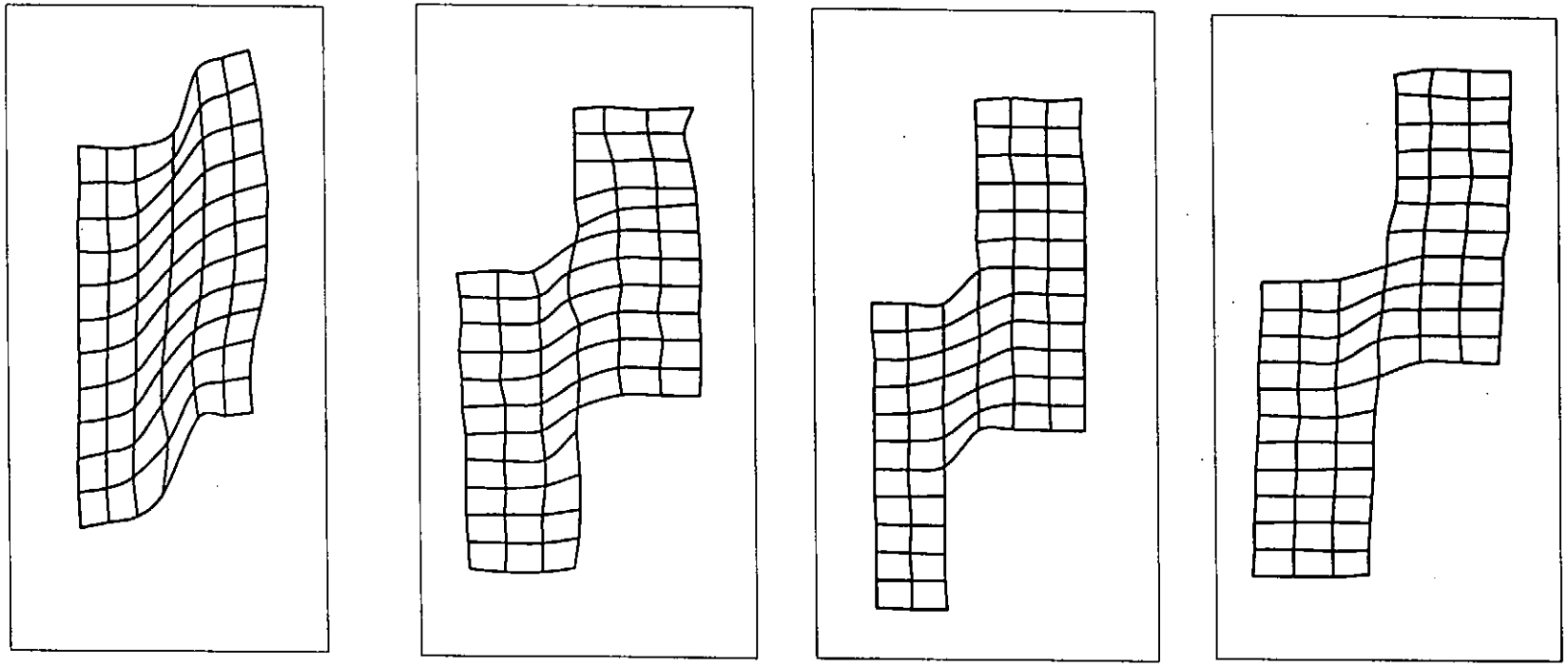

(a) 0-20% of Punch Penetration

(b) 20-40% of Punch Penetration

(c) 40-60% of Punch Penetration

(d) 60-80% of Punch Penetration

Fig.5.20 Graphical Presentation of Distorted Meshes

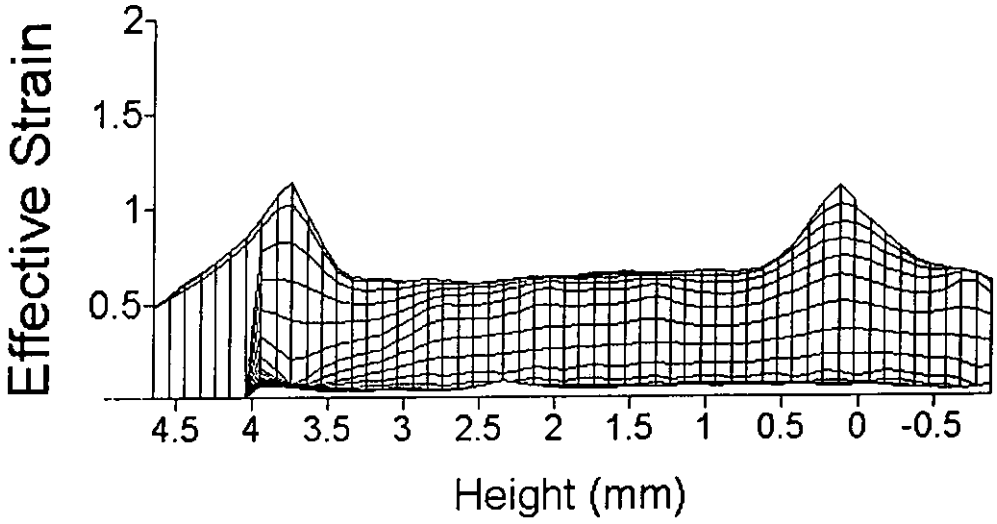

(a)

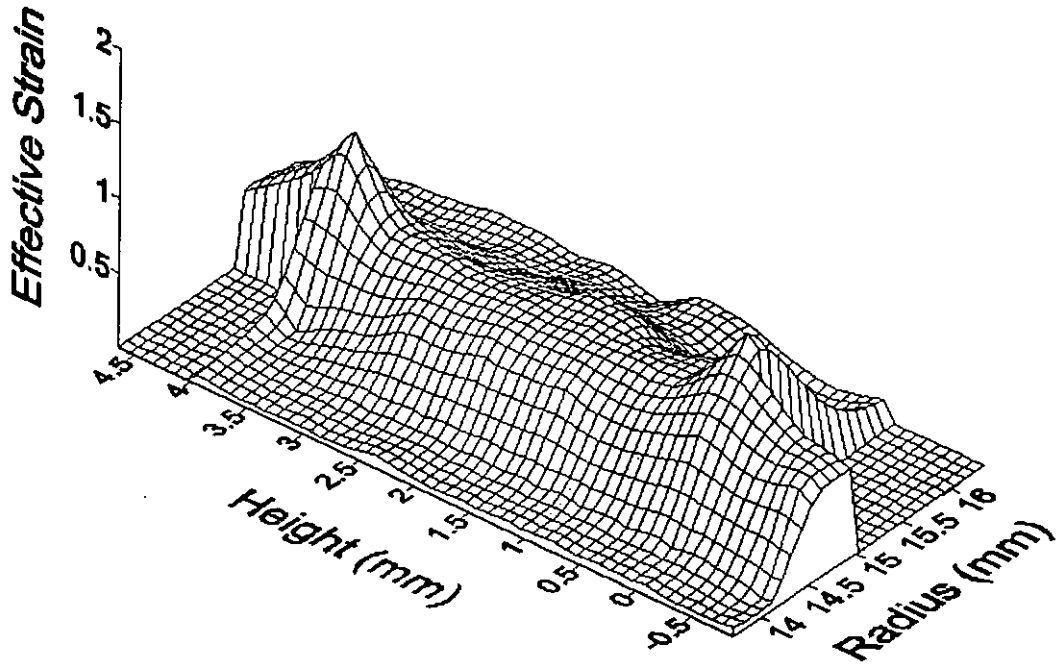

(b)

Fig.5.21 2-D and 3-D Contour Map of 0% - 20% Punch Penetration

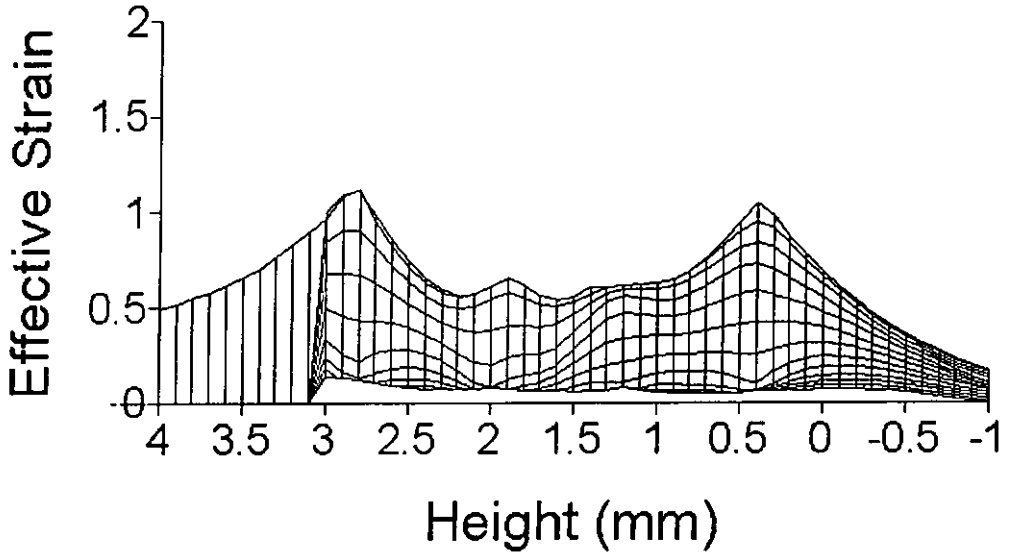

(a)

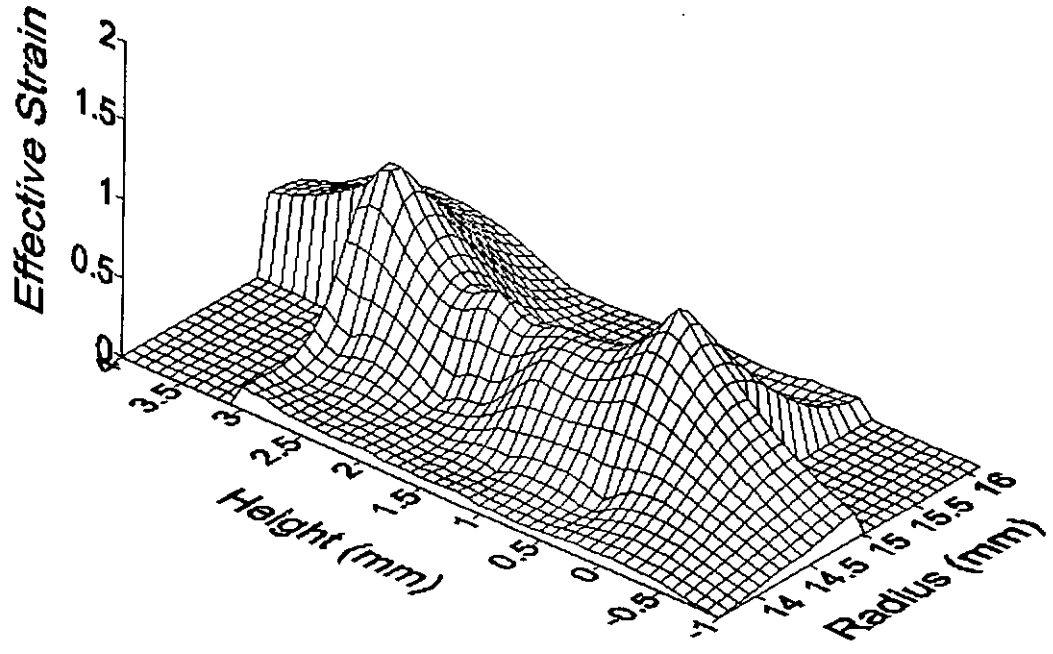

(b)

Fig.5.22 2-D and 3-D Contour Map of 20% - 40% Punch Penetration

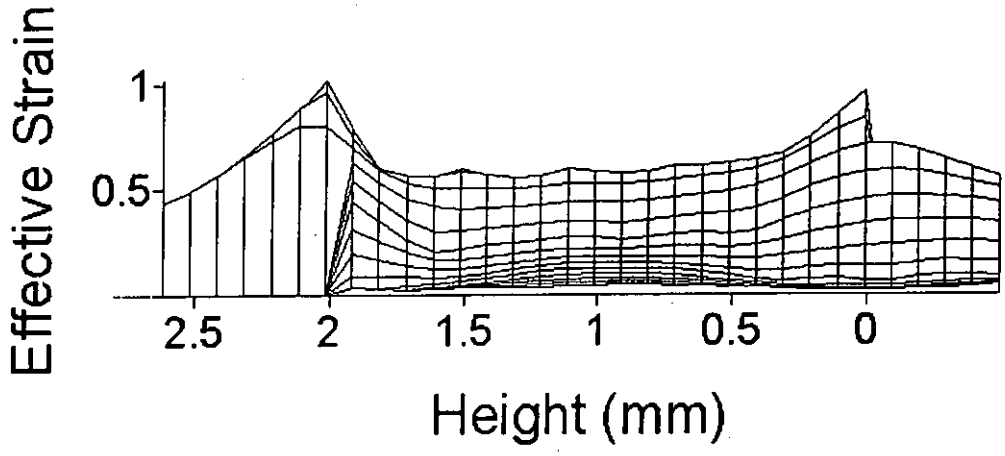

(a)

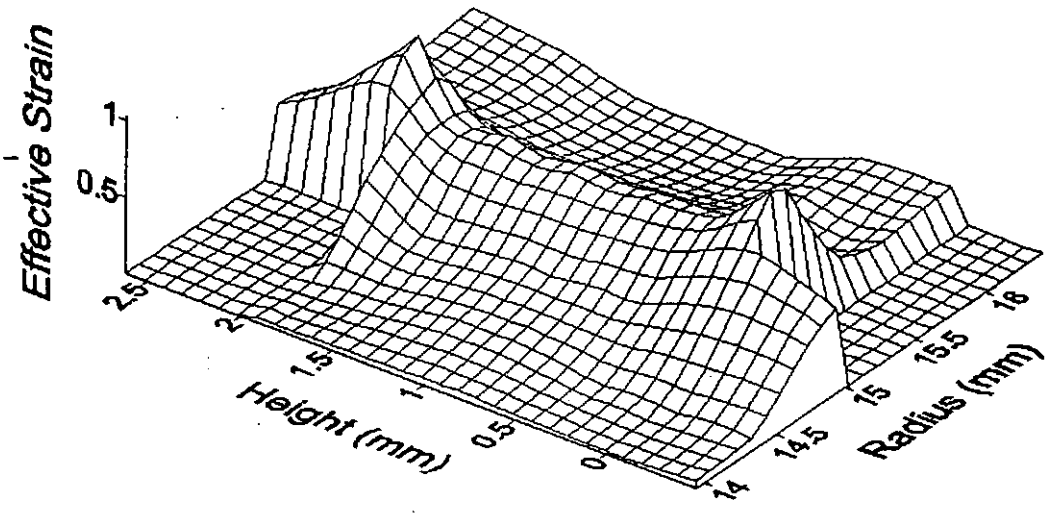

(b)

Fig.5.23 2-D and 3-D Contour Map of 40% - 60% Punch Penetration

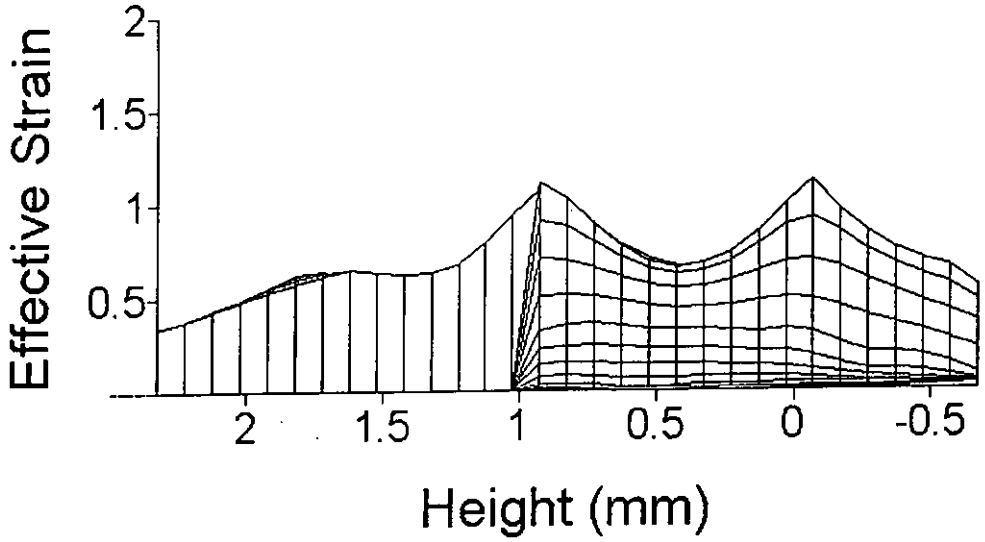

(a)

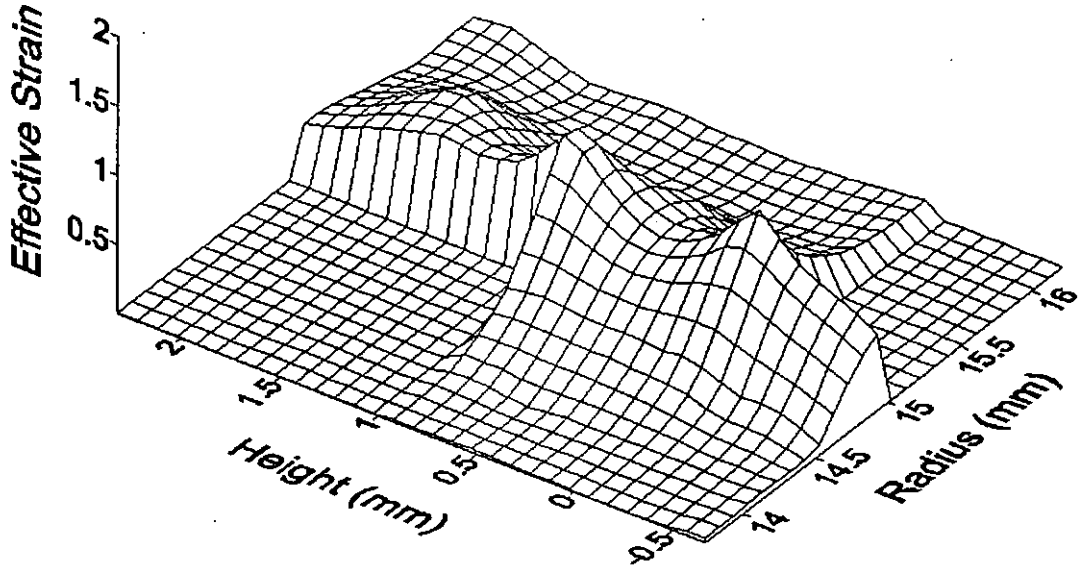

(b)

Fig.5.24 2-D and 3-D Contour Map of 60% - 80% Punch Penetration

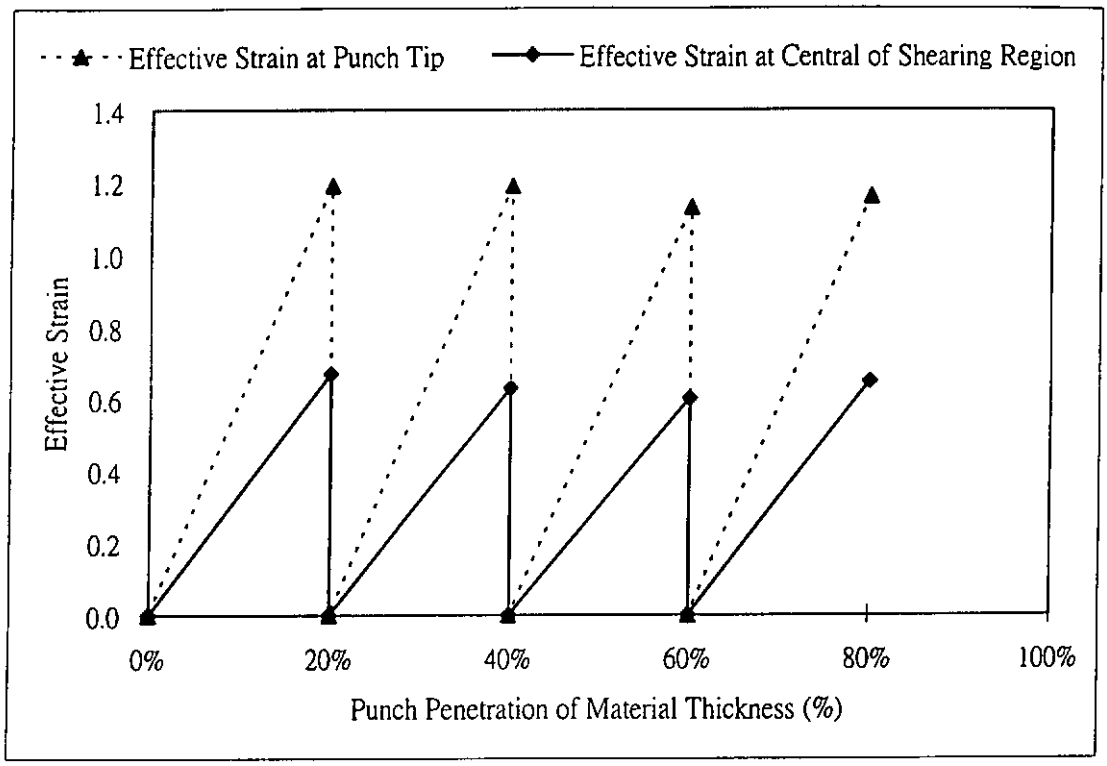

Fig.5.25 The Effective Strains at the Punch Tip and Central of the Shearing Region

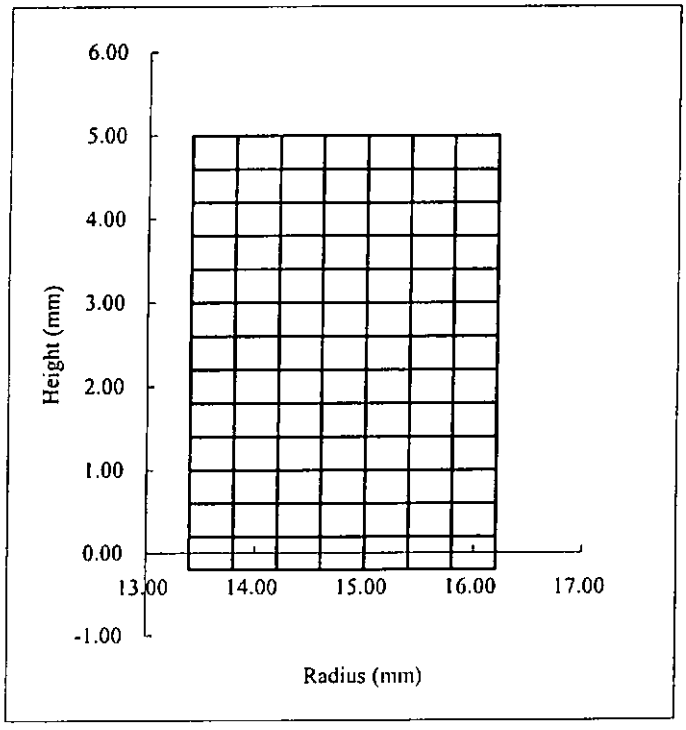

ig.5.26 Designed Coordinate System for Strain Measurement of Configuration in Fig.4.13

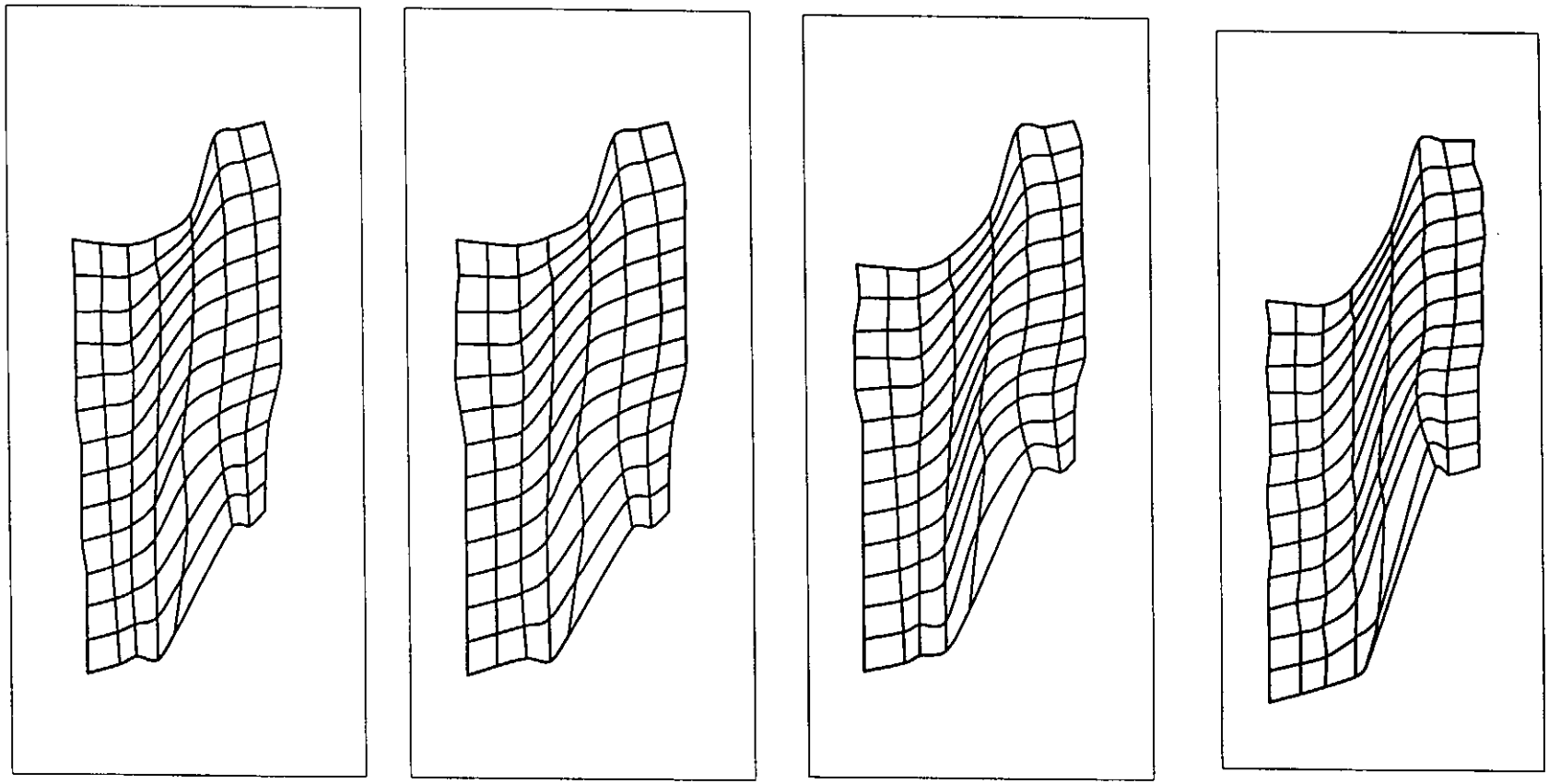

(a) 0-20% of Punch Penetration (b) 0-40% of Punch Penetration (c) 0-60% of Punch Penetration (d) 0-80% of Punch Penetration

Fig.5.27 Graphical Presentation of Distorted Meshes for Total Punch Penetration

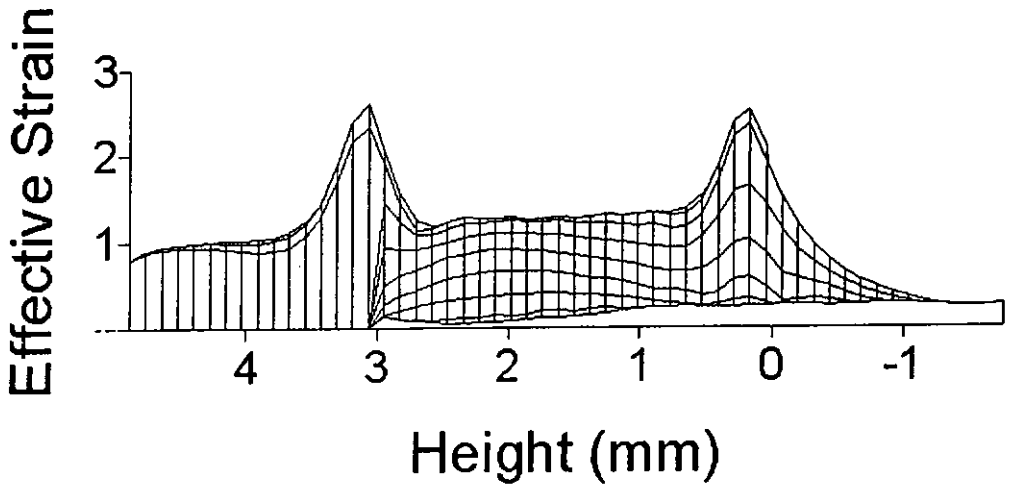

(a)

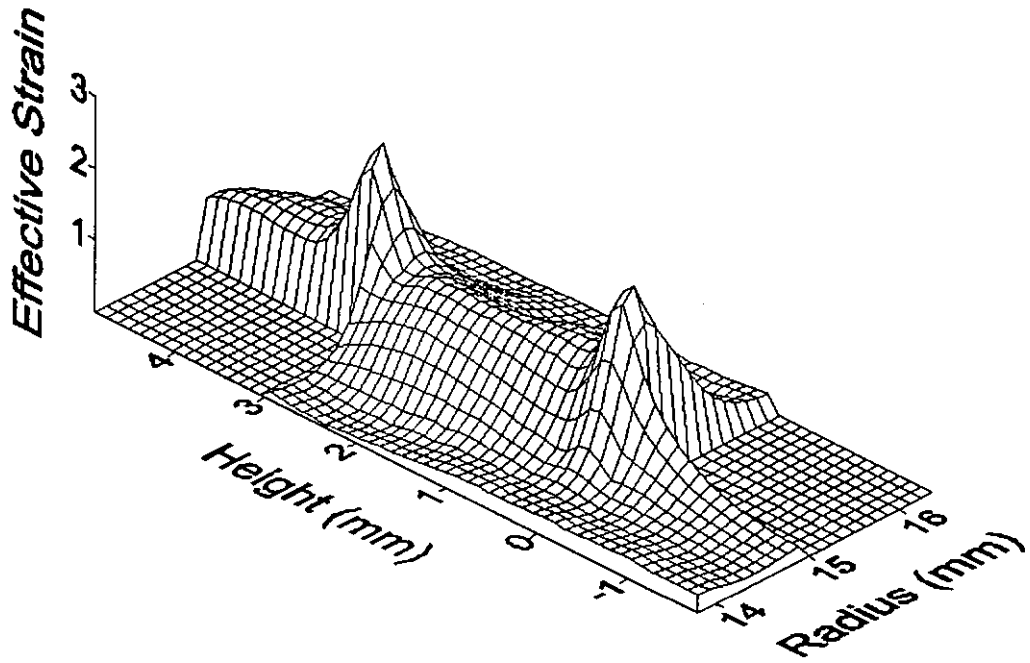

(b)

Fig.5.28 2-D and 3-D Contour Map of 0% - 40% Punch Penetration

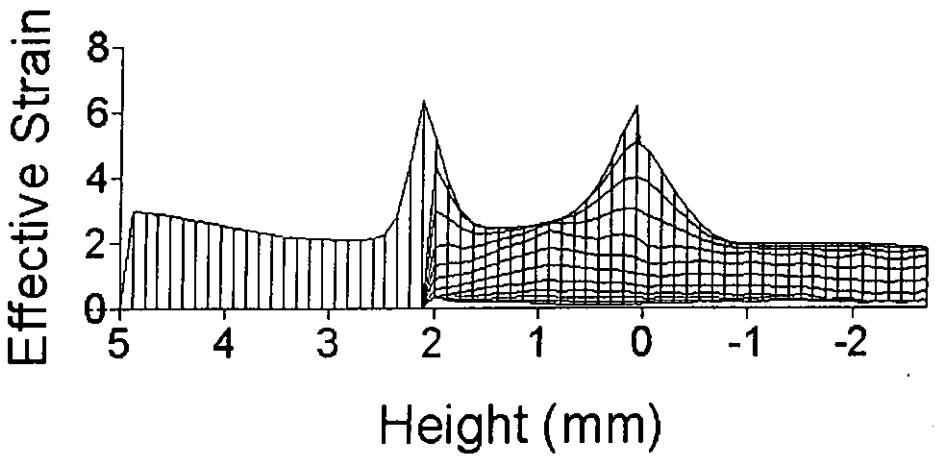

(a)

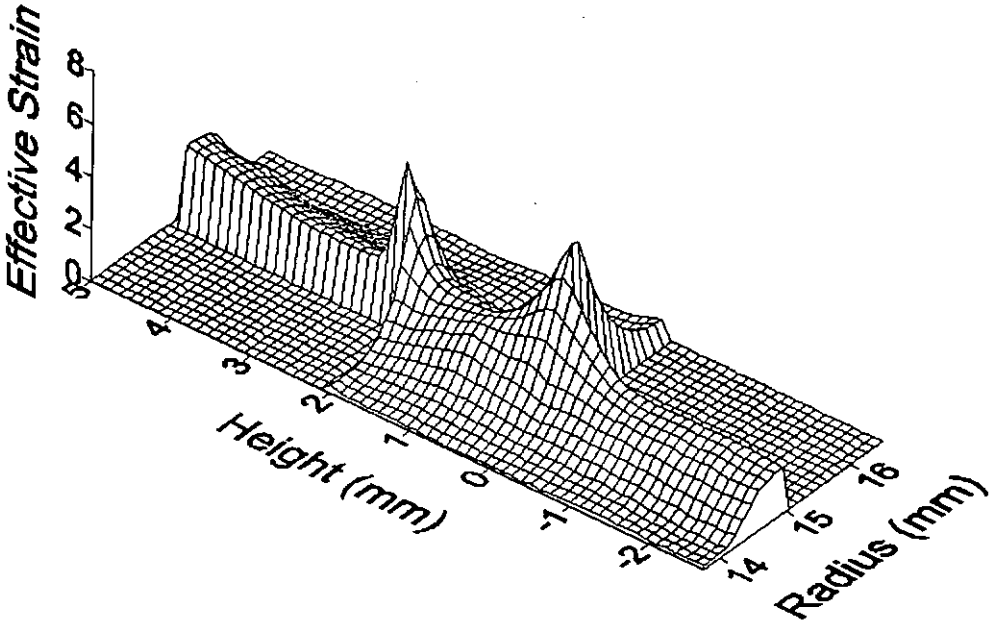

(b)

Fig.5.29 2-D and 3-D Contour Map of 0% - 60% Punch Penetration

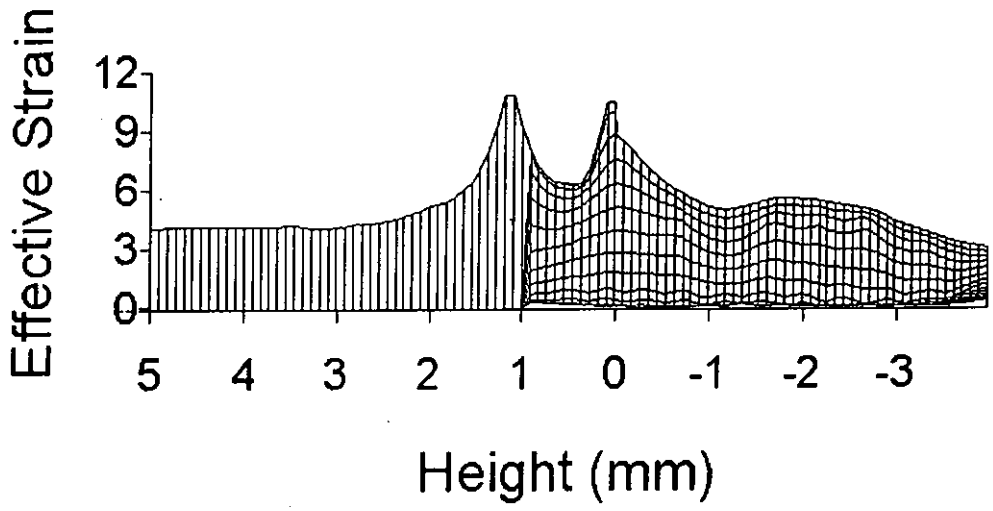

(a)

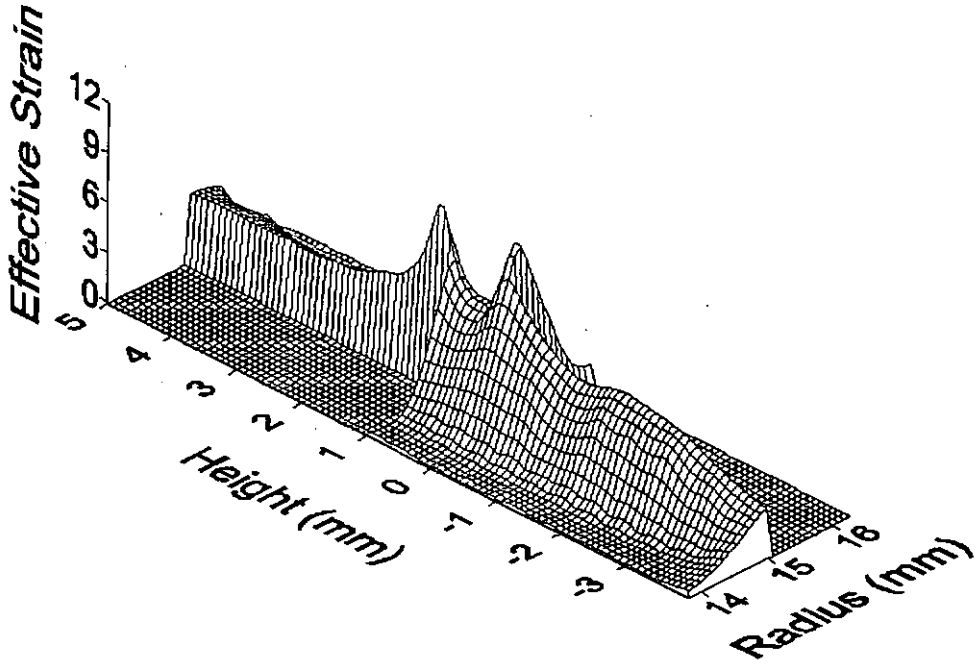

(b)

Fig.5.30 2-D and 3-D Contour Map of 0% - 80% Punch Penetration

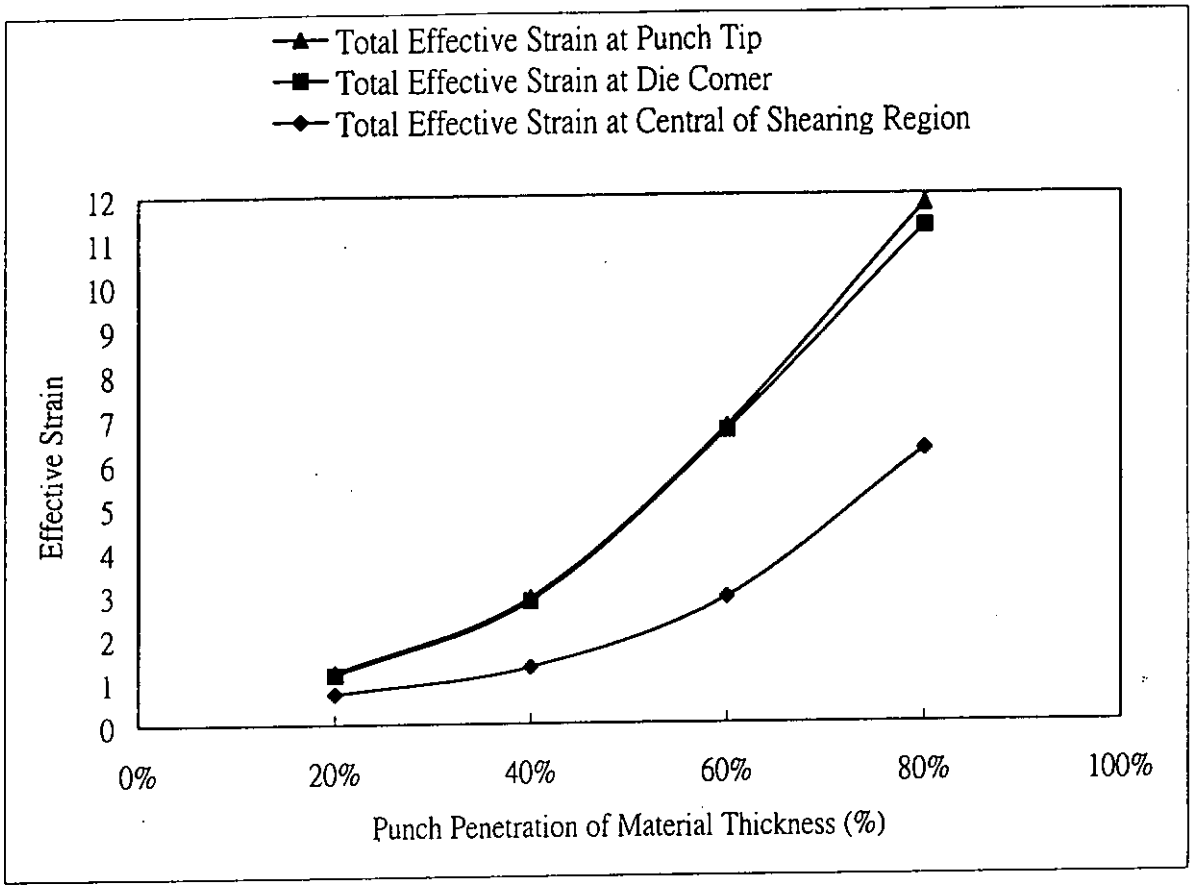

Fig.5.31 The Total Effective Strains at Different Locations

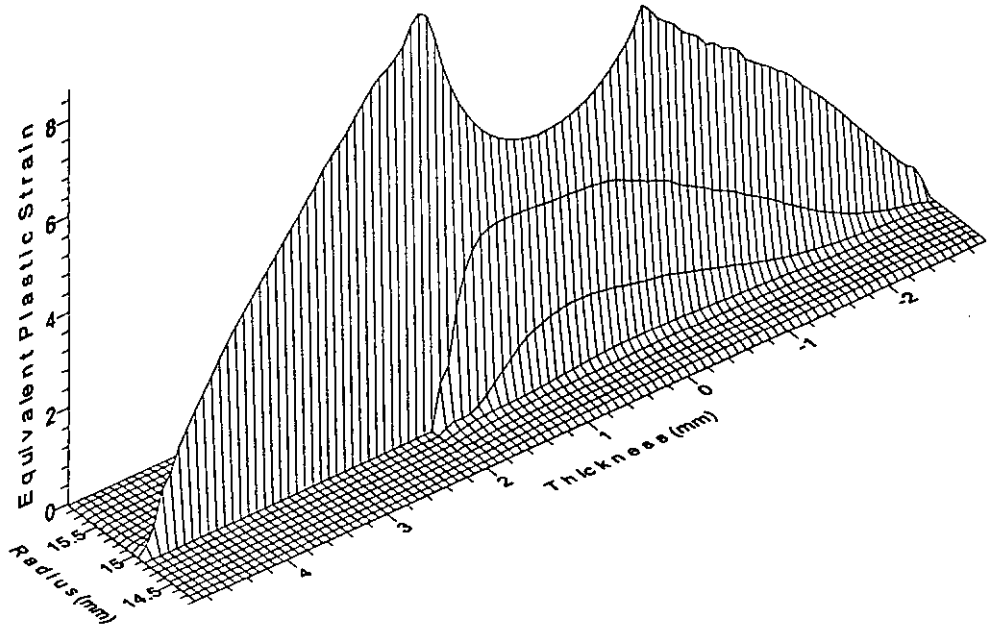

Fig.5.32 The Strain Distribution of Total Punch Penetration 0-60% (Chen,2002)

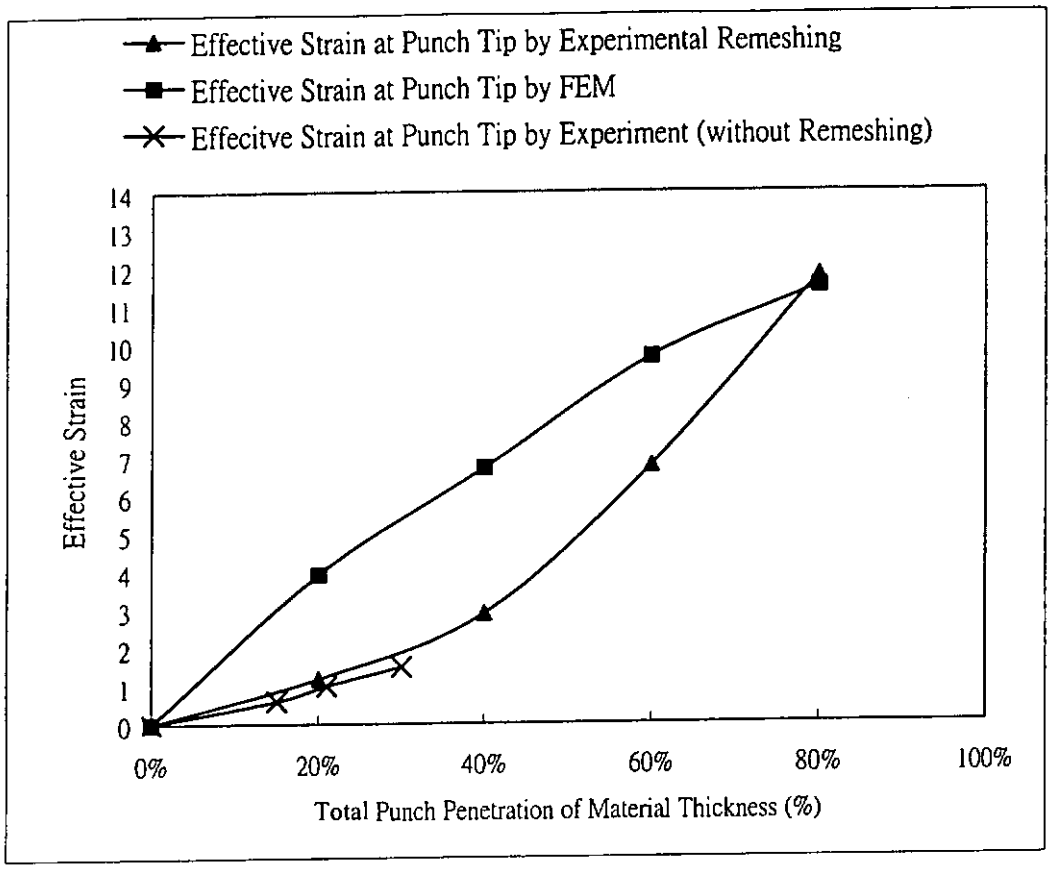

Fig.5.33 Comparison Between Experimental and FEM Findings

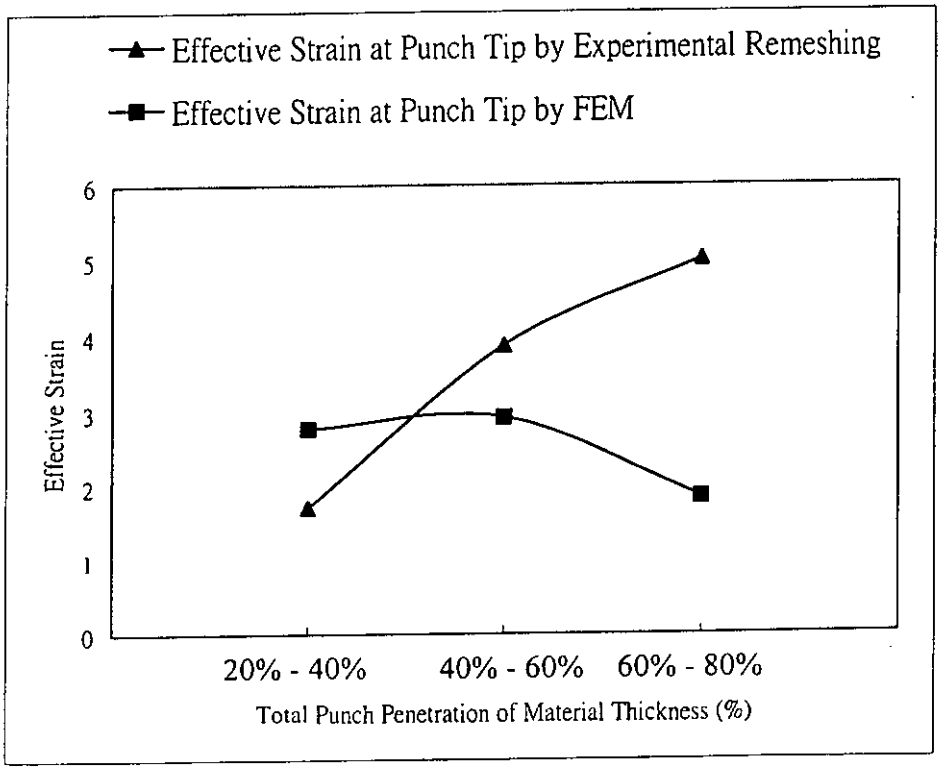

Fig.5.34 Increments of Effective Strain Against Total Punch Penetrations

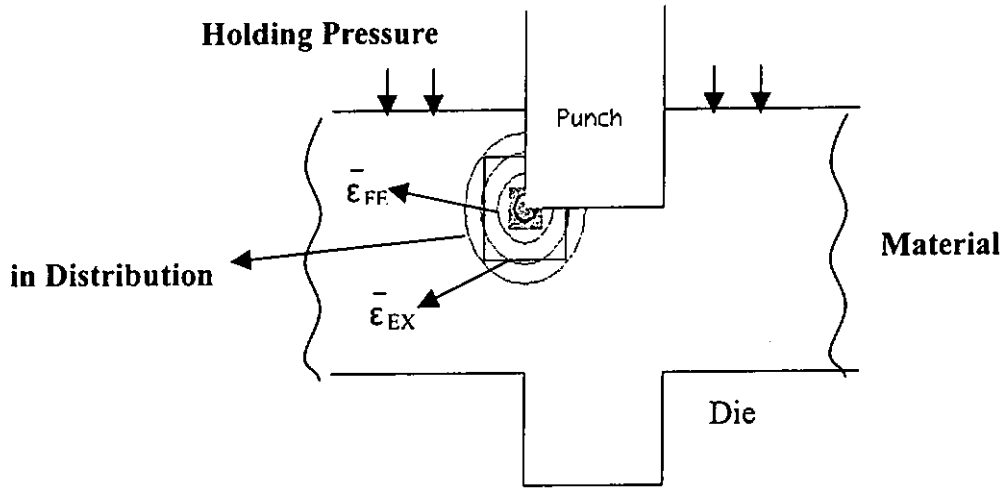

(a) For 20% of Punch Penetration

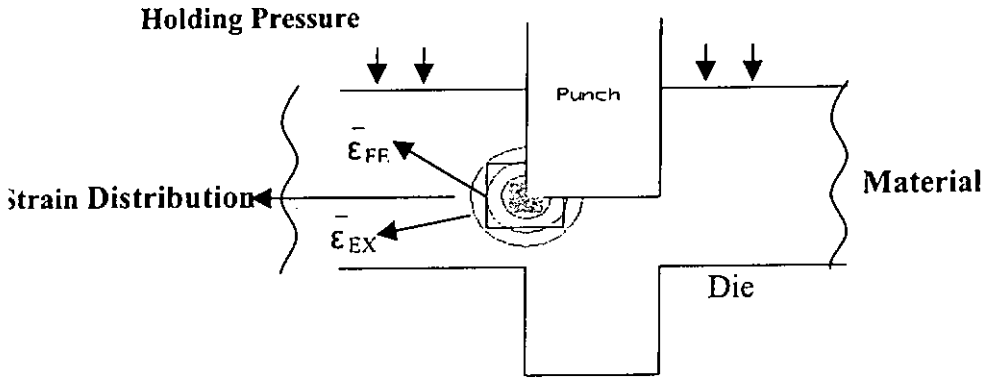

(b) For 60% of Punch Penetration

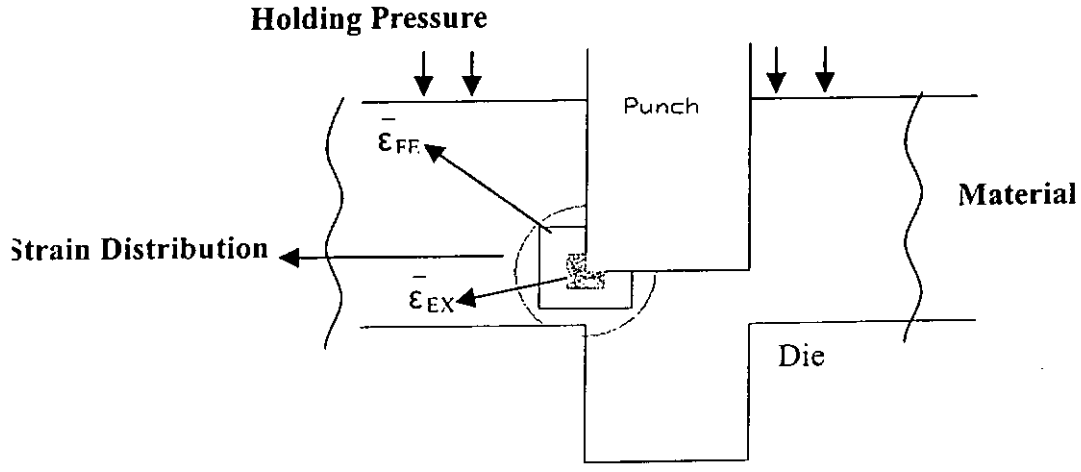

(c) For 80% of Punch Penetration

Fig.5.35 Difference of Strain Distributions between the Predictive and Experimental Values

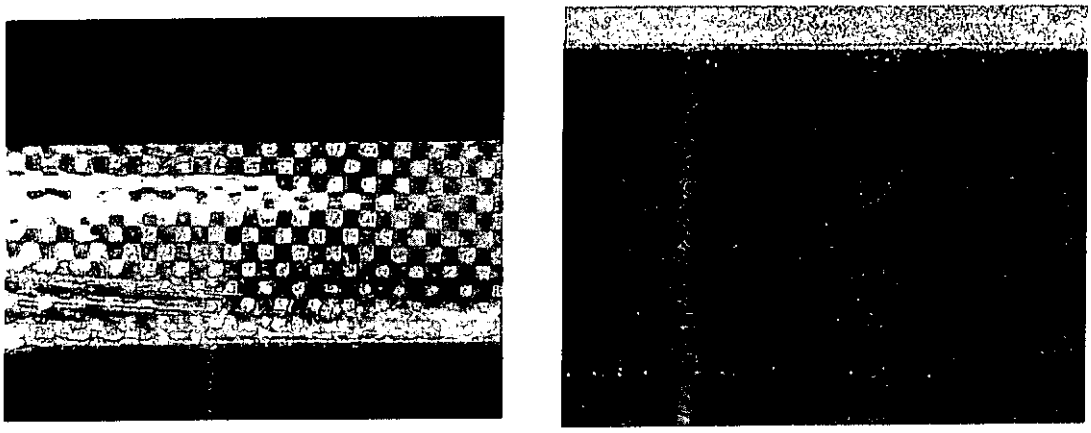

(a) Poor Lamination (b) Over Etching

Fig.5.36 Useless Mesh Etched on Specimens

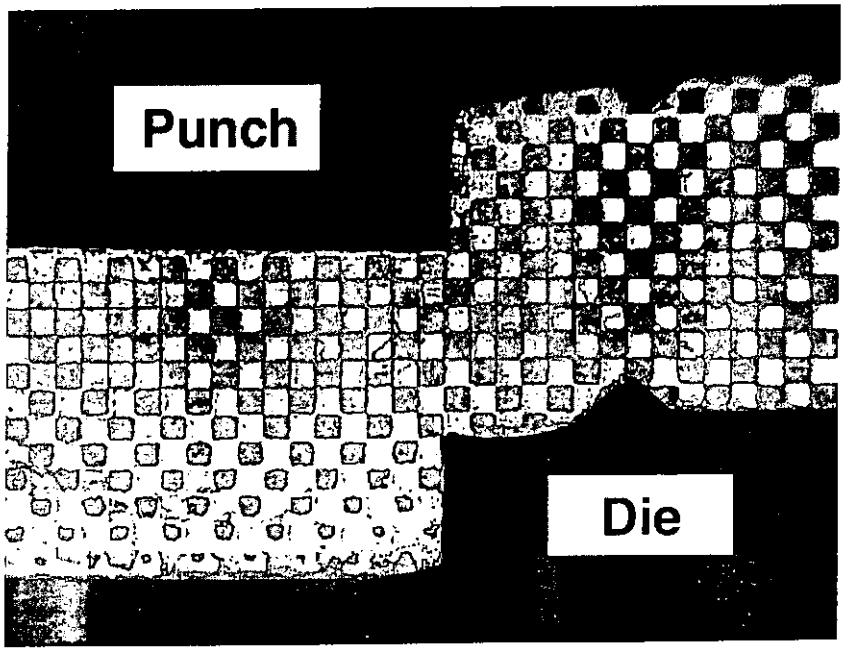

Fig.5.37 Remeshing of Over Polished Specimen

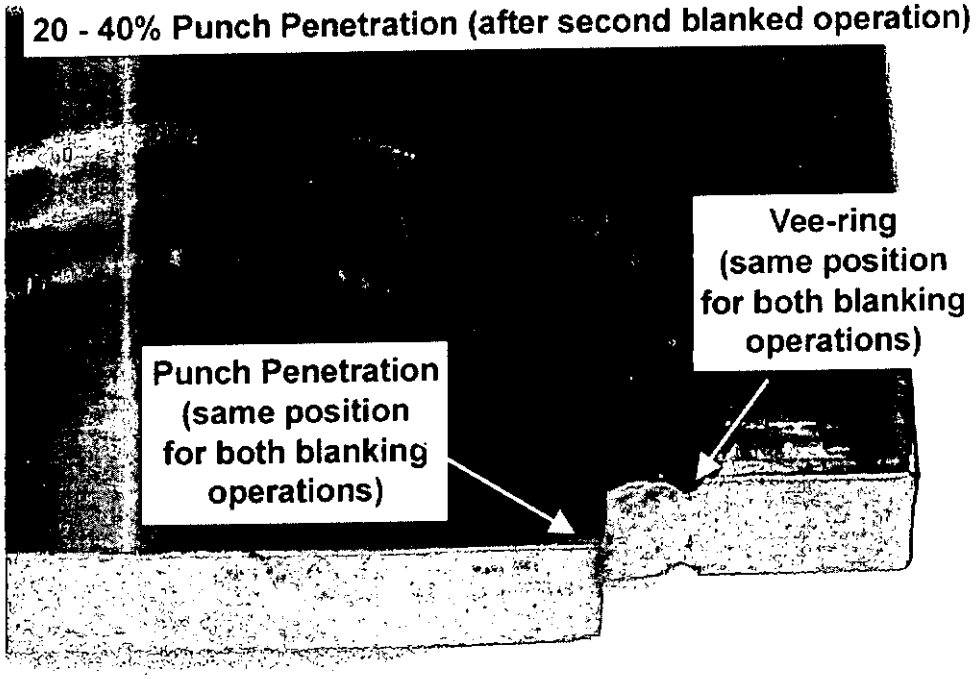

(a)

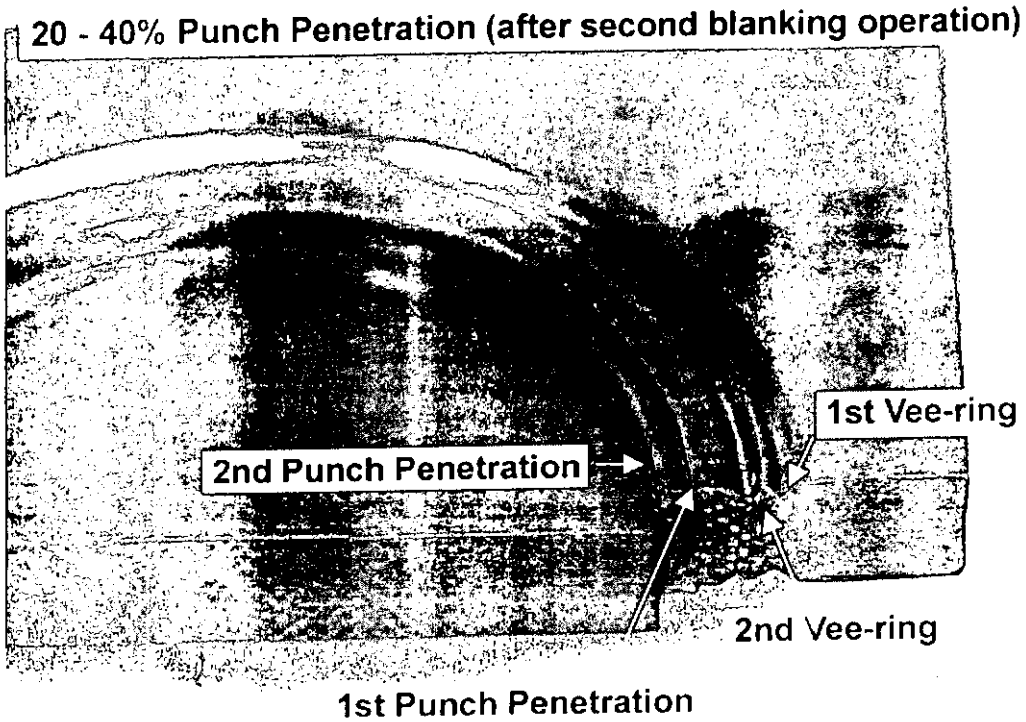

(b)

Fig. 5.38 Comparison of Accurate Alignment and Misalignment

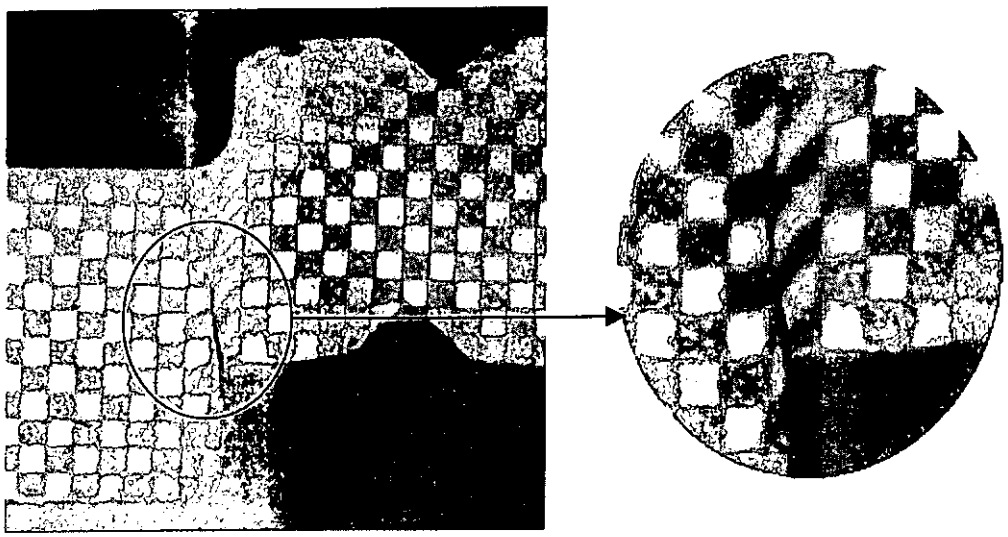

Fig.5.39 Remeshed specimen was Fine-blanked from 20% to 40% of material thickness

Fig.5.40 An Optical Micrograph Showing the Crack

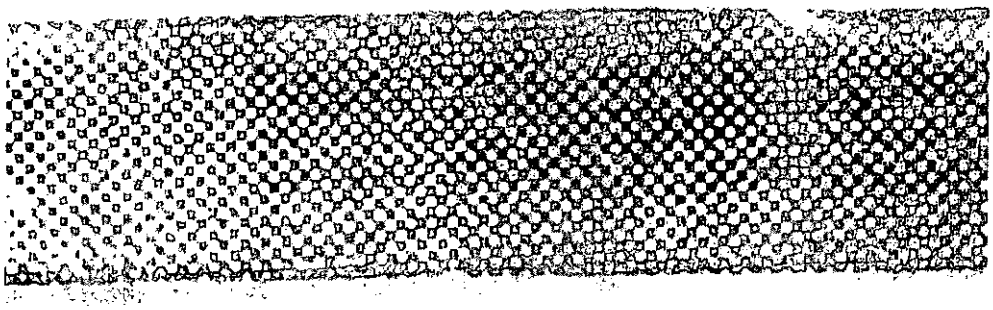

Fig.5.41 Specimen with Mesh of Grid Size 0.2mm x 0.2mm

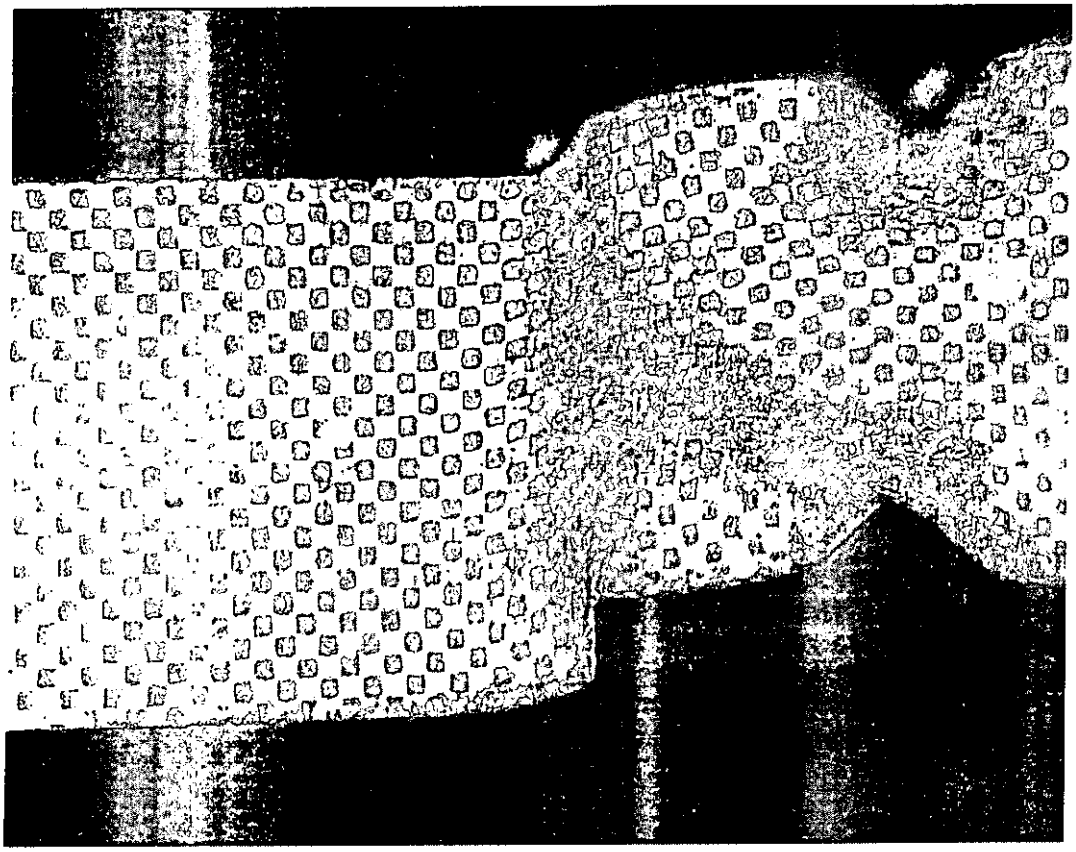

Fig.5.42 Punch Penetration of 10% Material Thickness (Grid Size: 0.2 x 0.2mm)